



NTNU – Trondheim
Norwegian University of
Science and Technology

Crystal Growth Kinetics of Calcium Carbonate Particles in Natural Gas Production

Charlotte Kleven Krossholm

Chemical Engineering and Biotechnology

Submission date: June 2012

Supervisor: Jens-Petter Andreassen, IKP

Co-supervisor: Ralf Beck, IKP

Norwegian University of Science and Technology
Department of Chemical Engineering

Preface

This master thesis was performed during the spring 2012 as a mandatory part of the final semester of the Master of Science degree in Chemical Engineering and Biotechnology. The project was given by the Department of Chemical Engineering, IKP, at the Norwegian University of Science and Technology, NTNU, in Trondheim. The title has been “Crystal Growth Kinetics of Calcium Carbonate Particles in Natural Gas Production”, and this topic has been studied through laboratory work.

Firstly, I would like to thank my main supervisor, Associate Professor Jens-Petter Andreassen, and my co-supervisor, Post Doc Ralf Beck, for their advices, support and patience during the semester. I would also like to thank Engineer Julian Tolchard for assisting me with the SEM and XRD analysis. PhD student Margrethe Nergaard has also been very helpful in the lab and with the report writing. Your enthusiasm for crystallization is admirable! At last, my two fellow students, Astrid Odland Barland and Torunn Kvam, deserve a big thank for sharing the time, laughter and frustration with me in the laboratory and study office throughout this months.

I declare that this is an independent work according to the exam regulations of the Norwegian University of Science and Technology.

Trondheim, 28th June 2012



Charlotte Kleven Krossholm

Abstract

Precipitation of calcium carbonate particles is an interesting area in natural gas production. The inorganic salt could be formed due to pH stabilization for corrosion control in the pipelines and during the regeneration of the hydrate inhibitor monoethylene glycol (MEG) onshore. Calcium carbonate is inverse soluble which implies a risk for precipitation at elevated temperatures, for example in heat exchangers, in the MEG regeneration process. Hence, it is desired to precipitate the ions; and to separate the particles from the MEG loop. Due to these issues, investigation of calcium carbonate growth is requested.

The purpose of this work has been to investigate crystal growth kinetics, by determining growth order and growth rate constants of calcium carbonate with MEG as co-solvent. Seeded growth experiments were performed for the polymorphs vaterite and calcite at 40 and 70 °C with 0 – 70 wt% MEG. Number and size measurements of the seeds were done by use of the Coulter Counter. The depleting calcium concentration was measured by automated titration and corresponding supersaturation ratios were calculated in MultiScale to give growth rates of calcium carbonate. The crystals were analysed by a scanning electron microscope (SEM) and by powder X-ray diffraction (XRD).

The results show that the growth of vaterite and calcite is reduced by increased amount of MEG. Additionally, an elevated temperature will enhance the growth. Increasing the co-solvent composition from 0 – 60 wt%, reduces the growth rate constants assuming parabolic rate law $k_{g=2}$ for vaterite from 1.81 to 0.24 nm/s at 40 °C and from 2.12 to 0.63 nm/s at 70 °C. The corresponding reduction for calcite with a MEG concentration raised from 0 – 70 wt% is from 0.52 to 0.02 nm/s at 40 °C and from 0.95 to 0.08 nm/s at 70 °C. It was concluded that calcite is the slowest growing polymorph in water at both temperatures.

A growth of second order was found for vaterite in water at 40 °C. For calcite the growth order at the same conditions was slightly higher. It is proposed that growth of both polymorphs in water is controlled by surface integration. The order of vaterite and calcite growth decreases with increased MEG concentration and temperature, and a change to first order kinetics is observed. Due to increased viscosity caused by the co-solvent, diffusion or adsorption controlled growth, when $g = 1$, is suggested. This could be explained by the lowered diffusivity of carbonate as a result of the non-stoichiometric reactant ratios.

Sammendrag

Utfelling av kalsiumkarbonatpartikler er et interessant felt innen naturgassproduksjon. Det uorganiske saltet kan dannes på grunn av pH-stabilisering for korrosjonskontroll i rørledningene, og i regenereringsprosessen av hydratinhibitoren monoetylglykol (MEG) på land. Kalsiumkarbonat er inverst løselig, noe som innebærer en risiko for utfelling ved høye temperaturer, for eksempel i varmevekslere, i regenereringsprosessen av MEG. Det er derfor ønskelig å felle ut ionene og separere partiklene fra MEG-sløyfen. På grunn av disse utfordringene, er undersøkelse av kalsiumkarbonatvekst anmodet.

Målet med dette arbeidet har vært å undersøke kinetikk for krystallvekst, ved å bestemme vekstorden og veksthastighetskonstanter, for kalsiumkarbonat med MEG som ko-solvent. Podede vekstforsøk ble utført for polymorfene vateritt og kalsitt ved 40 og 70 °C og med 0 – 70 vt% MEG. Antalls- og størrelsesmålinger av podepartiklene ble gjort ved bruk av Coulter Counter. Den avtagende kalsiumkonsentrasjonen ble målt ved automatisert titrering, og de tilsvarende overmetningsverdiene ble kalkulert i MultiScale, for å gi veksthastigheter for kalsiumkarbonat. Krystallene ble analysert med et elektronmikroskop (SEM) og ved pulverrøntgendiffraksjon (XRD).

Resultatene viser at vekst av vateritt og kalsitt reduseres ved økt mengde MEG. I tillegg vil en hevet temperatur fremme veksten. Ved å øke ko-solvent konsentrasjonen fra 0 – 60 vt% reduseres veksthastighetskonstanten, ved antagelse om parabolisk hastighetslov $k_{g=2}$, for vateritt, fra 1,81 til 0,24 nm/s ved 40 °C, og fra 2,12 til 0,63 nm/s ved 70 °C. Den tilsvarende reduksjonen for kalsitt ved en økt MEG-konsentrasjon fra 0 – 70 vt% er fra 0,52 til 0,02 nm/s ved 40 °C, og fra 0,95 til 0,08 nm/s ved 70 °C. Det ble konkludert at kalsitt er den tregest voksende polymorf i vann ved begge temperaturer.

En vekst av annen orden ble funnet for vateritt i vann ved 40 °C. For kalsitt var vekstordenen ved de samme betingelsene noe høyere. Det er foreslått at vekst av begge polymorfer i vann er kontrollert av integrasjon på overflaten. Vekstordenen for vateritt og kalsitt avtar ved økt MEG-konsentrasjon og temperatur, og det observeres en endring til førsteordenskinetikk. På grunn av økt viskositet forårsaket av ko-solventen er det foreslått diffusjons- eller adsorpsjonskontrollert vekst, når $g = 1$. Dette kan forklares av senket diffusiviteten av karbonat på grunn av de ikke-støkiometriske reaktantforholdene.

Table of content

| | |
|---|------------|
| Preface | i |
| Abstract | ii |
| Sammendrag | iii |
| 1 Introduction | 1 |
| 2 Theory | 3 |
| 2.1 Supersaturation | 3 |
| 2.2 Nucleation..... | 6 |
| 2.3 Crystal growth | 7 |
| 2.3.1 The adsorption-layer theories | 7 |
| 2.3.2 The diffusion-reaction theories | 7 |
| 2.3.3 Mechanisms of crystal growth | 9 |
| 2.4 Aggregation | 11 |
| 2.5 Calcium carbonate | 12 |
| 2.6 Polymorphism..... | 14 |
| 2.7 Solvent effects | 16 |
| 3 Alternative methods | 19 |
| 3.1 Determination of particle size..... | 19 |
| 3.2 Crystal growth determination | 21 |
| 4 Experimental | 23 |
| 4.1 Apparatus..... | 23 |
| 4.2 Seed preparation | 24 |
| 4.3 Seeded growth experiments..... | 25 |
| 4.4 Analysis techniques | 26 |
| 4.4.1 MultiScale | 26 |
| 4.4.2 Titration | 26 |
| 4.4.3 The Coulter-principle | 27 |
| 4.4.4 Scanning electron microscope (SEM) | 28 |
| 4.4.5 Powder X-ray diffraction (XRD) | 28 |
| 4.5 Growth calculations | 29 |
| 5 Results and discussion | 31 |
| 5.1 Seed particles | 31 |
| 5.1.1 Vaterite seed particles | 31 |
| 5.1.2 Calcite seed particles | 33 |
| 5.1.3 Comparison of vaterite and calcite seed particles | 35 |
| 5.2 Vaterite growth | 36 |

| | | |
|----------|--|--------------|
| 5.2.1 | Vaterite growth in water and MEG | 36 |
| 5.2.2 | Vaterite growth order and growth rate constants | 40 |
| 5.3 | Calcite growth..... | 44 |
| 5.3.1 | Calcite growth in water and MEG..... | 44 |
| 5.3.2 | Calcite growth order and growth rate constants | 50 |
| 5.4 | Comparison of vaterite and calcite growth | 55 |
| 5.4.1 | Growth order | 55 |
| 5.4.2 | Growth rate constants | 55 |
| 5.4.3 | Effect of MEG as solvent | 56 |
| 5.4.4 | Effect of temperature..... | 58 |
| 5.5 | Sensibility analysis and uncertainty | 59 |
| 5.5.1 | Number and volume of particles | 60 |
| 5.5.2 | Growth data | 60 |
| 6 | Conclusions | 63 |
| 7 | Further work | 65 |
| | References | 67 |
| | List of symbols | 71 |
| | List of abbreviations..... | 73 |
| | Appendix A – Chemicals..... | I |
| | Appendix B – Calculations | III |
| | B.1 Number and volume of seed particles | III |
| | B.2 Growth rates | III |
| | B.3 Supersaturation ratios | V |
| | B.4 Mother-liquids and solutions for growth experiments | VI |
| | B.4.1 Mother-liquids | VI |
| | B.4.2 Solutions | VII |
| | Appendix C – Experimental setup | IX |
| | Appendix D – Uncertainty | XIII |
| | Appendix E – Number and volume of seed particles | XV |
| | Appendix F – Additional graphs..... | XVII |
| | F.1 Vaterite growth experiments | XVII |
| | F.1 Calcite growth experiments | XVIII |
| | Appendix G – XRD scans | XXI |
| | Appendix H – Pictures of the reactor equipment..... | XXV |
| | Appendix I – Concentration of free ions for calcite growth..... | XXVII |
| | Appendix J – Risk assessment form | XXIX |

1 Introduction

Natural gas production from reservoirs along the Norwegian coast is one of the most important industries in Norway. Almost 20 % of the natural gas consumed in Europe is exported from Norway (Oljedirektoratet, 2011). Transportation of gas from the subsea production units to the processing facilities onshore faces different challenges. A potential risk of gas hydrate formation in the long carbon steel pipelines is one of them.

Gas hydrates are crystalline solid compounds of water molecules stabilized by small gas molecules in a lattice structure (Kaasa et al., 2005). The presence of liquid water and natural gas at a sufficient low temperature and a high pressure constitutes an ideal environment for gas hydrates formation. Pipelines blocked by gas hydrates are the one of the main flow assurance problem in natural gas production.

To prevent gas hydrate formation a hydrate inhibitor is used to decrease the temperature at which the gas hydrates are formed. A frequently employed chemical is monoethylene glycol, MEG (Kaasa et al., 2005), which is injected at the wellhead of the reservoir. The mixture of gas, condensate, MEG and formation water is transported to the processing plant where MEG is regenerated; returned to the seabed; and re-injected in the well stream. A process flow sheet of the MEG loop is shown in Figure 1.1.

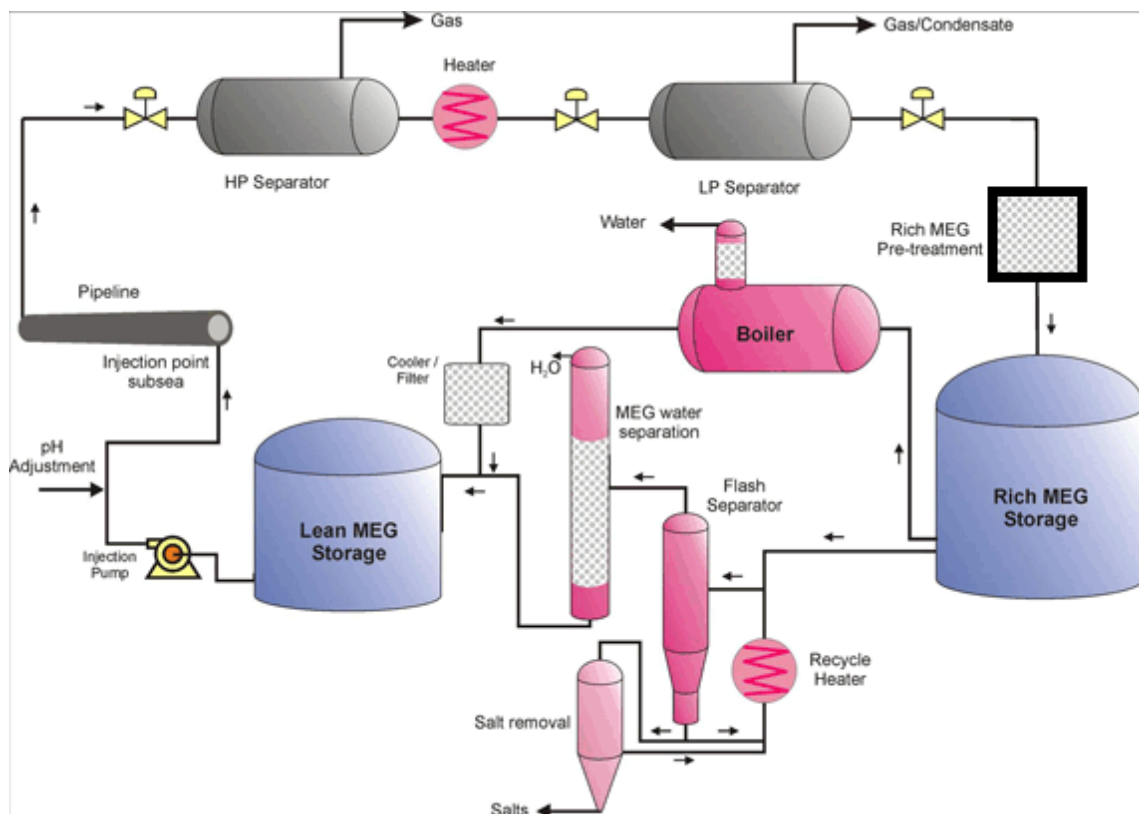


Figure 1.1: Flow sheet of the MEG loop (Institute for Energy Technology, 2011).

Another challenge in gas processing is to avoid uncontrolled precipitation of calcium carbonate, CaCO_3 . The salt is inverse soluble and may accumulate on the pipeline walls and the process equipment. Calcium ions from the formation water may form scale, a precipitated layer of solid material at a surface, in reaction with carbonate at elevated temperatures. Carbonate ions are formed from the carbon dioxide, CO_2 , in the gas. Scale inhibitors are widely used (Foss et al., 2006), but the necessity of physical removal of the ions as calcium carbonate particles through separation is crucial. Hence, crystal growth studies are necessary. A problem is to obtain large enough particles for simplification of the separation process. The formation of carbonate is favoured at high pH-levels induced by injection of sodium hydroxide, NaOH . This pH-adjustment is done to promote precipitation of FeCO_3 which is desirable as it acts as a corrosion protective layer inside the low-quality pipelines. (Olsen et al., 1999). Both the alkaline environment and the presence of MEG may affect the precipitation behaviour of CaCO_3 .

More knowledge on precipitation and growth kinetics of CaCO_3 particles in a MEG/water-system will make it possible to advance and economically improve the design and operation of the MEG regeneration process (Flaten, 2010). The objective of this project is to evaluate how different concentrations of MEG and varying temperature influence the growth of CaCO_3 . Growth order and growth rate constants will be determined. In the last decades, numerous of studies on crystal growth kinetics of CaCO_3 have been performed. Mostly, crystal growth in water has been determined, often in combination with studies on the influence on growth with various additives. Fewer kinetics studies on CaCO_3 in presence of mixed solvents have been published. Flaten (2010) directed a larger study on precipitation and growth of CaCO_3 in presence of MEG and her studies have been an important background for this work.

Calcium carbonate exhibits different crystal polymorphs. Two of them, vaterite and calcite, is studied in this work. The growth experiments are performed in batch operation seeded with vaterite and calcite particles. The crystal growth rates are measured by titration as the calcium concentration decreased during the growth. Determination of number and volume of the seeds is carried out by use of the Coulter Counter. SEM and powder XRD are used to analyse the crystal particles.

2 Theory

A solid crystal is material where the constituent parts, being molecules, atoms or ions, are arranged in repeating units in a lattice structure at locations which are characteristic of the substance (Mullin, 2001). Different substances form unique crystal systems depending on which symmetry the crystal comprises. A crystal may also form different polymorphs, meaning chemically identical substances with different crystalline forms (Mullin, 2001). For a substance to crystallize in a solution, the solution has to be supersaturated. The fundamental supersaturation may be expressed in terms of chemical potential.

2.1 Supersaturation

The fundamental driving force for crystallization is the difference in chemical potential between a substance in solution and in the crystal state expressed as

$$\Delta\mu = \mu_s - \mu_c \quad (2.1)$$

where μ_s is the chemical potential of the solution and μ_c of the crystal (Kashchiev, 2003). The definition of chemical potential, μ , can be expressed in terms of the standard potential, μ_0 , and the activity, a , as

$$\mu = \mu_0 + RT \ln a \quad (2.2)$$

where R is the gas constant and T the relative temperature. The expression of the fundamental driving force for crystallization can be written dimensionless by

$$\frac{\Delta\mu}{RT} = \ln\left(\frac{a}{a^*}\right) = \ln S \quad (2.3)$$

where a^* is the activity of a saturated solution and S is the fundamental supersaturation ratio. Calculations of the activity from experimentally found concentrations could be done from the following relation

$$a = c \cdot \gamma \quad (2.4)$$

where c is the concentration and γ is the activity coefficient. The activity coefficient denotes the influence of additional ions in the system, meaning that $a = c$ at infinite dilution (Mullin, 2001). The activity coefficient is given from the Debye-Hückel theory of electrolytes as

$$\log \gamma_{\pm} = -A |z_+ z_-| I^{1/2} \quad (2.5)$$

where A is the Debye-Hückel constant, z_+ and z_- are the valencies (charge) of the cation and anion, respectively. I is the ionic strength defined by

$$I = \frac{1}{2} \sum c_i z_i^2 \quad (2.6)$$

where c_i is the concentration in mol/L and z_i the valency, of the i^{th} ionic species. When the solution is not infinitely diluted it is more accurate to use activity instead of concentration in calculations of supersaturation.

The mean ionic activity, a_{\pm} , defined in equation (2.7), is appropriate to use for electrolyte solutions.

$$a = a_{\pm}^{\nu} \quad (2.7)$$

where $\nu = \nu_+ + \nu_-$ is the number of moles of ions, cations and anions respectively, in one mole of the solute. Equation (2.3) may therefore be rewritten as

$$\frac{\Delta\mu}{RT} = \nu \ln S_a \quad (2.8)$$

where $S_a = a_{\pm} / a_{\pm}^*$. The supersaturation could also be expressed as relative supersaturation:

$$\sigma_a = S_a - 1 \quad (2.9)$$

and the equation (2.8) is rewritten as

$$\frac{\Delta\mu}{RT} = \nu \ln(1 + \sigma_a) \quad (2.10)$$

The ionic activity product, IAP , is defined

$$IAP = (a_+)^{\nu_+} (a_-)^{\nu_-} \quad (2.11)$$

where a_+ and a_- are the ionic activities for the cation and the anion respectively. The activity product at equilibrium is called the solubility product, K_{sp} . The supersaturation could be expressed like

$$S_a = \left(\frac{(a_+)^{\nu_+} \cdot (a_-)^{\nu_-}}{K_{sp}} \right)^{\frac{1}{\nu}} = \left(\frac{IAP}{K_{sp}} \right)^{\frac{1}{\nu}} \quad (2.12)$$

Another definition for supersaturation is the saturation ratio, SR , which is related to the supersaturation ratio by

$$S = \sqrt{SR} \quad (2.13)$$

According to previous studies (Sandengen, 2006) the following relations are valid:

$SR < 1$: The solution is undersaturated.

$SR = 1$: At equilibrium. The solution is saturated.

$SR > 1$: The solution is supersaturated.

The solution is undersaturated in the stable region showed in Figure 2.1. There is no thermodynamic driving force for crystallization. Hence, dissolution takes place if solid particles are present. Through heating or evaporation, following the horizontal or vertical arrows respectively from A, it is possible to move into the metastable region and subsequently to the labile region. Crossing the line intersecting D and B, the solubility curve, the metastable region is reached where the solution is supersaturated. Spontaneous crystallization is unlikely to happen unless seed particles of the same compound as the solute are introduced to the system. When entering the labile region after crossing the supersolubility curve the solution is supersaturated and crystallization of the salt is probable. In addition to heating and evaporation, crystallization may occur by a chemical reaction. In reaction crystallization, also named precipitation, supersaturation is achieved by a chemical reaction between two solutions (Mersmann, 2001). Reaction crystallization is a good way to study growth, and this method has been used in this work.

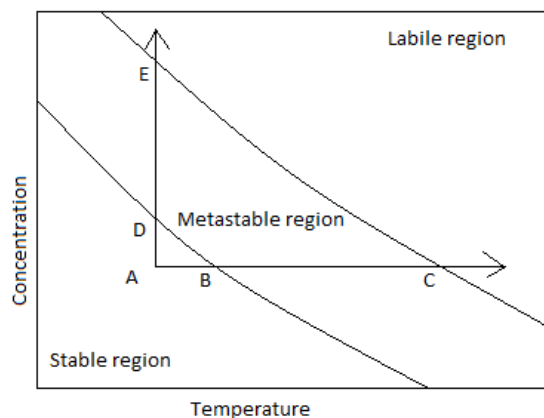


Figure 2.1: Concentration vs. temperature for an inverse soluble compound.

2.2 Nucleation

Nucleation is the formation of crystals when the solute precipitates, and may occur in a supersaturated solution. This phenomenon could happen spontaneously or be induced by an external force. Nucleation changes the number of particles in the system. A classification of different types of nucleation is shown in Figure 2.2.

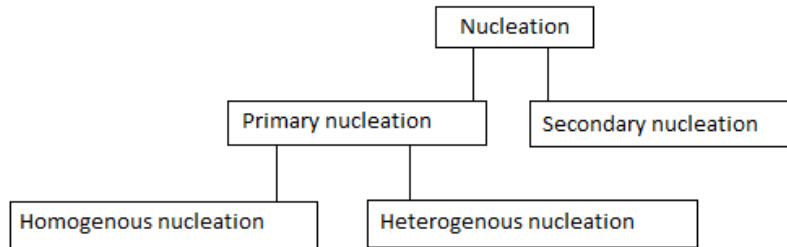


Figure 2.2: Classification of nucleation. The illustration is based on Mullin (2001).

A higher level of supersaturation is required for primary nucleation than for secondary nucleation, meaning that primary nucleation only happens in the labile region in Figure 2.1. Secondary nucleation may take place in the metastable region, with a lower level of supersaturation.

Formation of a solid phase caused by primary homogenous nucleation takes place spontaneously from a clear solution where the system has to create a surface to grow on itself. For a nucleus to be formed the constituent molecules have to coagulate, counteract re-dissolution and arrange themselves into a permanent lattice system. This process requires an energy barrier to be overcome and a high level of supersaturation (Ohtaki, 1998). The overall excess free energy, ΔG , between a small particle of solute and the solute in solution constitutes the basis for calculation of the rate of nucleation, J . ΔG is expressed like $\Delta G = \Delta G_s + \Delta G_v$. The term ΔG_s is a positive quantity expressing the difference in free energy between the crystal surface and the bulk. ΔG_v is negative, representing the difference between an infinite large particle and the solute in solution (Mullin, 2001). The nucleation rate is dependent on temperature, T , supersaturation ratio, S , and interfacial tension, γ , and could be expressed by the following equation

$$J = A' \cdot \exp\left(-\frac{16\pi\gamma^3 v^2}{3k^3 T^3 (\ln S)^2}\right) \quad (2.14)$$

where A' is a pre-exponential factor, k is the Boltzmann constant and v is the molecular volume (Mullin, 2001). J increases rapidly as the supersaturation is elevated.

When the nucleation is primary heterogeneous the surface for the ions to grow on is already present. This could be a foreign particle like an impurity. This nucleation process is more common and easier to achieve, due to that a lower overall excess free energy level is required

than the homogenous nucleation (Mullin, 2001). Hence, primary heterogeneous nucleation may occur at lower supersaturation ratios.

Secondary nucleation may occur when crystalline particles of the same compound as the solute, so-called seeds, are present in a supersaturated solution. The particles move around in the vessel, colliding with each other, the vessel walls and with the agitator. Contact between the particles and the agitator blades is the most important cause for secondary nucleation. When the particles collide, small fragments are abraded and new particles are created. When growth is studied by seeded experiments, nucleation is unwanted. If crystals still nucleate in this situation, the nucleation is classified as secondary, and a possible cause is a too high supersaturation.

2.3 Crystal growth

In a supersaturated solution a crystal initiates growing immediately after a stable nucleus is formed. The nucleus must be larger than a certain critical size to grow instead of being re-dissolved. Different theories of crystal growth have been suggested (Mullin, 2001). The adsorption-layer theories and the diffusion-reaction theories will be discussed below.

Generally, the crystal growth rate, G , could be written as a change of characteristic dimension, dL , divided by a change in reaction time, dt . G could also be expressed as function of relative supersaturation, $\sigma = S - 1$, and the following definition applies

$$G = \frac{dL}{dt} = k_g (S - 1)^g \quad (2.15)$$

where k_g is the growth rate constant and g is the growth order.

2.3.1 The adsorption-layer theories

The adsorption-layer theory, first proposed by Volmer, implies that the constituent ions are adsorbed on the particle surface layer by layer in a discontinuous process (Mullin, 2001). When a crystal grows, the solute ions are transported to the solid-liquid interface where they are free to move along the surface, and assemble into the crystal lattice at an energy-favoured spot, an 'active centre', having the greatest attractive forces. The growth will persist until the whole plane is completed. For the growth to continue, a new 'centre of crystallization' must be formed. There exist different mechanisms for this process as described in Chapter 2.3.3.

2.3.2 The diffusion-reaction theories

The diffusion-reaction theory indicates that the growth rate is proportional to the concentration difference between the point of deposition and the bulk of the solution as shown in Figure 2.3.

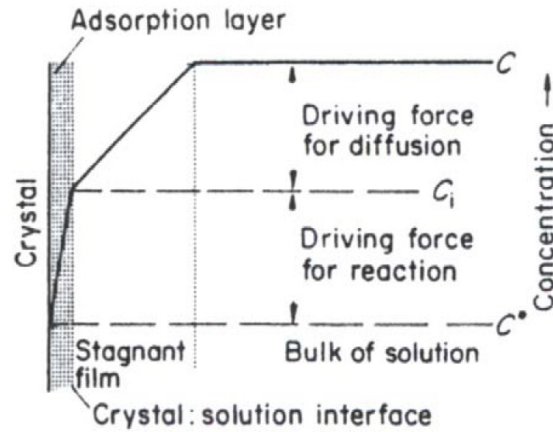


Figure 2.3: The diffusion-reaction model (Mullin, 2001).

The concept was originally an idea of Noyes and Whitney, but different modifications have been suggested later. Berthoud and Valetton stated that the crystal growth process comprises two steps; initially a diffusion step where the constituent ions are transported to the crystal surface; and thereafter a reaction step where the ions are organizing themselves into the crystal lattice. The two steps can be described by the following equations (Mullin, 2001); for diffusion

$$\frac{dm}{dt} = k_d A (c - c_i) \quad (2.16)$$

and for reaction

$$\frac{dm}{dt} = k_r A (c_i - c^*)^r \quad (2.17)$$

where m is the mass of solid deposited at the surface during the time t ; k_d is the mass transfer coefficient for diffusion; k_r is the surface reaction rate constant; A is the surface area of the crystal; c is the solute concentration in the supersaturated solution; c_i is the solute concentration in the solution at the solid-liquid interface; c^* is the equilibrium saturation concentration; and r is the reaction order.

By eliminating c_i and combining the equations (2.16) and (2.17), an equation expressing the ‘overall’ concentration driving force, $c - c^*$, could be written as

$$\frac{dm}{dt} = K_G A (c - c^*)^g \quad (2.18)$$

where K_G is the overall crystal growth coefficient.

Both steps in the diffusion-reaction model could be rate-determining. If the surface reaction is fast, the crystallization is controlled by diffusion. Otherwise, if the ions diffuse rapidly from the bulk to the surface, the reaction is rate determining.

2.3.3 Mechanisms of crystal growth

Different growth mechanisms could be classified for crystal growth according to their rate laws (Nielsen, 1984). Three kinetic models are proposed in literature named exponential, parabolic and linear rate law. The three rate laws could be explained by the following rate-determining mechanisms: Surface nucleation, spiral growth and rough growth, respectively. As mentioned above, the growth units will assemble in the crystal lattice at active centres, also called kinks, and when a plane is entirely filled a new ‘centre of crystallization’ must be created.

A mechanism for creating a crystallization centre is called two-dimensional, 2D, surface nucleation. A relatively high level of supersaturation in the solution is required, but when the first 2D nucleus is formed, new kinks are available for further growth. The nucleation may occur at the edges, corners and on the faces of the crystal surface as shown in Figure 2.4. Three possible growth models, all based on 2D surface nucleation, are described in literature (Sunagawa, 2005). They are the ‘birth and spread’, B+S, model; the ‘nuclei on nuclei’, NON, model; and the ‘polynuclear’, PN, growth model. The crystal surface may be smooth or rough depending on level of supersaturation. A higher level promotes a high nucleation rate causing a rough surface, while lower levels favour the growth rate and the surface becomes smooth.

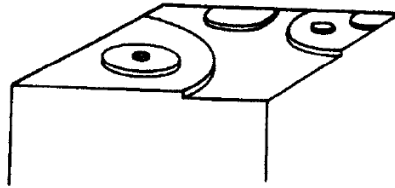


Figure 2.4: 2D surface nucleation (Mullin, 2001).

The crystal growth rate of 2D surface nucleation is exponential with a growth order, $g > 2$ and could be expressed as

$$G = k_1 S^{7/6} (S - 1)^{2/3} \ln(S)^{1/6} \exp\left(\frac{-K}{\ln S}\right) \quad (2.19)$$

where k_1 is the growth rate constant; and S is the supersaturation ratio (Flaten et al., 2010a). The growth order for PN growth is larger than for B+S growth, as seen from its steeper curve in Figure 2.6.

It is stated that many crystals grow rather fast at a relatively low degree of supersaturation, lower than the supersaturation required for 2D surface nucleation (Mullin, 2001). In this case the kinks appear from imperfections at the crystal surface. All real crystals reveal imperfections (Davey, 1982). One type of imperfection is the screw dislocation. This is formed when the atoms are not aligned at right angles, instead being displaced along a dislocation line (Mullin, 2001). Active centres are located along the screw dislocation allowing the crystal to grow in a spiral fashion as shown in Figure 2.5. Since active centres

always are present, the growth continuously follows the spiral pattern, and surface nucleation is not needed. The screw dislocation or spiral growth mechanism is also called BCF after Burton, Cabrera and Frank (Mersmann, 2001).

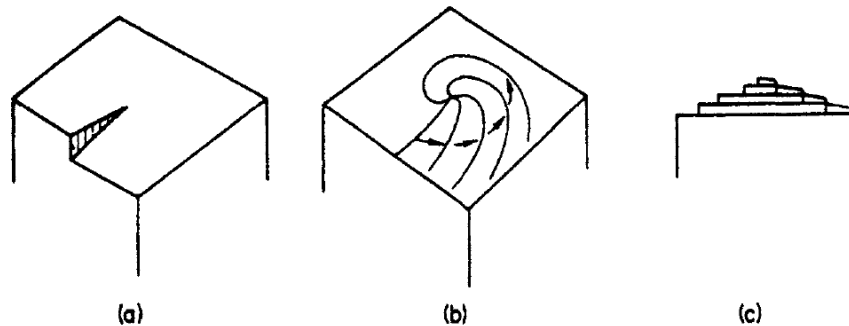


Figure 2.5: Screw dislocation, (a). Spiral growth, (b)-(c) (Mullin, 2001).

The spiral growth could be expressed with $g = 2$, like (Flaten et al., 2010a)

$$G = k_2(S-1)^2 \quad (2.20)$$

The rate determining step when $g = 2$ could be surface diffusion, integration or local diffusion at the kinks (Nielsen, 1984). The surface diffusion is the step where the growth unit reaches the crystal surface and diffuses onto the surface to find an energy favoured position (Sunagawa, 2005). The integration is the jump when the growth unit is brought into the kink. In this step the growth unit must be dissociated from its solvent compound in a desolvation or dehydration process. At very low supersaturations it should be considered that the rate controlling step could be linked to individual kinks and their separated diffusion fields (Nielsen, 1984).

The parabolic expression is valid for low supersaturation levels. At high levels of supersaturation the constituent ions attach over the entire surfaces and a rough crystal surface develops. This rough growth is diffusion limited since the surface reaction is fast. The transportation of constituent ions from the bulk to the crystal is slow. The growth rate is linear, $g = 1$ and could be expressed (Flaten et al., 2010a) by

$$G = k_3(S-1) \quad (2.21)$$

According to Nielsen (1984), the growth rate could also be determined by adsorption when $g = 1$. The term adsorption means here transition of ions from the bulk to the adsorption layer around the crystal. The linear rate law is valid for both diffusion and for adsorption.

Growth rate as a function of supersaturation ratio is showed in Figure 2.6. In principle, the overall growth rate follows the scheme illustrated by the black bold line (Mersmann, 2001).

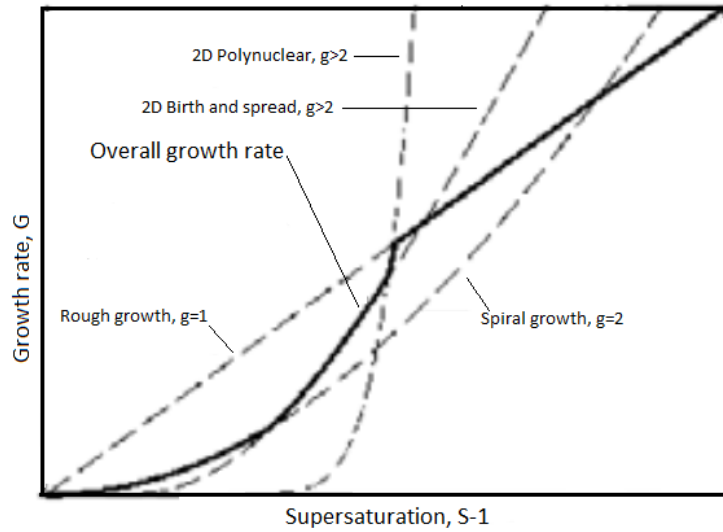


Figure 2.6: Crystal growth mechanisms. The figure is designed on the basis of Mersmann (2001).

There are several methods for determination of growth rates and evaluation of which mechanism the growth follows. One technique, done by seeded batch experiments, is to measure the depleting concentration of constituent ions and then calculate the increased volume of a particle as shown by

$$\Delta V = \frac{-\Delta c \cdot M_w}{\rho \cdot N} \quad (2.22)$$

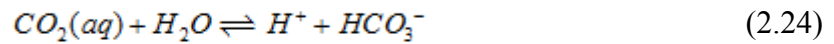
where M_w is the molecular weight and ρ is the density of the crystal. The number of seed molecules, N , must be determined (Flaten et al., 2010a). The increased volume could be related to the characteristic dimension, L , of the crystal, and subsequently the growth rate could be expressed as in equation (2.15). For further determination of growth order, g , and growth rate constants, k_g , various plots of G and S should be designed and evaluated. This is examined in more detail in Chapter 4.5.

2.4 Aggregation

Besides growing in the supersaturated solution, nucleated crystal particles tend to cluster together causing a decline of the total number of particles in the suspension. However, the volume of the particles is still the same. If the clustered particles are small enough so the van der Waals forces are larger than the gravitational forces, they may permanently stick together and grow collectively (Mullin, 2001). This phenomenon is often called aggregation although other terms as ‘agglomeration’, ‘coagulation’ and ‘flocculation’ are widely used. The shape of the aggregate crystal will change when two or more particles grow together. Aggregation could be a source of uncertainty in seeded growth experiments.

2.5 Calcium carbonate

Calcium carbonate differs from other known inorganic salts since it is inverse soluble. This means that when the temperature increases, the solubility decreases leading to precipitation at elevated temperatures. CaCO_3 is also classified as a sparingly soluble salt and may be formed after the following equilibrium equations, (2.23) - (2.26):



In growth studies of CaCO_3 two methods of setting the experimental conditions have been employed (Ohtaki, 1998). The first is to use gaseous CO_2 as the carbonate source, and equilibrate the carbonate ions in a NaOH solution with CO_2 gas. This gives low pH-experiments (~ 7). The other is by using bicarbonate from for instance sodium carbonate, Na_2CO_3 , as the carbonate source, giving a high pH of ~ 10 . The former method is used in the growth experiments in this work. The two aqueous solutions that are mixed are NaOH and calcium chloride, CaCl_2 . Both solutions are bubbled with gaseous CO_2 to reach a stable pH of approximately 7 (Olderøy et al., 2009).

The log-log diagram in Figure 2.7 shows the concentration for various carbonate species as a function of pH. If the pH is increased the activity of carbonate does the same. This could also be seen in the equilibrium equations (2.24) - (2.25). The initial pH of the present growth experiments is ~ 7 , marked with the red line, and the distribution of carbonate species at this pH could be seen in Figure 2.7.

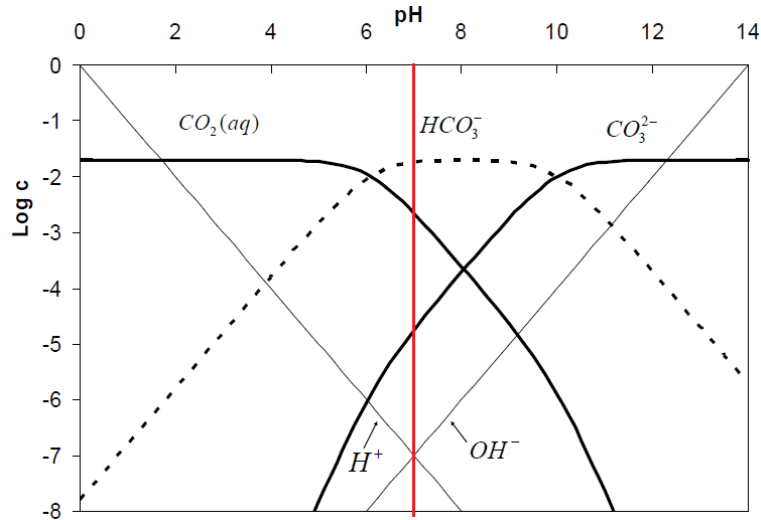


Figure 2.7: Logarithm of concentration of carbonic acid (H_2CO_3), bicarbonate (HCO_3^-) and carbonate (CO_3^{2-}) as a function of pH. The figure is designed on the basis of Sandengen (2006) and Flaten (2010). The red line indicates pH 7.

The supersaturation ratio for calcium carbonate could be written from equation (2.12) as

$$S_{\text{CaCO}_3} = \left(\frac{a_{\text{Ca}^{2+}} \cdot a_{\text{CO}_3^{2-}}}{K_{sp}(\text{CaCO}_3)} \right)^{\frac{1}{2}} \quad (2.27)$$

With the aim of calculating concentrations of NaOH needed to obtain a sufficient level of initial supersaturation the alkalinity of the system must be known. Alkalinity could be defined as the sum of all titratable bases (Sandengen, 2006). Alkalinity could also be described as the system's ability to resist a change in pH when different species are added. From the electro neutrality equation of the calcium carbonate system an expression for alkalinity could be made. By summing positive and negative ions on each side, the electro neutrality equation could be expressed in terms of molality, m , like

$$2 \cdot m_{\text{Ca}^{2+}} + m_{\text{CaHCO}_3^+} + m_{\text{Na}^+} + m_{\text{H}^+} = 2 \cdot m_{\text{CO}_3^{2-}} + m_{\text{HCO}_3^-} + m_{\text{OH}^-} + m_{\text{Cl}^-} \quad (2.28)$$

Calcium is not only present as free ions, but also bound in complexes. The total amount of calcium could therefore be expressed as

$$m_{\text{Ca,tot}} = m_{\text{Ca}^{2+}} + m_{\text{CaHCO}_3^+} + m_{\text{CaCO}_3^0} \quad (2.29)$$

Equation (2.29) could be rearranged, expressed by $m_{\text{Ca}^{2+}}$, and inserted in equation (2.28). Then, by arranging pH-independent and pH-dependent species on the left and right hand side, respectively, one obtains:

$$2 \cdot m_{Ca,tot} + m_{Na^+} - m_{Cl^-} = 2 \cdot m_{CO_3^{2-}} + m_{HCO_3^-} + m_{CaHCO_3^+} + 2 \cdot m_{CaCO_3^0} + m_{OH^-} - m_{H^+} \quad (2.30)$$

By eliminating species that do not affect the pH, the expression for alkalinity is obtained from the right side of equation (2.30):

$$A_T = 2 \cdot m_{CO_3^{2-}} + m_{HCO_3^-} + m_{CaHCO_3^+} + 2 \cdot m_{CaCO_3^0} + m_{OH^-} - m_{H^+} \quad (2.31)$$

In the case where the solutions are bubbled with CO₂ gas, as mentioned above, all initial alkalinity comes from addition of NaOH and equation (2.31) could be reduced to

$$A_T = m_{OH^-} \quad (2.32)$$

As soon as the growth is initiated the alkalinity is expressed all species in equation (2.31) will be present.

2.6 Polymorphism

Polymorphism is the ability a substance has to crystallize into different crystal structures that are chemically identical. Polymorphs of a particular crystal have different physical properties (Mullin, 2001). Calcium carbonate exhibits different polymorphs. Three of them are illustrated in Figure 2.8; vaterite, aragonite and calcite, here ordered after increasing stability. The most stable polymorph has the lowest solubility. Vaterite and aragonite are regarded as metastable polymorphs. Vaterite is polycrystalline and forms spherical particles in a hexagonal crystal system. Aragonite tends to form particles with the shape of needles in an orthorhombic symmetry system. Calcite particles are often cube-shaped and structured into a trigonal-rhombohedral crystal lattice (Flaten et al., 2010a). The cube shape of calcite could differ somewhat due to the preparation method. By varying the temperature spherulitic calcite or aggregated cubes of calcite with smooth surfaces could be made. The latter was used in this work as showed in Figure 2.8. Both aragonite and calcite are mono-crystalline. Amorphous calcium carbonate, ACC, is another solid phase of calcium carbonate, also this one is metastable.

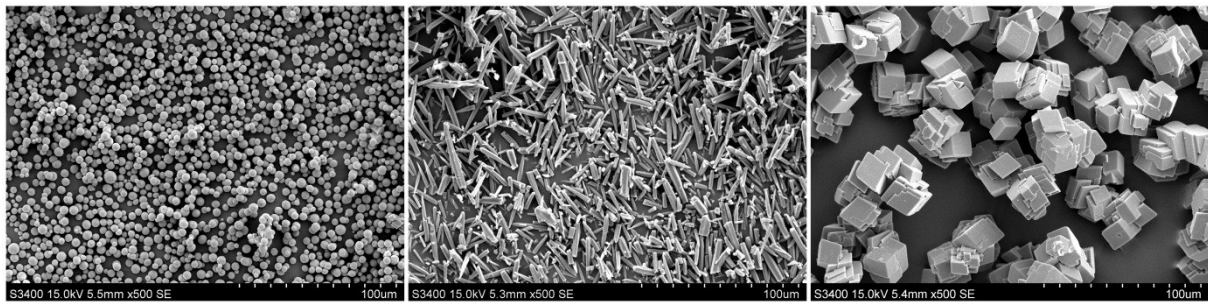


Figure 2.8: Polymorphs of CaCO₃. Vaterite (left), aragonite (middle) (Barland, 2012) and calcite (right). The scale bar is 100 μm.

Generally, if the IAP of a solution exceeds $K_{sp,ACC}$, ACC will precipitate spontaneously before transformation to a more stable polymorph takes place. The growth rate of the more stable polymorph is rate determining for the transformation process (Andreassen, 2001). Transformation into a more stable polymorph occurs through dissolution and re-precipitation over time. The polymorph that will form depends on temperature and level of supersaturation. The temperature dependency of the different polymorphs at a given initial supersaturation is shown in Figure 2.9.

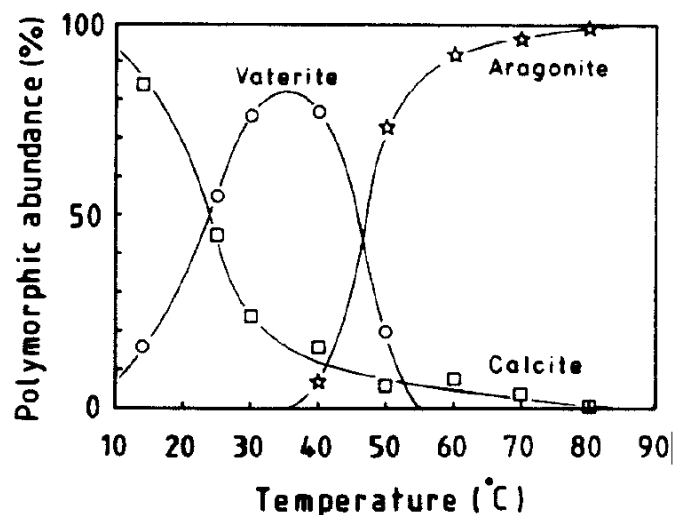


Figure 2.9: Polymorphic abundance as a function of temperature at a specific initial supersaturation (Ogino et al., 1987).

The solubility products for the three polymorphs could be determined by the following equations (Plummer and Busenberg, 1982) and is shown in Figure 2.10. Temperatures are in Kelvin.

$$\log K_{sp,cal} = -171.9065 - 0.077993 \cdot T + \frac{2839.319}{T} + 71.595 \log T \quad (2.33)$$

$$\log K_{sp,arag} = -171.9773 - 0.077993 \cdot T + \frac{2903.293}{T} + 71.595 \log T \quad (2.34)$$

$$\log K_{sp,vat} = -172.1295 - 0.077993 \cdot T + \frac{3074.688}{T} + 71.595 \log T \quad (2.35)$$

Vaterite is the most soluble but the least stable polymorph, whereas calcite is least soluble and most stable. Solubility products for ACC are also shown in Figure 2.10. In literature, two different theories are proposed (Clarkson et al., 1992) and (Brečević and Nielsen, 1989) as shown below. The temperatures, T , in equation (2.36) and (2.37) are in Kelvin and Celsius respectively.

$$\log K_{sp,ACC,Clarkson} = \frac{1247}{T} - 10.224 \quad (2.36)$$

$$\log K_{sp,ACC,Brečević} = -6.1987 + 0.005336 \cdot T + 0.0001096 \cdot T^2 \quad (2.37)$$

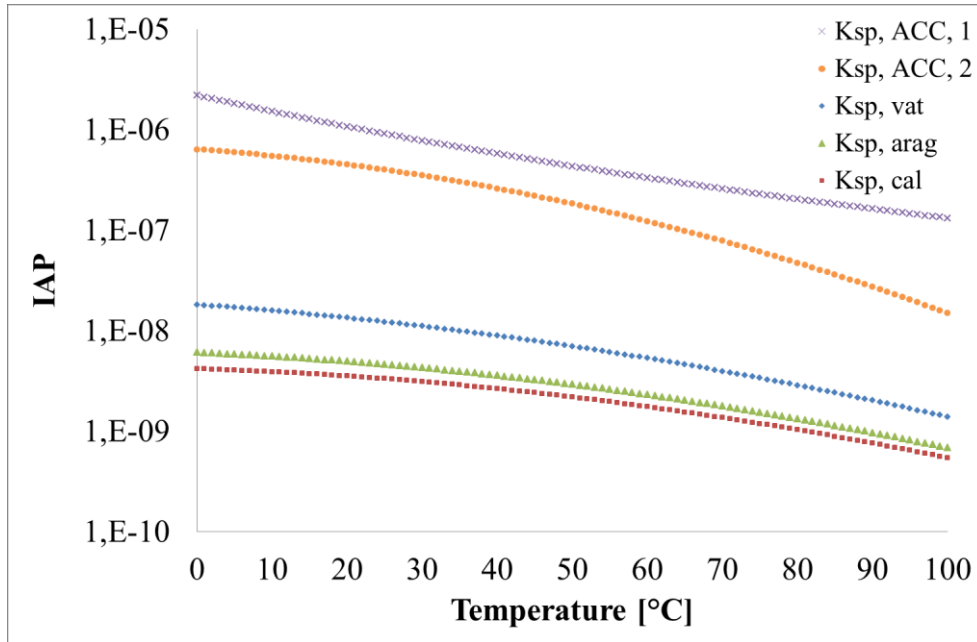


Figure 2.10: IAP as a function of temperature for the ACC, vaterite, aragonite and calcite. The y-axis is logarithmic. $K_{sp, \text{vat}}$, $K_{sp, \text{arag}}$ and $K_{sp, \text{cal}}$ from Plummer and Busenberg (1982), $K_{sp, \text{ACC}, 1}$ from Clarkson et al. (1992) and $K_{sp, \text{ACC}, 2}$ from Brečević and Nielsen (1989).

The relation between the supersaturation for the different polymorphs, exemplified with vaterite and calcite, could be expressed by

$$S_{\text{vat}} = S_{\text{cal}} \cdot \sqrt{\frac{K_{sp, \text{cal}}(T)}{K_{sp, \text{vat}}(T)}} \quad (2.38)$$

2.7 Solvent effects

According to Flaten (2010) both the thermodynamics and the kinetics of the system may change when a co-solvent is added. Consistent with equation (2.15), the growth rate, G , is a function of supersaturation, S . However, the physical parameters of a given system will also affect the growth rate (Söhnel and Garside, 1992). These parameters are for example solubility, surface roughness, α , viscosity, μ , and interfacial tension, γ . A co-solvent like monoethylene glycol, MEG, could change these parameters.

Introduction of MEG as co-solvent in a calcium carbonate system, will cause a change in the solubility (Kaasa et al., 2005). Solubility is an important factor in relation to supersaturation. According to equation (2.12), there is a direct relation between supersaturation and the solubility product of a salt. A change in solubility will thus vary the supersaturation which again will influence the growth. Kaasa et al. (2005) reported a reduced solubility of calcite when the mole fraction MEG rises as illustrated in Figure 2.11. Flaten (2010) indicates that the same trend applies to vaterite and aragonite as well. It is emphasized that the solubility product, K_{sp} , could be based on either activities or concentrations of the ions. Furthermore,

MEG is only influencing the concentration based solubility, and not the activity based. The solubility described by Kaasa et al. (2005) is based on concentrations.

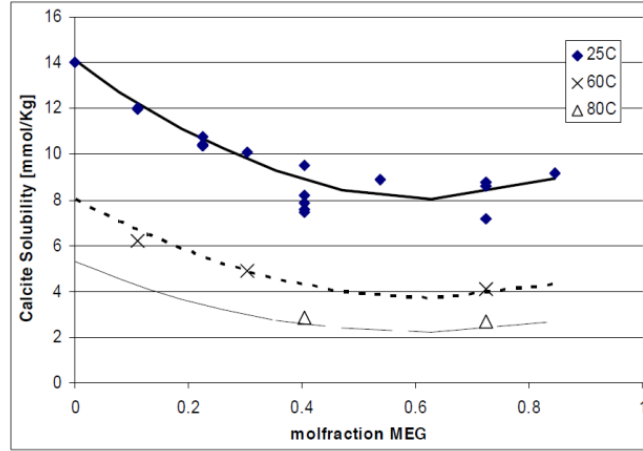


Figure 2.11: Solubility of calcite as a function of mole fraction MEG in 0.5 M NaCl at temperatures between 25 and 80 °C. The lines represent thermodynamic models and the points represent experimental data (Kaasa et al., 2005).

Another parameter that is influenced by the solvent is the surface roughness. The surface roughness is expressed by the roughness factor, α , also called alpha factor, and could be defined as

$$\alpha = \frac{\xi \cdot \Delta H}{kT} \quad (2.39)$$

where ξ is an anisotropy factor related to the bonding energies in the crystal surface layers, ΔH is the enthalpy of fusion, k is the Boltzmann constant and T the temperature (Mullin, 2001). The roughness factor is linked to solubility. As the solubility decreases, with a higher MEG concentration, the α -factor will increase. This implies a smooth crystal surface and a growth controlled by integration. In contrast, when the solubility increases, a rough crystal surface develops and the growth is diffusion controlled. In this work, α -factors have not been investigated.

The viscosity of the supersaturated solution has an impact on crystal growth due to its influence on diffusion. In accordance with Davey (1982), at a given temperature, if the viscosity of the solution increases, the diffusivity coefficient reduces. This means that the diffusion or transport of growth units gets slower and could be rate determining for the growth. The viscosity of aqueous solutions of MEG rises by increased mole fraction of MEG, and for pure MEG the viscosity reduces by elevated temperature (Hayduk and Malik, 1971) as shown in Figure 2.12.

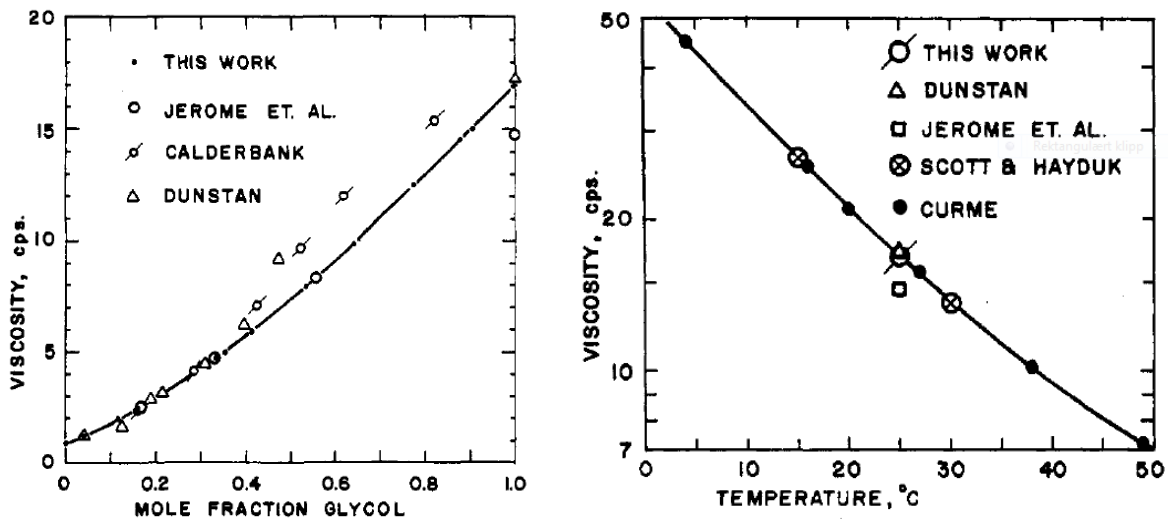


Figure 2.12: Viscosity of aqueous ethylene glycol at 25 °C as a function of mole fraction (left) and viscosity of pure ethylene glycol as a function of temperatures between 0 and 50 °C (Hayduk and Malik, 1971).

The interfacial tension, γ , between the surface of a crystalline particle and the solution is an important parameter in nucleation and growth processes (Mullin, 2001). Interfacial tension is also called surface energy and is defined as the increase in the free energy of the system per unit of surface area produced (Davey, 1982). The parameter is strongly related to the interactions between the crystal and the solvent (Ålander and Rasmuson, 2007).

3 Alternative methods

A literature review on alternative methods for determination of particle size and crystal growth were performed as a part of the specialization project fall 2011. The review is given in the following subsections.

3.1 Determination of particle size

Throughout all experiments in this work the Coulter Counter method for determination of seed particle size was used. Alternatively, as accomplished by Kralj et al. (1990), the crystal particles could have been manually counted under a microscope (Olympus model AHBT optical microscope). Differing from the experiments in this work, the researchers did not use seeds in the experiments, but counted the nucleated particles in the solution. The microscope counting was done by use of a blood cell counting chamber, a hemocytometer.

This method was originally used for determination of blood cell concentration, but could also be used for counting other substances in a suspension. The average volume of the crystals is calculated by dividing total volume of particles by the counted number of particles. Volume of particles is determined from the density and mass of precipitate, where the mass being calculated from the difference between initial and final concentrations found by pH-measurements during the growth (Kralj et al., 1990). It could be argued that unseeded experiments for crystal growth determination are unsuitable. When employing seeds the crystal surface is well-defined with known area and morphology (Kazmierczak et al., 1982). This is necessarily not known, or could vary, during unseeded growth experiments.

It could be claimed that vision-based counting is less reliable than counting with an instrument like the Coulter Counter. However, the Coulter Counter may register an aggregate of particles as one particle, thus giving a slightly wrong result. In addition, the Coulter Counter does not evaluate the shape of the crystals counted, always assuming spherical particles. When cubic calcite particles are present, this is not detected. When determining particles manually by a hemocytometer the crystals with a shape deviating from spherical will be identified. On the other hand, SEM images could also reveal crystal shape. The hemocytometer method is anyhow more time-consuming and less efficient than the Coulter Counter method; hence the latter method is preferred.

Another method for size determination of particles, employed by Njegić-Džakula et al. (2009), is the multiple BET method, after Brunauer, Emmett and Teller. This technique defines the specific surface area of the crystal, A_s , by use of nitrogen gas adsorbing on the particle surface. The specific surface area is determined by the volume of a monomolecular layer of nitrogen, V_m , when the specific surface area of the gas, A_{sp} , is known (Mørk, 2004). V_m is calculated from the BET-equation:

$$\frac{P}{V(P_0 - P)} = \frac{1}{V_m \cdot C} + \frac{(C-1)}{V_m \cdot C} \cdot \frac{P}{P_0} \quad (3.1)$$

where P and P_0 is vapour pressure and saturation pressure, respectively, for nitrogen, and C is a constant given for the specific system. V_m is obtained by evaluating the slope, $(C-1)/V_m \cdot C$, and the intersection with the y-axis, $1/ V_m \cdot C$, from a plot of $P/V(P_0-P)$ versus P/P_0 . An advantage with use of nitrogen as the adsorbate is that the value of C is high resulting in a sharper break of the adsorption isotherm. This makes it easier to determine the border between monomolecular and polymolecular layers of nitrogen.

The specific area, A_s , of the crystal is determined from

$$A_s = \frac{\rho V_m}{Mw} \cdot \frac{A_{sp}}{m} \cdot N_A \quad (3.2)$$

where ρ and Mw is the density and the molecular weight, respectively, for nitrogen. m is the mass of the crystal sample and N_A is the Avogadro constant (Mørk, 2004).

The researchers studied crystal growth of calcite and used calcite seed crystals in their experiments. The BET method for surface determination requires a weighed amount of dried particles. Hence, calcium and carbonate containing solutions were mixed, stirred for five hours, aged for three days and later filtered. The crystals were rinsed with water to eliminate any remaining chloride ions and subsequently resuspended in deionized water before putting them aside for ageing. After five months, the suspension was filtered and dried, and the seed particles could be used for the growth experiment (Njegić-Džakula et al., 2009).

The preparation of seeds as described by Njegić-Džakula et al. (2009) is circumstantial due to long-term ageing. Scheduling of the experiments has to be done a long time in advance. Possibly, a larger amount of seeds could be prepared and stored for future experiments. The BET technique has been criticized by specialists who think that the method frequently gives misleading information (Mullin, 2001). While particles investigated by the Coulter Counter are gently dispersed in a liquid, the BET method requires dried particles with a potential risk of particle damage and distortion resulted by the filtrating, washing and drying processes.

Njegić-Džakula et al. (2009) determined the growth rate from depletion of calcium concentration divided by time, which also could be expressed in terms of supersaturation by

$$G = \frac{\Delta c_{Ca^{2+}}}{\Delta t} = k_n A_s (S-1)^n \quad (3.3)$$

Specific surface area of the precipitated crystals could be denoted as $A_s = f \cdot V_p^{2/3}$ where V_p is the volume of precipitate; $V_p = c_{ppt} \cdot V_{m,p}$ and f is an expression for the volume and surface

shape factors, $f = \beta \cdot \alpha^{2/3}$. $V_{m,p}$ is the specific molar volume and c_{ppt} is the precipitated calcium concentration.

The growth rate equation could then be rewritten as

$$G = K \cdot f \cdot (c_{ppt} V_{m,p}) \cdot (S-1)^n = k_n \cdot c_{ppt}^{2/3} \cdot (S-1)^n \quad (3.4)$$

where K and k_n are the crystal growth rate constants. The calcite seed particles prepared by the above described technique are illustrated in a paper by Njegić-Džakula et al. (2009). Compared to other pictures of calcite (Beck and Andreassen, 2010) the calcite particles of Njegić-Džakula et al. (2009) appear like aggregates of many particles with different sizes without any well-defined surface area. It seems that surface area determination of the particles will give different results for each experiment, since there is a possible variation of surface area relative to amount of seed particles weighed out.

Njegić-Džakula et al. (2009) state that they used a moderately supersaturated calcium concentration solution in the growth experiment to avoid nucleation. From the pictures of the grown calcite particles it emerges that nucleation has occurred. This was tried avoided, but if it has any effect on the growth kinetics results is uncertain.

3.2 Crystal growth determination

This project work was carried out with batch experiments. Alternatively, the experiment could have been operated continuously with a constant concentration of the solution. Kazmierczak et al. (1982) performed calcium carbonate growth experiments with use of this method.

The aim is to maintain a constant level of supersaturation throughout the growth experiment. This is achieved by continuously measurements of pH in the solution; and controlled simultaneously addition, by automatic burettes, of a calcium chloride; and a mixture of sodium carbonate and bicarbonate. The purpose of the two titrants is to replace calcium and carbonate, respectively, when the ions are consumed during the growth. The ionic strength is kept constant by adding potassium chloride.

When the level of supersaturation is held steady throughout the run, extensive data for one value of the growth rate, G , is obtained since G is a function of supersaturation. This method is more comprehensive, thus providing better statistics. When the growth rate is studied in a batch operation the supersaturation decreases, thus giving many values of G .

An advantage with the constant composition method is that through several measurements at each level of supersaturation, more accurate data is obtained. The solution concentration should then be changed between parallel experiments to achieve values of G for different level of supersaturation. Additionally, the method allows for a higher level of supersaturation

compared to the batch method (Flaten, 2010). For growth mechanism studies the constant composition method is convenient. Furthermore, the technique is appropriate for investigation of secondary nucleation and influence of foreign ions (Kazmierczak et al., 1982).

A challenge with the constant composition method is the sensitivity the system experiences according to CO_2 in the atmosphere. There is a risk for interaction between the solution and CO_2 in the gas phase above the solution in the reactor according to the equations (2.23) and (2.24). When the growth is monitored by pH-measurements, the fact that there is CO_2 in the gas phase could decrease the pH of the solution and therefore disturb the measurements. To counteract this disturbance the gas space in the crystallization vessel is kept to a minimum. This problem is avoided in the batch experiment at low pH in the present work. Since CO_2 is bubbled continuously in the solution, with a constant partial pressure, the interaction between the CO_2 in the atmosphere and the solution is not an issue.

4 Experimental

Seeded growth experiments were conducted for the calcium carbonate polymorphs vaterite and calcite at varying temperatures and MEG concentrations in lab scale reactors. The experiments were based on reaction crystallization of CaCO_3 from aqueous solutions done in batch operation. The experiments were carried out according to Table 4.1.

Table 4.1: Experimental procedure. The column ‘Reactor type’ denotes if the impellor and baffles were completely made of steel or coated with Teflon.

| Polymorph of seeds | Temperature [°C] | MEG [wt%] | # of experiments | Reactor type |
|--------------------|------------------|-----------|------------------|--------------|
| Vaterite | 40 | 0 | 1 | Steel |
| Vaterite | 40 | 40 | 1 | Steel |
| Vaterite | 40 | 60 | 1 | Steel |
| Vaterite | 70 | 0 | 1 | Steel |
| Vaterite | 70 | 40 | 1 | Steel |
| Vaterite | 70 | 60 | 1 | Steel |
| Calcite | 40 | 0 | 5 | Steel |
| Calcite | 40 | 30 | 3 | Steel |
| Calcite | 40 | 50 | 2 | Steel |
| Calcite | 40 | 70 | 2 | Steel |
| Calcite | 70 | 0 | 5 | Steel/Teflon |
| Calcite | 70 | 30 | 1 | Teflon |
| Calcite | 70 | 70 | 2 | Teflon |

4.1 Apparatus

The reactor used for the growth experiments is shown in Figure 4.1, designed on basis of Andreassen and Hounslaw (2004). A similar vessel was used for the vaterite seed preparation. The reactor for calcite seed preparation was of the same type, but larger (3 L). It had baffles and propeller made of glass to avoid corrosion. The reactor for vaterite seed preparation had 4 baffles made of steel. The lid with steel propeller and baffles was replaced by one coated with Teflon for some experiments. This will be explained in Chapter 5.3. The experimental set up is explained in Table 4.2.

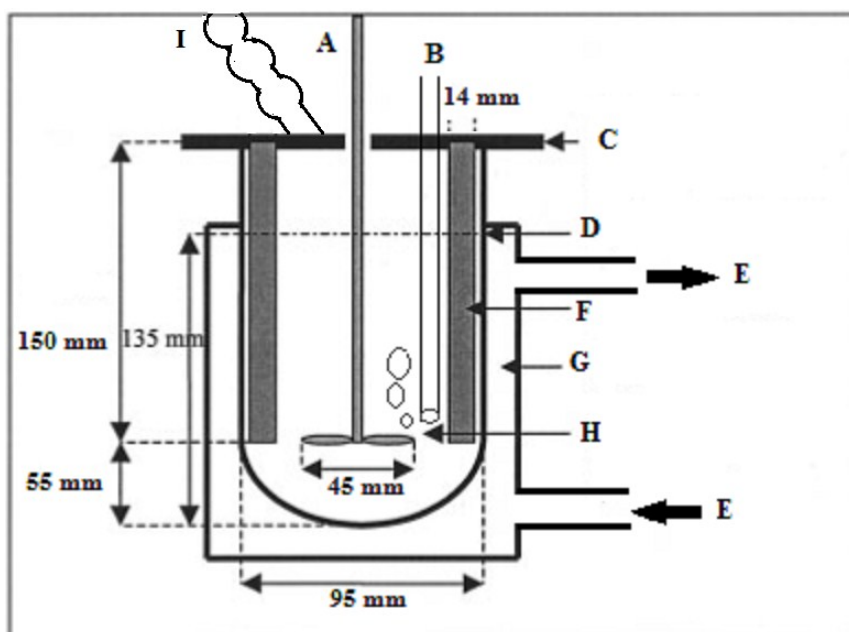


Figure 4.1: Double-walled batch reactor.

Table 4.2: Experimental apparatus.

| Symbol | Explanation |
|--------|---|
| A | Digital stirrer engine (Eurostar digital IKA [®] -Werke) |
| B | CO ₂ inlet |
| C | Lid with openings for sample withdrawal, CO ₂ inlet and cooling column |
| D | Liquid level |
| E | Temperature control, inlet and outlet of water bath |
| F | Two baffles attached to the lid for flow purposes |
| G | Double-walled glass vessel with heating jacket |
| H | Four-bladed impeller |
| I | Cooling column |

4.2 Seed preparation

Vaterite seeds were freshly prepared for each growth experiment. The seeds were prepared by mixing 250 mL 0.2 M CaCl₂ · 2H₂O and 250 mL 0.2 M Na₂CO₃ at 30 °C in a 1 L double-walled vessel at a stirring rate of 1500 ± 10 rpm (Andreassen and Hounslow, 2004). A list of all chemicals used could be found in Appendix A. The solutions were prepared with distilled and deionized water and preheated to 30 ± 0.10 °C in a Julabo 12 ME water bath before mixing. The prepared seed solution consists in a 500 mL 0.1 M CaCO₃ solution. After 15 minutes the stirring rate was decreased to 800 ± 10 rpm, and two 15 mL seed samples were withdrawn from the vessel with an automatic 5.0 mL pipette. One sample was used for number and volume determination of the seed particles, and the other for the growth experiment.

Calcite seeds were prepared the same way as vaterite seeds, only that a larger volume was made, to give the 0.1 M CaCO₃ solution. A 500 mL 0.6 M CaCl₂ · 2H₂O solution and a 500 mL 0.6 M Na₂CO₃ solution was poured in 2.0 L distilled water at 30 °C in a 3 L vessel. The two solutions were preheated to 30 ± 0.10 °C. The stirring was continued for 48 hours at a rate of 500 ± 10 rpm, to ensure complete transformation to calcite, before the seeds were used. For each calcite growth experiment 60 mL seed solution was withdrawn by a syringe at a stirring rate of 1200 ± 10 rpm. Calcite seeds from one batch were used for all growth experiments. The stirring rate was maintained at 500 ± 10 rpm between each calcite growth experiment.

4.3 Seeded growth experiments

The growth experiment was performed after the method of Olderøy et al., 2009 by mixing equal weight of a calcium (CaCl₂ · 2H₂O) and carbonate (NaOH/CO₂) solutions diluted with distilled and deionized water and 0 – 70 wt% MEG as co-solvent. All solutions were made from mother-liquids to minimize uncertainty when weighting out reactants. Calculations could be found in Appendix B.

The solutions were preheated in a Lauda E200 water bath and bubbled with CO₂ for approximately 30 minutes to saturate the solution with CO₂ and reach a stable pH (Olderøy et al., 2009). The pH was approximately 7 for all experiments. The solutions were mixed in a 1 L double-walled vessel to a final weight of 750 g with a stirring rate of 600 ± 10 rpm. The temperature was 40 ± 0.5 °C or 70 ± 1.0 °C adjusted by a Julabo F33 MC water bath. The initial calcium concentration in the growth reactor was 5.0 mmol/kg_{solvent} for all experiments. The concentration of the NaOH-solution varied depending on temperature and concentration of MEG. Details are given in Appendix C. Calculations for this was done in MultiScale to obtain an initial supersaturation of $S_{\text{vat}} = 3.0$ for vaterite growth as suggested by Flaten et al. (2010a). For calcite growth an initial supersaturation, $S_{\text{cal}} = 5.0$ was chosen. The initial level of supersaturation was chosen to a sufficient low level so that nucleation could be avoided. Precipitation should not occur in absence of seed material. The initial supersaturation for calcite was for some experiments decreased to $S_{\text{cal}} = 4.0$ due to nucleation of aragonite in experiments at 70 °C.

It emphasized that when calculation of supersaturation in MultiScale and preparing solutions for calcite growth, volume and concentrations of additional ions in the 60 mL seed solution is taken into account, as explained in Appendix B.

The seed solution was added to the vessel immediately after mixing of the CaCl₂ and NaOH solutions. The sampling started directly after this. The vessel operated with constant CO₂-bubbling, being the source of carbonate ions. The reaction time for growth experiments varied between 40 and 200 minutes depending on operating temperature and MEG concentration.

4.4 Analysis techniques

Different equipment and techniques were utilized for analysing the particles and experimental results. The principles of MultiScale, automated titration, Coulter Counter, scanning electron microscope and powder X-ray diffraction are described below.

4.4.1 MultiScale

Design of the experiments and calculations of results were partly done with the computer programme MultiScaleTM, version MultiMEGScale 7.0©. The multiphase equilibrium programme determines necessary concentrations of reactants, supersaturation ratios and equilibrium constants based on the Pitzer model. MultiScale takes into account several equilibria when determining supersaturation ratios. The co-existence of different ions in the solutions may result in formation of other chemical species, for instance various complexes. When calculating activity based supersaturations it is necessary to consider the presence of all ions. Important equilibrium equations, in addition to equation (2.23) to (2.26) are listed below:



The species at the right hand side of equation (4.2) and (4.3) are calcium complexes. MultiScale determines saturation ratios for calcite, thus supersaturations for vaterite must be calculated by equations (2.13) and (2.38). An advantage with MultiScale is that the K_{sp} based on activities, is constant when the MEG concentration varies, as long as the temperature is the same.

4.4.2 Titration

The depleting calcium concentration during the growth was determined by automated titration with 0.01 M EDTA in a Mettler Toledo DL53 Titrator. Samples of approximately 10 mL were withdrawn from the growth vessel with a syringe. Initially, this was done every 30 seconds and subsequently with a time interval varying between one and 10 minutes as the calcium concentration decreased. The samples were immediately filtered through a 0.22 μ m Millipore filter-paper to remove any $CaCO_3$ -particles. The filtrate was added to titration cups with an already weighed mixture of ~40 mL distilled water and ~1 mL 0.1 M HCl. The latter was added to remove any remaining CO_2 gas in the sample, hence ending the growth process. The samples were weighted again, to determine amount of calcium solution before ~0.3 mL of a NH_3/NH_4^+ buffer solution was added to ensure sufficient level of pH = ~10.

4.4.3 The Coulter-principle

Multisizer™ 3 Coulter Counter® version 3.51 from Beckman Coulter was used to obtain particle size distributions (PSD) of seed particles by number and volume. Particles in a suspension of an electrolyte solution, which is electrically conductive, pass through a small orifice. As a particle passes the channel, a change in electrical resistance is registered and counted, resulting in a number-volume distribution of the particles (Mullin, 2001). It is assumed that the particles are spherical.

The electrolyte solution used was 0.15 M NaNO₃. Two solutions saturated with vaterite and calcite, respectively, were prepared. This was done by adding previous prepared and dried particles, and stirring the solution with a magnet. The saturated solution with respect to vaterite, $S_{vat} = 1$, was stirred for approximately three hours. A Zeiss Axio Imager.A1m light microscope was used to determine that the added particles still were vaterite, without transforming to calcite. The calcite solution was stirred for 24 hours to obtain $S_{cal} = 1$. Both solutions were filtered through a 0.22 μm filter twice before they were used in the Coulter Counter measurements.

Since vaterite seeds were prepared freshly before every experiment, the seeds had to be investigated with the Coulter Counter each time. For determination of vaterite seeds a volume of 750 mL of the vaterite saturated NaNO₃-solution and 15 mL vaterite seed solution were added to a 1 L double-walled vessel with a stirring rate of 600 ± 10 rpm. A sample of approximately 150 mL was withdrawn by a 50 mL pipette and placed in the Coulter Counter instrument. The stirring was started and a volume of 100 μL was imbibed through the 100 μm- sized orifice where the particles were counted and measured. Two 15 mL samples of seed solution were withdrawn from each seed population, i , and added to two separate saturated solutions as illustrated in Figure 4.2. Two samples were withdrawn from this, each measured three times. This resulted in 12 measurements for each vaterite growth experiment.

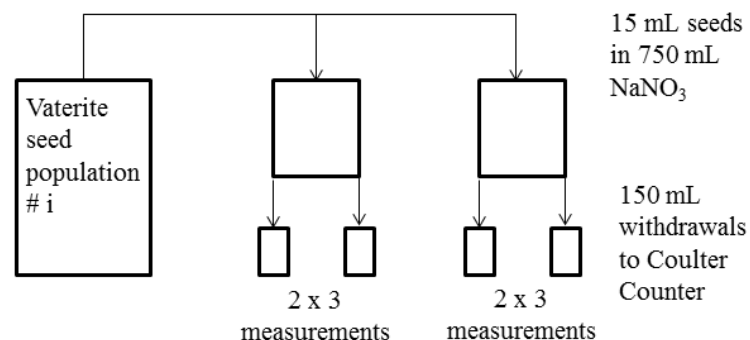


Figure 4.2: Measurements each seed population of vaterite seeds in Coulter Counter.

For calcite seed determination 690 mL calcite saturated NaNO₃ was mixed with 60 mL calcite seed solution to obtain a final volume of 750 ml, assumed equivalent with 750 g, which is the same as in the growth reactor. The procedure in Coulter Counter was the same as for vaterite, except for the volume imbibed through the orifice which was 2 000 μL and the orifice size

which was 200 μm . One seed population was used for all calcite experiment. Four 60 mL samples of seed solution were withdrawn from this batch and added to four separate saturated solutions as shown in Figure 4.3. Three samples from each of these were investigated in the Coulter Counter where three measurements were done, resulting in 36 measurements in total.

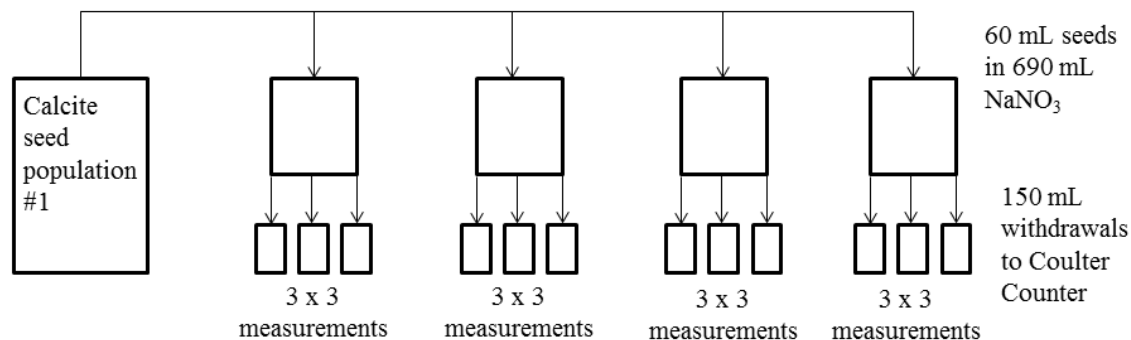


Figure 4.3: Measurements of calcite seeds in Coulter Counter.

4.4.4 Scanning electron microscope (SEM)

A quantitative indication of which polymorphs that are present in a sample could be determined by a scanning electron microscope. Particle morphology and topography may also be examined by SEM. The seed solutions and the solutions containing the grown particles were filtrated separately through 2.5 μm Whatman filter-papers, washed with 96 % ethanol and dried at 64 °C overnight. The calcium carbonate powder was glued on to a piece of double-sided carbon tape stuck to a sample holder and coated with gold particles with an Edwards Sputter Coater S150B to avoid accumulation of electrons. The SEM pictures were captured in a Hitachi S-3400N adjusted to an accelerating voltage level of 15.0 kV. Secondary electron emission was employed throughout the analysis.

4.4.5 Powder X-ray diffraction (XRD)

Powder X-ray diffraction was used to provide a qualitative determination on which polymorphs a sample consist of by, comparing the diffraction pattern of the sample with characteristic peaks from the software EVA. The crystals, both seeds and grown particles, were then analysed by XRD with a Bruker AXS D8 Focus. The scanning time was approximately three hours for each sample. The diffraction angle interval was between 20° and 60° for all scans. A slit setting of 0.02 was employed.

4.5 Growth calculations

Throughout the calculations it is assumed that nucleation, agglomeration and fracture of particles could be neglected. Details on calculations are carefully given in Appendix B.

Growth calculations are made based on calcium concentration from titration, and number and volume measurements from the Coulter Counter. The Coulter Counter counts and gives volume values as if all particles were spheres. For growth calculation of calcite this is therefore not exactly true. However, growth calculations of calcite are based on both cubic volume and spherical volume for comparison. The increasing volume of a particle during its growth is calculated by equation (2.22). The density values used in the calculations are 2.440 g/cm^3 (Flaten et al., 2010a) and 2.710 g/cm^3 (Nývlt and Ulrich, 1995) for vaterite and calcite, respectively. The equations (4.4) – (4.6) are used in calculations of growth rates, G .

$$V_{\text{vat}} = \frac{4}{3} \pi \cdot r^3 \quad (4.4)$$

$$V_{\text{cal}} = s^3 = (2L)^3 \quad (4.5)$$

where r is the radius of a spherical vaterite particle and L is half the length of one side of a calcite cube.

$$G = \frac{\Delta V}{\Delta t} \quad (4.6)$$

The supersaturation decreases according to consumption of calcium and carbonate. The supersaturation ratios during the experiments were calculated from the reduced calcium concentrations by the software MultiScale. The alkalinity reduces during the growth when the crystals grow. The alkalinity of the system is equal to $2 \cdot c_{\text{CO}_3^{2-}} = 2 \cdot c_{\text{Ca}^{2+}}$. This results in a decrease in alkalinity, from $A_{T,0}$ to $A_{T,1}$, for each calcium concentration calculated by

$$A_{T,1} = A_{T,0} - 2 \cdot \Delta c_{\text{Ca}^{2+},1} \quad (4.7)$$

Linearization of a plot of $\log(G)$ against $\log(S-1)$ gave the growth order as the slope and the logarithm of growth rate constant as the intersection with the y-axis as shown in equation (4.8). This equation is obtained from equation (2.15).

$$\log G = g \cdot \log(S-1) + \log(k_g) \quad (4.8)$$

Moreover, by plotting of $G^{0.5}$ against $(S-1)$ the growth rate constant, $k_{g=2}^{0.5}$, is given as the slope when assuming a second order growth, $g = 2$, see equation (2.20), as shown in equation (4.9):

$$G^{0.5} = k_{g=2}^{0.5} (S-1) \quad (4.9)$$

The latter method of plotting makes it possible to compare obtained rate constants with literature and to compare rate constants between experiments with different temperature and MEG concentrations in this work.

Additionally, in the examination of viscosity in Chapter 5.4, by assuming linear growth law, the growth rate constant, $k_{g=1}$, could be found as the slope when plotting G versus $(S - 1)$ according to

$$G = k_{g=1}(S - 1) \quad (4.10)$$

5 Results and discussion

5.1 Seed particles

5.1.1 Vaterite seed particles

Vaterite seeds particles were made freshly for each experiment due to the polymorph's ability of transforming into the more stable polymorph calcite over time. Samples of all individual seed populations were investigated by SEM to obtain a quantitative determination of the seeds. Two parallels are shown in Figure 5.1. The pictures reveal a seed population of almost pure spherical vaterite and a uniform particle size distribution. Since vaterite has the tendency to transform into calcite is difficult to eliminate calcite completely. All SEM pictures show a small amount of cubic calcite among the spherical vaterite.

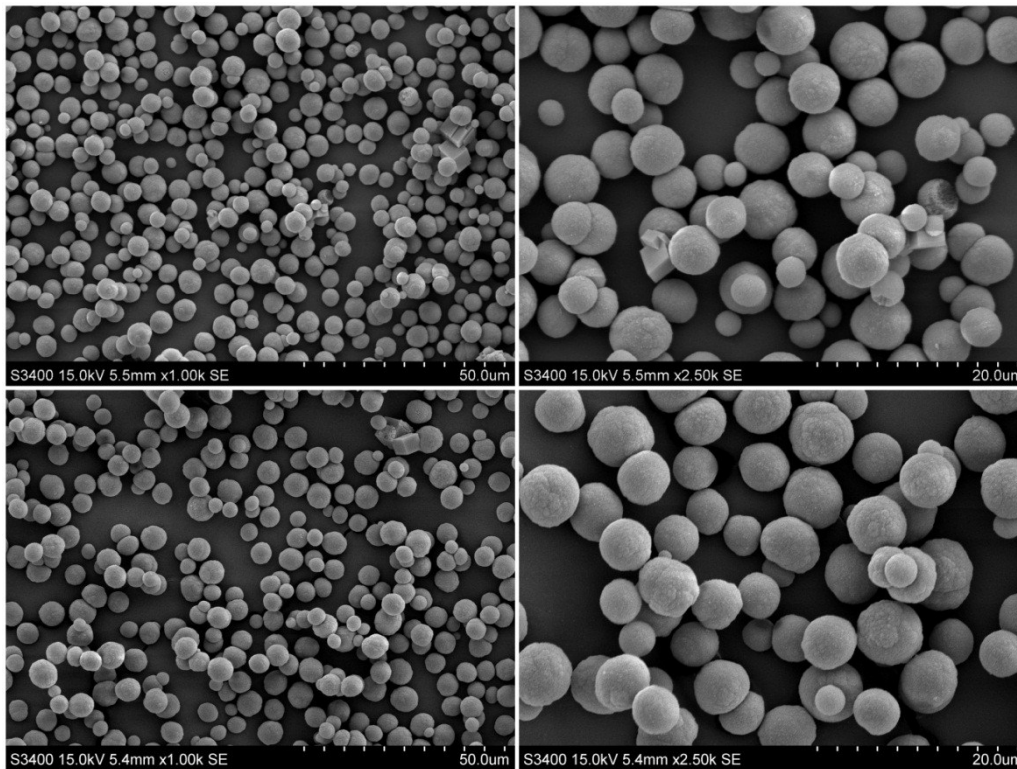


Figure 5.1: SEM pictures of two samples of vaterite seeds. The scale bar is 50 μm (left) and 20 μm (right).

Polymorphic characterisation of the seed particles were done by powder XRD. The unique diffraction peaks of a vaterite sample are shown in Figure 5.2. The peaks confirm that the only constituent elements in a seed sample were calcium carbonate vaterite and calcite. XRD was used for qualitative determination of the constituent polymorphs only.

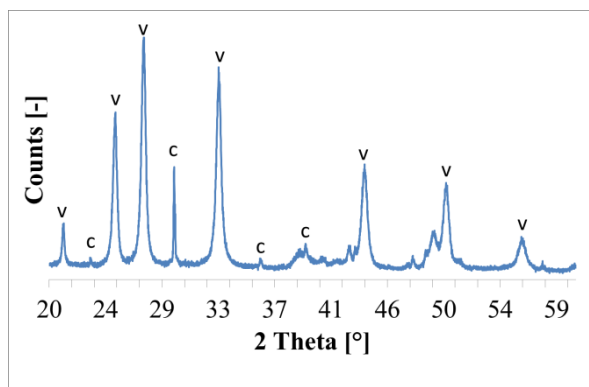


Figure 5.2: Powder XRD for vaterite seed particles. The labels ‘v’ and ‘c’ at the characteristic peaks represent vaterite and calcite respectively.

Particle size distributions, PSD, of seed particles are determined by the Coulter Counter. Number and volume of particles are needed for growth calculations. PSD by number and by volume from the same seed population and from different seed populations are shown in Figure 5.3 and Figure 5.4, respectively. The diameter axis in the PSDs by number starts from 3 μm due to observation of noise in the Coulter Counter measurements between 0 and 3 μm . According to the SEM pictures no seed particles were found at a size smaller than 3 μm . The size interval of vaterite seeds ranges between 3 – 12 μm in diameter which corresponds to the SEM pictures.

PSDs by number of seeds from different populations vary more than from the same population. A possible explanation for this is the stochastic nature of nucleation (Jiang and ter Horst, 2011). It is difficult to obtain repeatability in nucleation rates experiments. This implies that varying nucleation rates results in a varying number of particles. On the other hand, the total volume of particles will not necessarily differ to the same extent since the same amount of reactants has been used in each preparation of a batch of seeds.

When comparing the PSDs by volume in Figure 5.3 and Figure 5.4 the curves vary relatively much. However, it is the total area under each curve that gives the overall volume of seeds, so each curve must not be equal. The appearance of larger particles in the PSDs by volume is assumed to be calcite. This is not seen so clearly in the PSDs by number. Calcite is larger than vaterite, and consequently will calcite contribute with a larger volume even though the number of the large particles is low. The larger particles could also be clustered particles of either vaterite or calcite which are counted as one particle when passing through the orifice in the Coulter Counter.

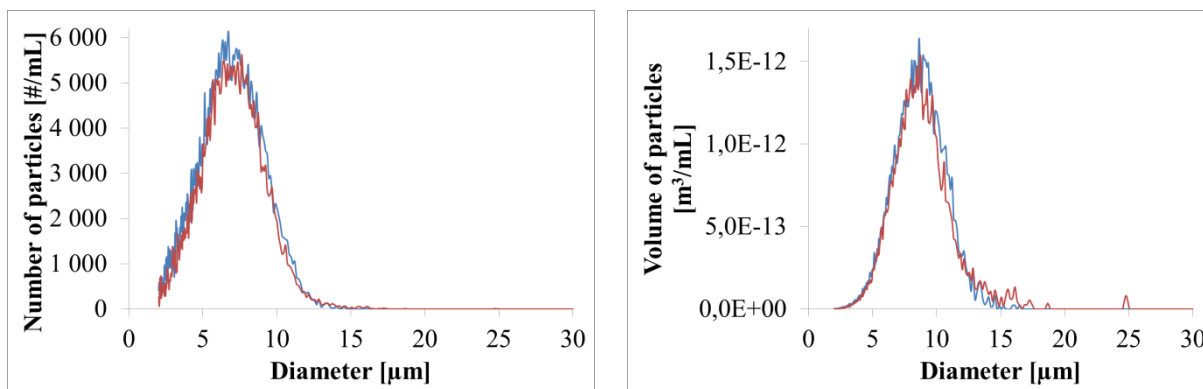


Figure 5.3: PSD for two samples of vaterite seeds from the same seed population by number of particles per mL (left) and by volume of particles per mL (right).

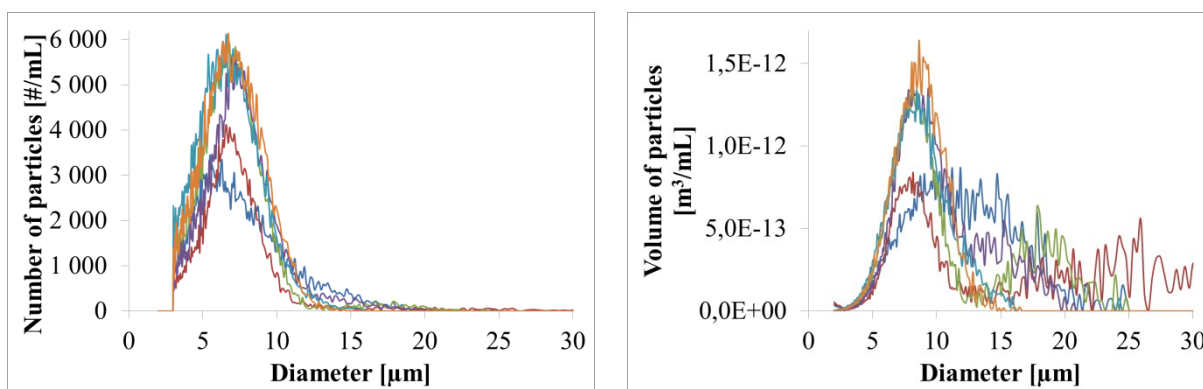


Figure 5.4: PSD for vaterite seeds from six different seed populations by number of particles per mL (left) and by volume of particles per mL (right).

5.1.2 Calcite seed particles

Calcite seed particles were prepared only once and seeds from this batch were used for all experiments. The polymorph is stable after transforming from vaterite. As long as a constant stirring rate is maintained there should be no problems using seeds from the same population several times. A sample from the seed population was investigated by SEM as seen in Figure 5.5.

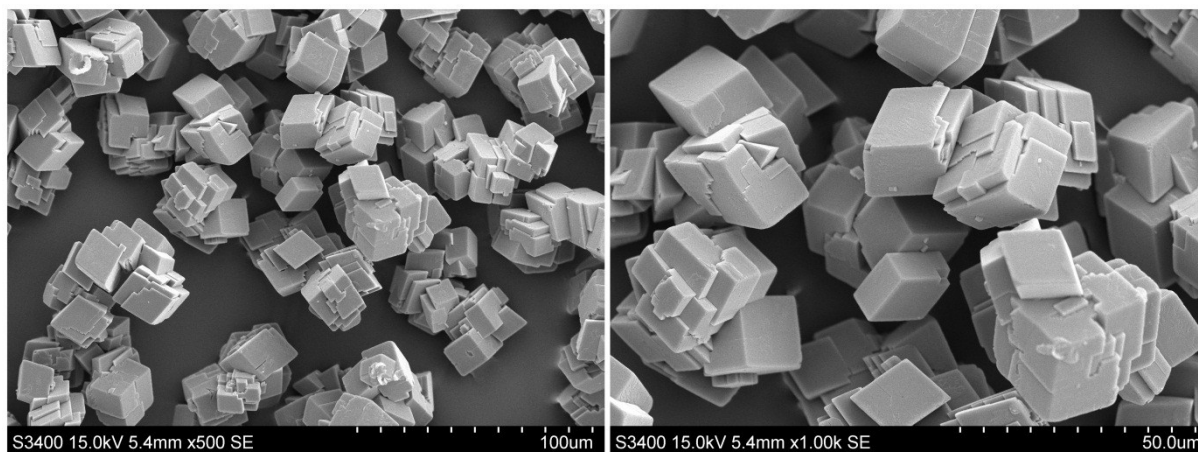


Figure 5.5: SEM picture of calcite seeds. The scale bar is 100 μm (left) and 50 μm (right).

The pictures disclose aggregates of cubic calcite particles with smooth surfaces. The difficulty of generating non-aggregated calcite particles with smooth surfaces have been reported by researchers previously (Flaten, 2010). It is stated that calcite tends to aggregate more efficient, than for instance spherically shaped vaterite, due to its well-defined faces (Andreassen and Hounslow, 2004).

A scan of calcite seeds from powder XRD is illustrated in Figure 5.6. The characteristic peaks confirm that the crystals seen in Figure 5.5 are 100 % pure calcite.

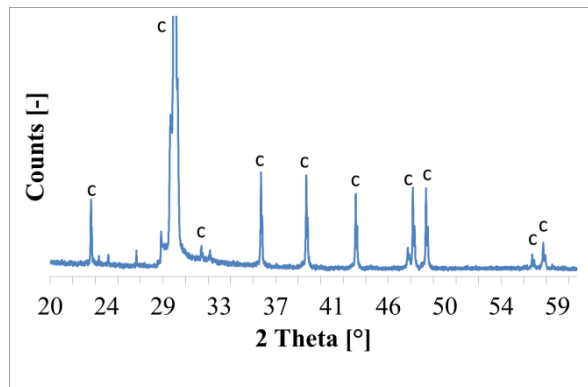


Figure 5.6: Powder XRD for calcite seed particles. The label ‘c’ at the characteristic peaks represents calcite.

PSD of calcite seeds by number and volume are shown in Figure 5.7. The size distributions measurements are from the same seed population and show a good reproducibility. Due to Coulter Counter’s assumption of spherical particles, the PSD of calcite is not as accurate as for vaterite. The x-axis is expressing particle size in diameter. This is not exactly right for calcite which is cubic shaped.

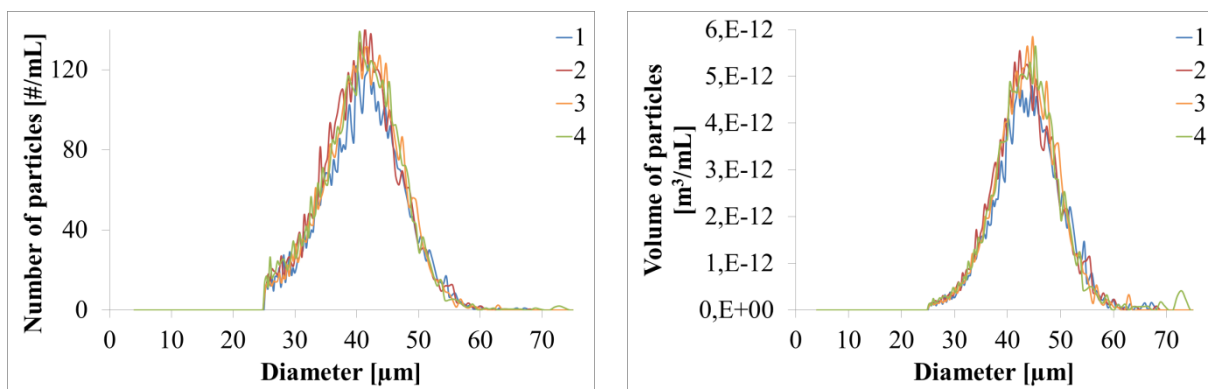


Figure 5.7: PSD for calcite seeds from four measurements of the same batch of seeds by number of particles per mL (left) and by volume of particles per mL (right).

5.1.3 Comparison of vaterite and calcite seed particles

Values of number and volume of particles per mL final volume in the growth reactor for vaterite and calcite are shown in Table 5.1. For a description of uncertainty and calculations of average and standard deviation it is referred to Appendix D. Details on all Coulter Counter measurements are given in Appendix E.

Table 5.1: Number and volume of seed particles per mL.

| Polymorph | Number of particles [10³ # part./mL] | Volume of particles [10⁻¹² m³/mL] | Volume pr. particle [10⁻¹⁶ m³/part.] |
|------------------|--|--|---|
| Vaterite | 313 ± 78 | 70 ± 8 | 2.30 ± 0.40 |
| Calcite | 4.50 ± 0.40 | 161 ± 14 | 361 ± 9 |

The volume per particle has been calculated by dividing volume of particles per mL by number of particles per mL. The average diameter for vaterite calculated from volume per particle in Table 5.1 is 7.6 μm. This is within the diameter intervals obtained from Coulter Counter in Figure 5.3 and Figure 5.4. Flaten et al. (2010a) obtained an average vaterite particle diameter of 6.4 μm. For calcite, the average “diameter” (length of one cube side) from Table 5.1 for calcite is 33 μm.

Comparison of uncertainty of the values from Table 5.1 is illustrated in Table 5.2. The values, given in percentage, are obtained by dividing standard deviation by the average.

Table 5.2: Comparison of percentage standard deviation for vaterite (several seed populations) and calcite (one seed population).

| Polymorph | Number of particles [%] | Volume of particles [%] |
|------------------|------------------------------------|------------------------------------|
| Vaterite | 25 | 11 |
| Calcite | 9 | 8 |

Two observations are done from these values. Firstly, the percentage standard deviations for vaterite are larger than for calcite. Secondly, for vaterite, the uncertainty in number of particles is significantly larger than for volume of particles. Hence, it is confirmed that there is more variation between different seed populations than within the same batch, and there is less variation between volumes of particles than number of particles. As explained in Chapter 5.1.1 the stochastic feature of nucleation gives rise to a large variation in number of particles between each seed population. Total volume of particles differs less due to that the same amount of chemicals are used each time.

During withdrawal of seeds to the growth reactor it was observed how fast the calcite sedimented compared to vaterite. An explanation could be given by Stokes law due to the large particle size difference of vaterite and calcite. The free settling velocity increases with increased diameter of a particle as long as the viscosity of the solution and the densities of the

particles remain the same (Geankoplis, 2003). The densities of vaterite and calcite are comparable, and the viscosity of the solutions is the same. This could be a source of uncertainty in the experiments.

5.2 Vaterite growth

Vaterite seeded experiments were performed at 40 °C and 70 °C with a solvent composition of 0, 40 and 60 wt% MEG. All experiments were executed once. The initial supersaturation was $S_{\text{vat}} = 3.0$.

5.2.1 Vaterite growth in water and MEG

The growth commences immediately after the seed particles are introduced to the reactor. The particles grow by consuming calcium and carbonate ions. The depleting calcium concentration with reaction time for 0, 40, and 60 wt% MEG at 40 °C is shown in Figure 5.8. Corresponding concentration profiles at 70 °C is illustrated in Appendix F.

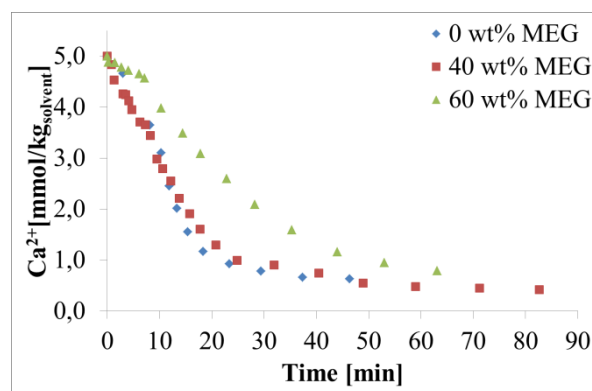


Figure 5.8: Decreasing calcium concentration over time for vaterite with varying MEG concentration at 40 °C.

Increased weight percentage of MEG retards the growth. While the water solution reaches equilibrium after 30 minutes, the solution with 60 wt% MEG needs more than 60 minutes. An initial slow calcium depletion is observed at 40 °C in 60 wt% MEG. Nucleation has been suggested as an explanation for this. This is later shown in the SEM picture in Figure 5.12.

Supersaturation ratios were calculated from the decreasing calcium concentrations in MultiScale. The supersaturation of the solution reduces in the same way as calcium concentrations according lowered ionic activity as seen in equation (2.12). Supersaturation profiles for all vaterite experiments are illustrated in Figure 5.9.

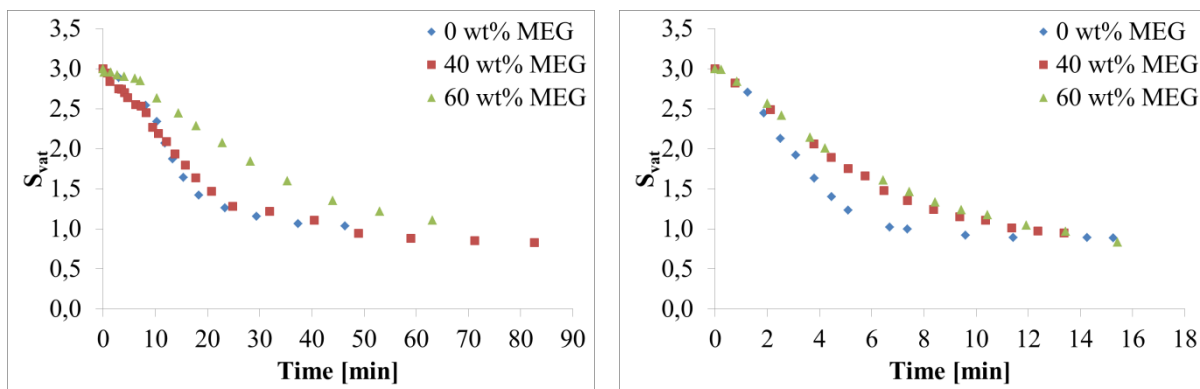


Figure 5.9: Decreasing supersaturation over time for vaterite with varying MEG concentration at 40 °C (left) and 70 °C (right). Note the different units of time at the x-axis.

It is obvious that an elevated temperature promotes the growth. For growth in water, the solution reaches equilibrium after 30 minutes at 40 °C while it only takes 10 minutes at 70 °C.

The initial supersaturation was chosen to a value of $S_{\text{vat}} = 3.0$ to avoid nucleation. To ensure correct determination of growth rates it is desirable that the decreasing calcium concentration is a result of enlargement of the seeds particles exclusively. The curves flatten out at $S_{\text{vat}} = 1$ when the solution is saturated. There is no more driving force for vaterite growth.

Samples of vaterite crystals from all six experiments were investigated by powder XRD and SEM. XRD scans of vaterite crystals grown at all experimental conditions were compared with scans of vaterite seeds. This is shown in Appendix G. All characteristic peaks shown in the XRD scans are representing vaterite or calcite. It is emphasized that XRD analysis were used for qualitative determination of the crystals only.

Comparison of seed particles and grown particles grown in water at varying temperature are illustrated in the SEM pictures in Figure 5.10.

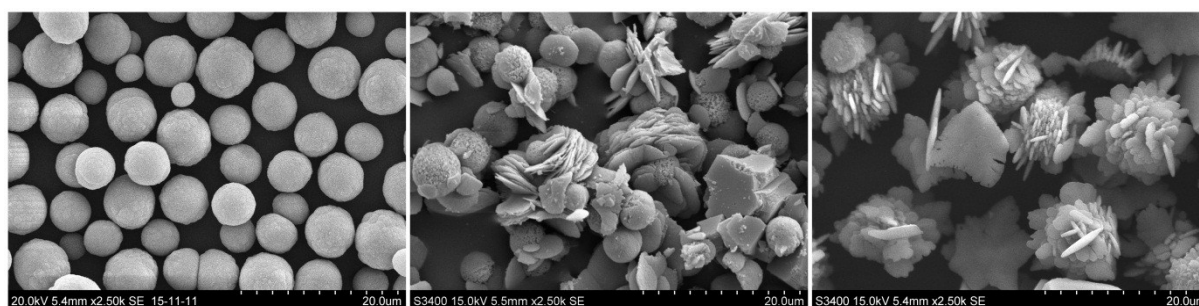


Figure 5.10: Vaterite seeds (left), vaterite grown in water at 40 °C (middle) and at 70 °C (right) after 50 minutes. The scale bar is 20 μm.

A conspicuous particle enlargement is less visible in the SEM pictures and better illustrated by the PSDs from the Coulter Counter as shown in Figure 5.11. It appears that the diameter size interval has increased from 3 – 12 μm to 5 – 20 μm. The PSD by number for grown crystals is lower and wider than for seeds. This is probably due to unwanted particle

aggregation and nucleation. From the PSD by volume it is clear that the total volume of particles (area under the curve) has increased significantly during the growth.

Some of the grown particles in Figure 5.10 appear as clusters and it should be remembered that the Coulter Counter possibly counts clustered particles as one. Additionally, the larger calcite particles, which are seen in the SEM pictures, will also contribute to uncertainty in the Coulter Counter measurements.

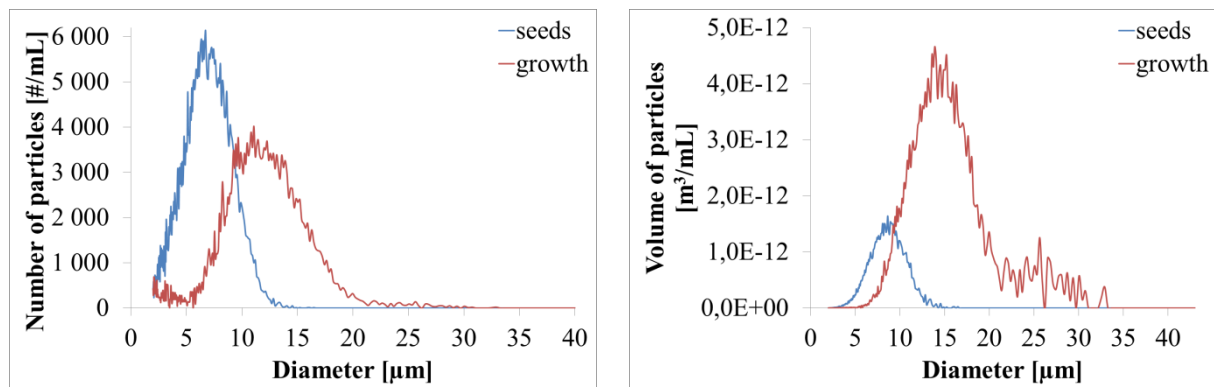


Figure 5.11: PSD for vaterite seeds and vaterite grown in water at 40 °C by number of particles per mL (left) and volume of particles per mL (right).

Nucleation of vaterite appears in the water experiments both at 40 °C and 70 °C. The nucleation should be classified as secondary since seeds are present in the solution. At 40 °C the nucleated substances emerge as layer by layer of thin plates.

Vaterite grown in varying concentrations of MEG at 40 °C and 70 °C is illustrated in Figure 5.12. Some calcite is present also here. Additionally, vaterite has nucleated in the experiment at 40 °C with 60 wt% MEG. This correspond to the statement that MEG induces nucleation (Flaten et al., 2010b). However, there is not observed nucleation at 70 °C with 60 wt% MEG, so one should be careful with drawing any conclusions about this.

The crystal surface of vaterite, grown at 70 °C, looks differently than at 40 °C. Flaten et al. (2010a) suggest that vaterite crystals at a higher temperature have grown with a different mechanism. The crystal surface from growth at 70 °C in both Figure 5.10 and Figure 5.12 appears with hexagonal plates. Vaterite is polycrystalline with a hexagonal unit cell. Growth of mono-crystalline plates in solution is rarely observed (Flaten et al., 2010a), since vaterite often transforms to aragonite at elevated temperatures (Ogino et al., 1987).

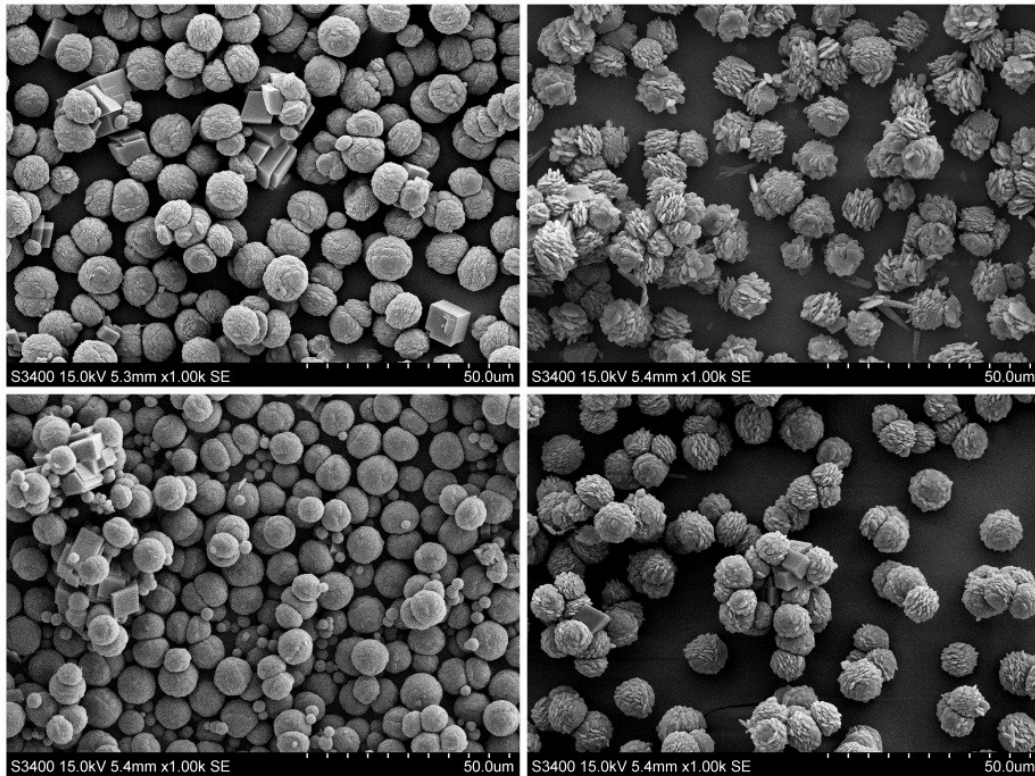


Figure 5.12: Vaterite growth with 40 wt% MEG at 40 °C (upper left), 70 °C (upper right) and with 60 wt% MEG at 40 °C (lower left), 70 °C (lower right) after 50 minutes. The scale bar is 50 μm.

Flaten et al. (2010a) proposed that when vaterite seed are introduced to the supersaturated solution at high temperatures, the system is forced to continue the vaterite growth with enlarged separated crystalline units. Hence, mono-crystalline hexagonal plates will be formed, as shown in Figure 5.13. However, some of the plates, especially in water as shown in Figure 5.10, look like bulk nucleation of vaterite, shaped as plates.

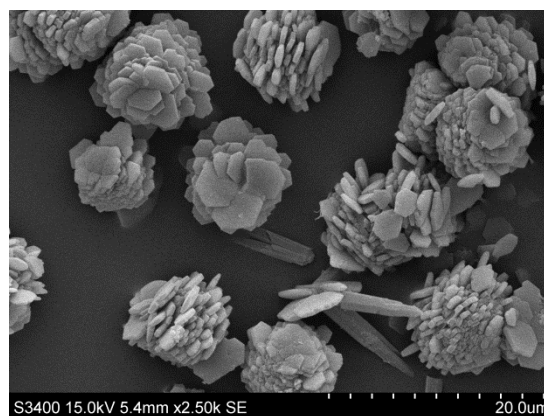


Figure 5.13: Vaterite growth with 40 wt% MEG at 70 °C exhibits hexagonal plates. The scale bar is 20 μm.

More calcite appears in the SEM pictures of grown vaterite crystals compared to pictures of the seeds. This may originate from transformation, nucleation or from growth of calcite which was already present in the seed solution. Transformation from vaterite to calcite is possible

when the vaterite growth has reached $S_{vat} = 1$. Then, dissolution of vaterite and precipitation of calcite is probable. Calcite could also have nucleated in the bulk either during the growth or in the small time interval between mixing of CaCl_2 and NaOH and adding of seeds.

5.2.2 Vaterite growth order and growth rate constants

In order to determine growth order, g , and growth rate constants, k_g , for vaterite, growth rates and supersaturation as $\log(G)$ and $\log(S-1)$, respectively, is plotted as shown in equation (4.8). This gives the growth rate, g , as the slope, and the growth rate constant, k_g , as the logarithm of the intersection with the y-axis. Detailed calculation of G and S is given in Appendix B. The plots are shown in Figure 5.14 for varying MEG concentrations at 40 °C and 70 °C.

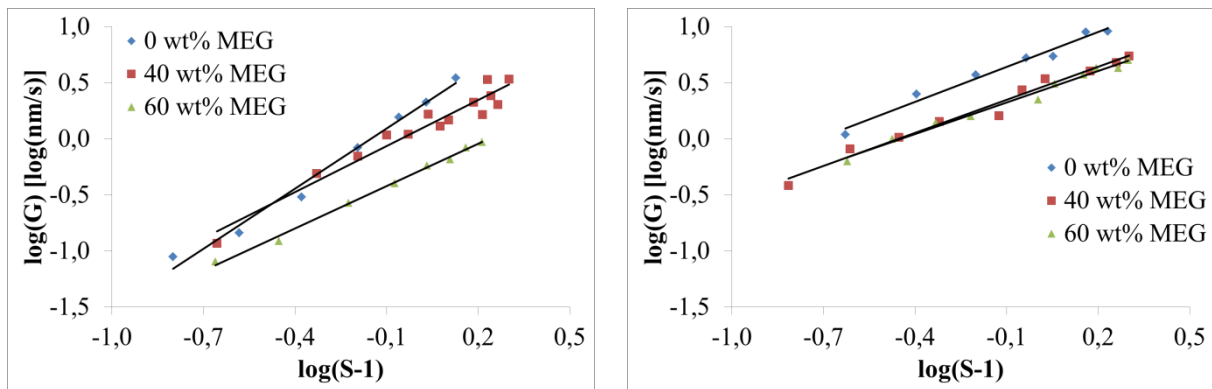


Figure 5.14: Log(G) as a function of log ($S-1$) for vaterite with 0, 40 and 60 wt% MEG at 40 °C (left) and 70 °C (right).

The incline of all graphs 70 °C appear lower than at 40 °C. Hence, a lower growth order is observed when the temperature rises. Additionally, the linear regression lines at 70 °C seem relatively parallel compared to at 40 °C. This indicates that the growth orders at 70 °C, independent of MEG concentration, are fairly the same. The growth orders and growth rate constants determined from the plots in Figure 5.14 are presented in Table 5.3. The growth rate constants are related to the given growth order and could be used to calculate growth rates, G , at a given supersaturation. The data points fit acceptably to the linear regression models. The correlation coefficients related to the regression are reported in Table 5.4. Details on determination of uncertainty are given in Appendix D.

Table 5.3: Growth order and growth rate constants for vaterite. One parallel of each experiment.

| MEG [wt%] | g (40 °C) | g (70 °C) | k_g [nm/s] (40 °C) | k_g [nm/s] (70 °C) |
|-----------|-------------|-------------|----------------------|----------------------|
| 0 | 1.79 | 1.04 | 1.86 | 5.56 |
| 40 | 1.37 | 0.98 | 1.22 | 2.78 |
| 60 | 1.26 | 0.94 | 0.51 | 2.60 |

Table 5.4: Correlation coefficient from the linear regression models of $\log(G)$ versus $\log(S-I)$ for vaterite.

| MEG [wt%] | R ² (40 °C) | R ² (70 °C) |
|-----------|---------------------------|---------------------------|
| 0 | 0.99 | 0.98 |
| 40 | 0.94 | 0.98 |
| 60 | 0.99 | 0.99 |

A growth order of 1.79 is obtained for vaterite growth in water at 40 °C. According to previous studies by Flaten et al. (2010a) the growth order at the same conditions was 2.01 ± 0.34 , whereas Olderøy et al. (2009) proposed a growth order of 2.02 ± 0.11 . A growth of second order follows a parabolic rate law. Hence, the mechanism proposed is spiral growth. The growth could be controlled by integration at the surface.

Furthermore, Flaten et al. (2010a) reported a lowered growth order at 40 °C when the MEG concentration increases, and an order closer to one at 70 °C. The same trends were found in this work. A first order growth follows the linear rate law and the mechanism is rough growth. This implies that the growth is controlled by diffusion or adsorption, meaning that the surface reaction is fast. This causes high growth rates as seen in Figure 2.6. At 70 °C the growth rates are high so a diffusion controlled growth could be justified by the high temperature. This is also stated in literature. Both Söhnel and Garside (1992) and Mullin (2001) report that at high temperatures crystal growth rates are likely to become diffusion controlled. However, diffusion controlled growth is not expected at low growth rates which is the case when the MEG concentration increases. Flaten et al. (2010a) suggest that a different explanation of the low growth rate orders is needed.

As a result of the experimental design, with an initial supersaturation. $S_{vat} = 3.0$ and an initial calcium concentration of 5.0 mmol/kg_{solvent}, the carbonate concentration turn out to be considerably low compared to calcium. To maintain the same level of supersaturation, independent of temperature and MEG content, less NaOH must be added when the temperature and MEG concentration increase. Hence, the carbonate concentration decreases correspondingly. The concentrations of free ions of calcium and carbonate, initially and in the end of the growth, are shown in Table 5.5.

Table 5.5: Concentration of free ions in mmol/kg_{solvent}. *) The initial calcium concentration is slightly lower than 5.00 due to that some calcium ions are bound in complexes as shown in equation (4.2) and (4.3).

| Temperature [°C] | MEG [wt%] | Initial Ca ²⁺ * | Initial CO ₃ ²⁻ | End Ca ²⁺ | End CO ₃ ²⁻ |
|------------------|-----------|----------------------------|---------------------------------------|----------------------|-----------------------------------|
| 40 | 0 | 4.82 | 0.30 | 0.64 | 0.26 |
| 40 | 40 | 4.82 | 0.08 | 0.72 | 0.06 |
| 40 | 60 | 4.82 | 0.03 | 0.76 | 0.02 |
| 70 | 0 | 4.81 | 0.06 | 0.69 | 0.04 |
| 70 | 40 | 4.81 | 0.02 | 0.83 | 0.01 |
| 70 | 60 | 4.81 | 0.01 | 0.84 | 0.002 |

It is clear that the ratio between the calcium and carbonate concentrations is strongly non-stoichiometric. The largest difference of the concentrations asserts itself in experiments with high MEG content. Consequently, diffusion controlled growth could be explained by reactant limitation of carbonate at these conditions. Flaten et al. (2010a) decided to make clear the effect of reactant limitation by carrying out experiments with stoichiometric ratios. It was found out that the growth order remained close to two when the MEG concentration was increased from 0 to 50 wt%. Due to these findings it was believed that low concentrations of carbonate limit the crystal growth in the non-stoichiometric experiments.

With the purpose of determining to which extent MEG influences the growth rates, a growth of second order is assumed. Hence, the growth rate constants for different solvent compositions could be compared. Growth data when assuming parabolic growth mechanism is obtained from equation (4.9). The graphs in Figure 5.15 demonstrate how the growth rate constants are influenced by increased MEG concentration and elevated temperature. The figure exemplifies variation in MEG concentration at 40 °C and variation in temperature in water. The same trends were found for MEG concentrations at 70 °C and temperatures with 40 and 60 wt% MEG, respectively. These graphs are shown in Appendix F.

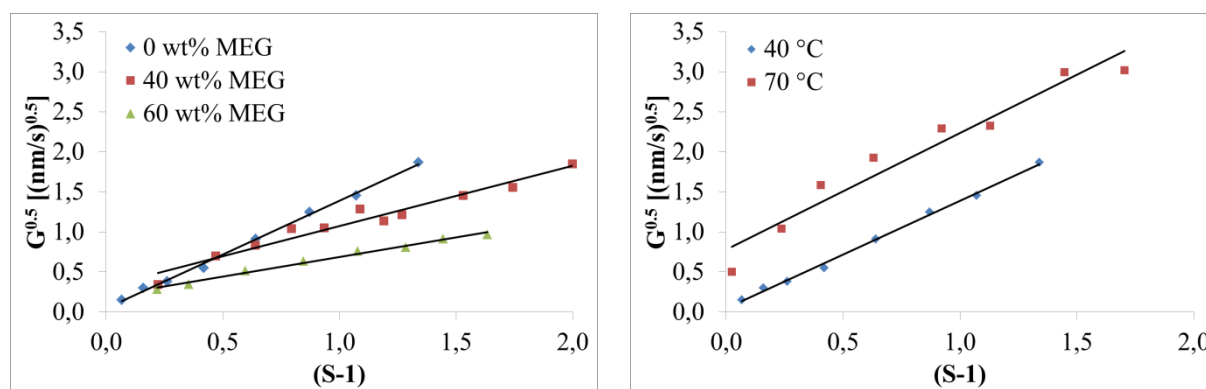


Figure 5.15: $G^{0.5}$ as a function of $(S-1)$ for calcite with varying MEG concentration at 40 °C (left) and varying temperature in water (right).

Data points at the given conditions are used to obtain a linear regression model. A steeper slope gives a larger growth rate constant, hence a faster growth. The slopes from experiments

in water at varying temperatures (to the right in Figure 5.15) seem relatively parallel and it could look like the growth rate constant is about the same. This is not the case as seen in Table 5.6, where the growth rate constants determined from the graphs are reported. Correlation coefficients from the linear regression models are shown in Table 5.7.

Table 5.6: Growth rate constants for vaterite when assuming parabolic growth mechanism, $g = 2$. One parallel of each experiment.

| MEG [wt%] | $k_{g=2}$ [nm/s] | |
|-----------|------------------|---------|
| | (40 °C) | (70 °C) |
| 0 | 1.81 | 2.12 |
| 40 | 0.57 | 0.93 |
| 60 | 0.24 | 0.63 |

Table 5.7: Correlation coefficient from the linear regression models of $G^{0.5}$ versus $(S-I)$ for vaterite.

| MEG [wt%] | R^2 | |
|-----------|---------|---------|
| | (40 °C) | (70 °C) |
| 0 | 0.98 | 0.94 |
| 40 | 0.96 | 0.95 |
| 60 | 0.99 | 0.98 |

It is observed that the growth rate constant reduces as the co-solvent concentration is increased and increases as the temperature is elevated. The same tendencies for were described by Flaten et al. (2010a). The growth rate constant is reduced more than 7 times at 40 °C and slightly more than 3 times at 70 °C when the co-solvent concentration increases from 0 – 60 wt%. The rate constant for growth in water at 40 °C was found to be 1.81 nm/s, which is in proper accordance with previous reported rate constants shown in Table 5.8.

Table 5.8: Growth rate constants for vaterite in water at 40 °C reported in literature. *) This value was estimated from a polynomial function made on the basis of growth rate constants at 11.4 – 42.5 °C reported by Kralj et al. (1990).

| Work | $k_{g=2}$ [nm/s] |
|--------------------------------|------------------|
| Kralj et al. (1990) | 1.80* |
| Andreassen (2001) | 2.0 ± 0.3 |
| Andreassen and Hounslow (2004) | 1.98 ± 0.08 |
| Olderøy et al. (2009) | 1.71 ± 0.12 |
| Flaten et al. (2010a) | 1.94 ± 0.30 |
| This work | 1.81 |

Even though the growth determination methods used by the researchers in Table 5.8 are not identical, the variation of $k_{g=2}$ is relatively small. As discussed in Chapter 3, Kralj et al. (1990) measured the growth with recording pH in the solution. Additionally, they did not use vaterite seeds, but determined the number of precipitated crystals by counting under a microscope.

Despite use of this alternative method, the growth rate constant obtained is close the one found in this work.

5.3 Calcite growth

Calcite seeded experiments were executed with 0, 30, 50 and 70 wt% MEG at 40 °C and with 0, 30 and 70 wt% MEG at 70 °C. The initial supersaturation was $S_{cal} = 5.0$ at 40 °C, but was reduced to 4.0 for some experiments at 70 °C due to unwanted nucleation of aragonite with $S_{cal} = 5.0$. Throughout this chapter only concentration profiles are shown due to different initial supersaturation among the experiments. All corresponding de-supersaturation curves are showed in Appendix F. The experiment notation X-Y-I, for example 40-0-1, means 40 °C, 0 wt% MEG, parallel number 1. This system is used throughout the chapter.

5.3.1 Calcite growth in water and MEG

Five seeded calcite growth experiments were performed in water at 40 °C to examine reproducibility. Concentration profiles for all of them are shown in Figure 5.16.

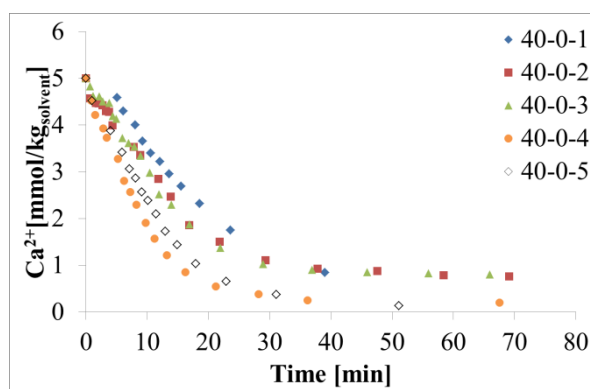


Figure 5.16: Decreasing calcium concentration over time for calcite in water at 40 °C for five parallel experiments. The notation 40-0-i means temperature - wt% MEG - parallel number.

A satisfactory reproducibility of calcite growth in water at 40 °C was difficult to obtain. None of the parallels stands out from the other, so it was decided to include all of them for further calculations. However, the solution in all parallels needs approximately 35 minutes to reach equilibrium. The reduced supersaturation over reaction time for calcite growth is determined the same way as for vaterite from measured calcium concentrations.

Powder XRD was accomplished for all experiments at 70 °C and for one of each MEG concentration at 40 °C. All XRD scans are shown in Appendix G. All peaks in the XRD scans were characterised as calcite.

All calcite experiments were investigated by SEM. For comparison, calcite seeds and three parallels of calcite grown in water at 40 °C are illustrated in Figure 5.17.

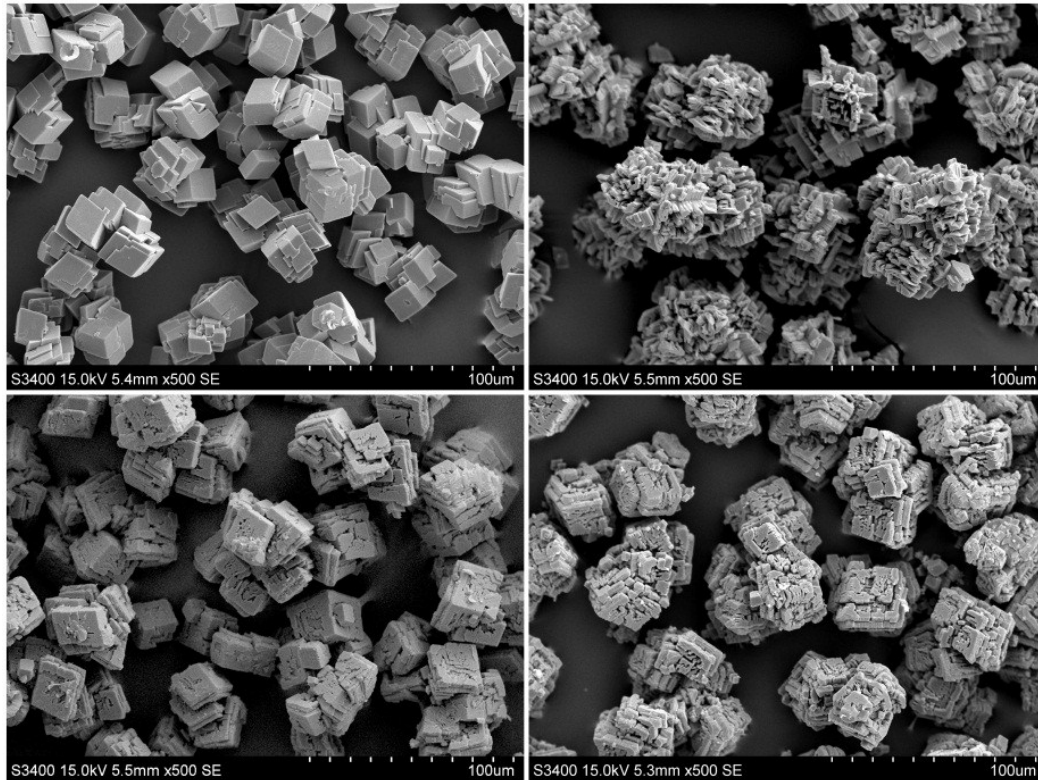


Figure 5.17: Calcite seeds and three parallel calcite grown in water at 40 °C after 50 minutes. Upper row from left: Seeds and 40-0-1. Lower row from left: 40-0-4 and 40-0-5. The scale bar is 100 μm.

Crystals from the two parallels not shown in the figure, 40-0-2 and 40-0-3 from Figure 5.16, appeared with a similar surface feature as 40-0-1. These three parallels, having a rugged surface, exhibits the slowest calcium depletion curves in Figure 5.16. This may indicate that the growth has been inhibited by an impurity substance. However, none of the parallels reveal a surface feature similar to the seeds. This could imply that the growth of all parallels have been inhibited, though to a different degree. According to Mullin (2001) impurities may affect the crystal growth rates in numerous of ways. Reduced growth or changes of the crystal habit are possible consequences of impurities.

Depleting calcium concentration curves for growth experiments at 40 °C with MEG as co-solvent are illustrated in Figure 5.18. Three parallels were performed with 30 wt% MEG, and two parallels with 50 and 70 wt% MEG, respectively. The reproducibility in these experiments is better than in the water experiments. The solutions with MEG as co-solvent reach equilibrium slower than water solutions. The time needed is 60, 90 and 200 minutes with increased MEG concentration. This implies that increased concentration of MEG retards the growth of calcite, similarly as for vaterite.

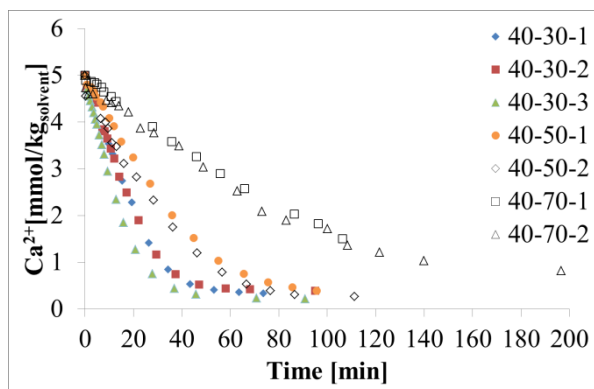


Figure 5.18: Decreasing calcium concentration over time for calcite in 30, 50 and 70 wt% MEG at 40 °C.

SEM-pictures of calcite seeds and three parallels grown in 30 wt% MEG at 40 °C are shown in Figure 5.19. Similarly as for growth in water, the calcite grown in 30 wt% MEG exhibits a crystal surface differing from the seed crystals. The two parallels with the most rugged surface, 40-30-1 and 40-30-2, reveal a slightly slower decreasing calcium concentration than 40-30-3 as seen in Figure 5.18. Again, it could look like inhibition of growth has occurred.

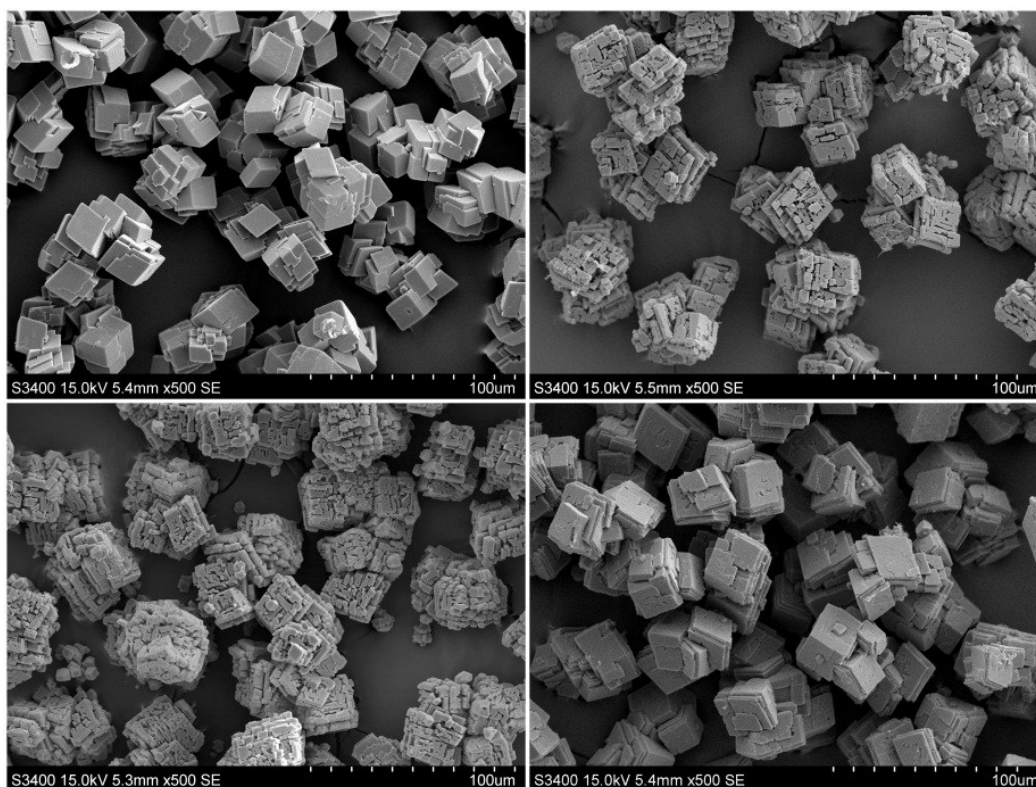


Figure 5.19: Calcite seeds and three parallels calcite grown in 30 wt% at 40 °C after 50 minutes. Upper row from left: Seeds and 40-30-1. Lower row from left: 40-30-2 and 40-30-3. The scale bar is 100 µm.

Two parallels of calcite grown in 50 and 70 wt% MEG, respectively, are illustrated in Figure 5.20.

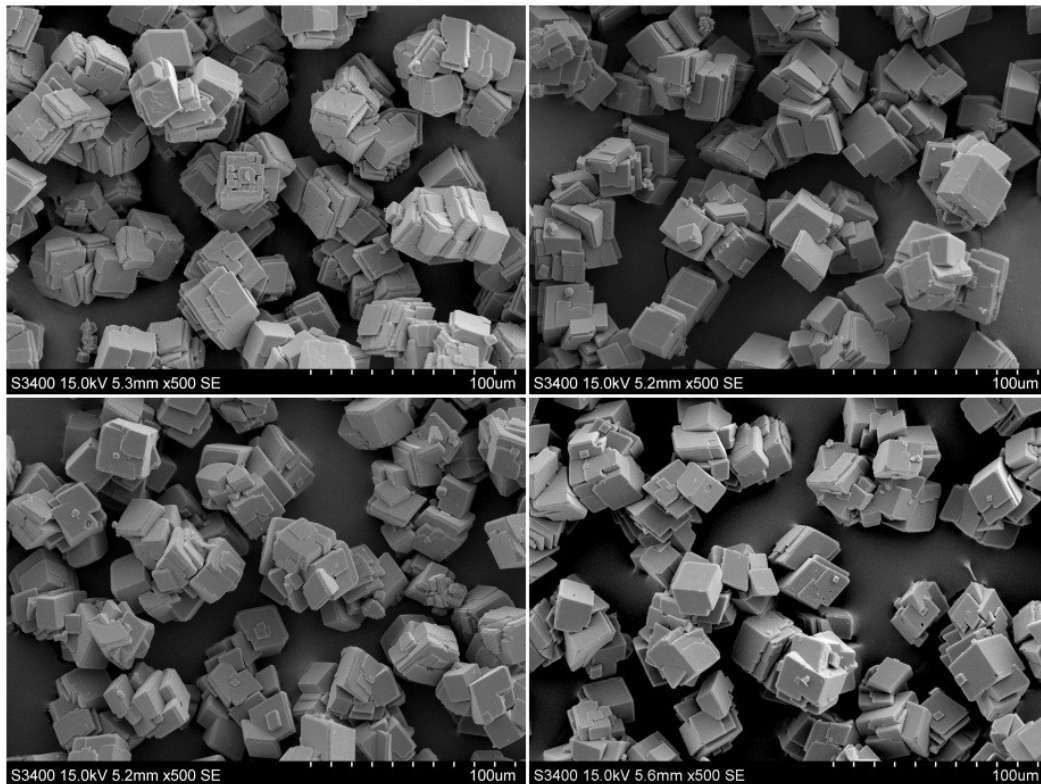


Figure 5.20: Two parallel calcite experiments grown in 50 and 70 wt% at 40 °C after 50 minutes. Upper row from left: 40-50-1 and 40-50-2. Lower row from left: 40-70-1 and 40-70-2. The scale bar is 100 μm .

In contrast with calcite grown in water and in 30 wt% MEG the crystals grown with higher concentration of MEG have a surface similar to the seeds. According to the concentration profiles in Figure 5.18, parallel calcite growth in 50 and 70 wt% MEG show the most respectable reproducibility of all.

Reproducibility in water at 70 °C is, likewise in water at 40 °C, difficult to achieve, as shown from the concentration profiles for five parallel experiments in Figure 5.21.

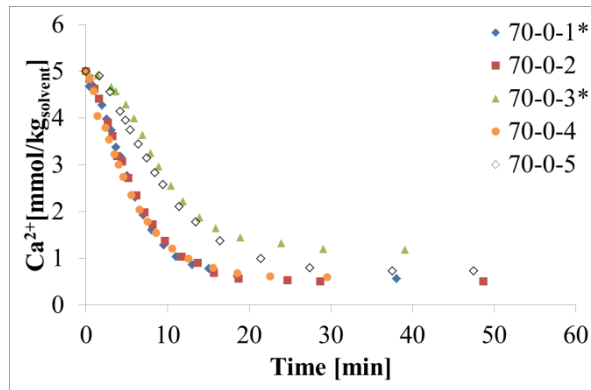


Figure 5.21: Decreasing calcium concentration over time for calcite in water at 70 °C for five parallel experiments. The symbol * denotes experiments where rust was observed in the reactor during the growth.

The solutions reach equilibrium after 20-30 minutes, thus faster than at 40 °C. In the same way as for vaterite it seems that an elevated temperature promotes the growth. The two first experiments, 70-0-1 and 70-0-2, were performed with an initial supersaturation, $S_{cal} = 5.0$. By investigation with SEM aragonite was seen among the calcite as illustrated in Figure 5.22. It is probable that the nucleation of aragonite was a result of the combination high temperature and high initial supersaturation. To options, a lowered initial supersaturation or inoculation of less seed particles, were discussed as solutions to avoid aragonite formation. It was decided to decrease the initial supersaturation from 5.0 to 4.0 for the remaining water experiments.

In two of the water experiments at 70 °C, 70-0-1* and 70-0-3*, rust was observed in the reactor during the experiment. The rust appeared as some brown coloured particles on the filtration paper. After the appearance of rust in the first experiment, 70-0-1*, it was decided to replace the propeller and baffles made of steel with equivalent equipment coated with Teflon to avoid corrosion. A drawback with the Teflon coated propeller is that the framework inside is made of steel. At the point where the propeller blades are connected to the framework a small steel bolt is visible. Pictures of the two propellers are shown in Appendix H. Despite attempts of covering the bolt with Teflon tape, the corrosion problem was not eliminated. Thus, in the third experiment, 70-0-3*, rust was observed again. Since none of the concentration profiles for experiments with rust problems deviated from the other profiles it was decided to include both of them for further investigation. Characteristic peaks for iron oxides (rust) were not found from the XRD analysis. It has probably not been enough iron oxides.

It should be mentioned that the propellers and baffles in the two experimental setups, made of steel and Teflon respectively, are not identical in terms of size. This could influence the flow conditions in the reactor and consequently have an impact on the determination of growth. It was, however, assumed that the different propellers did not affect the growth studies to a large extent. It was decided that the attempt of eliminating rust was more important than to use identical propellers.

SEM pictures of calcite seeds and five parallels calcite growth in water at 70 °C is shown in Figure 5.22.

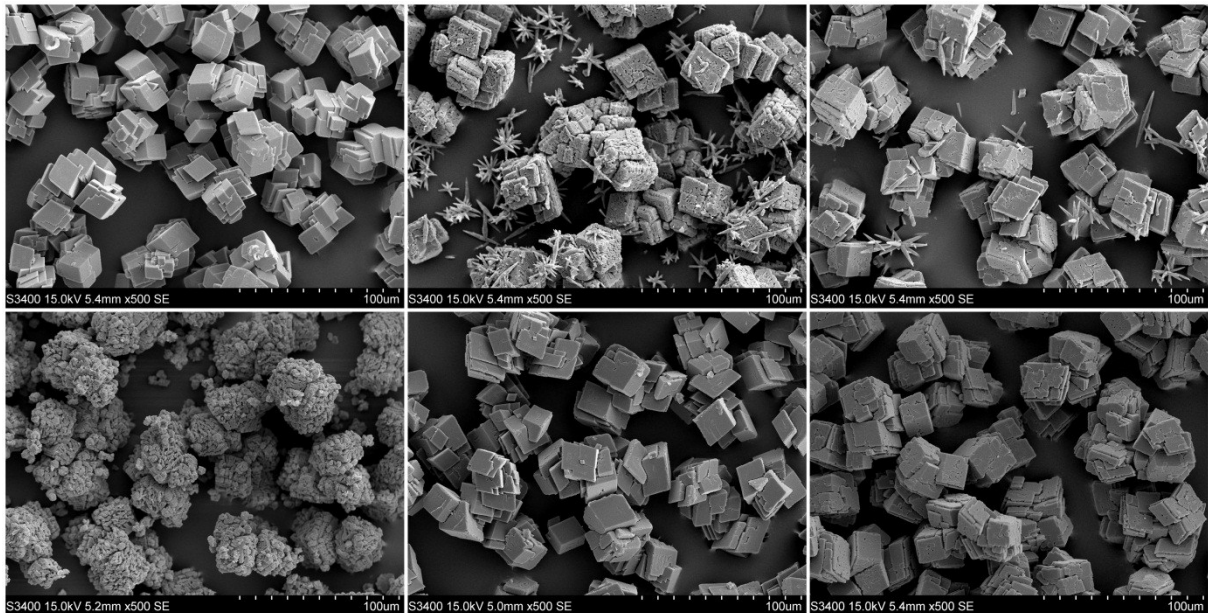


Figure 5.22: Calcite seeds and five parallels calcite grown in water at 70 °C after 50 minutes. Upper row from left: Seeds, 70-0-1* and 70-0-2. Lower row from left: 70-0-3*, 70-0-4 and 70-0-5. The symbol * denotes experiments where rust was observed in the reactor during the growth. The scale bar is 100 μm.

As mentioned above, SEM pictures of the two experiments executed with an initial supersaturation, $S_{cal} = 5.0$, reveal nucleation of aragonite. The polymorph exhibits as needle or star-shaped particles as described in literature (Flaten et al., 2009). Despite observation of aragonite in some experiments, no traces of this polymorph were found by the XRD analysis. Even though aragonite has characteristic peaks between the employed diffraction angles (20 – 60 °) (Beck and Andreassen, 2010), it could be that its amount was insufficient to be detected.

Crystals from the two experiments where rust was detected, 70-0-1* and 70-0-30*, appear with varying surface features as seen in Figure 5.22. Additionally, nucleation of calcite is seen in 70-0-30*. Interestingly, the surface is reminiscent of the surfaces seen at calcite grown in water at 40 °C from Figure 5.17. If traces of corrosion in the growth reactor result in crystals with a rugged surface, it could be argued that the water experiments at 40 °C also suffered from corrosion problems. Hence, there is a possibility that experiments experienced corrosion even though no rust was observed in the reactor or at the filtration paper. However, it could not be concluded that rust inhibits the growth. The concentration profile for the experiment, 70-0-1*, did not reach equilibrium slower than parallel experiments even though rust was observed.

Concentration profiles for three experiments performed at 70 °C in solutions with MEG are demonstrated in Figure 5.23. One and two experiments were conducted with 30 and 70 wt% MEG, respectively.

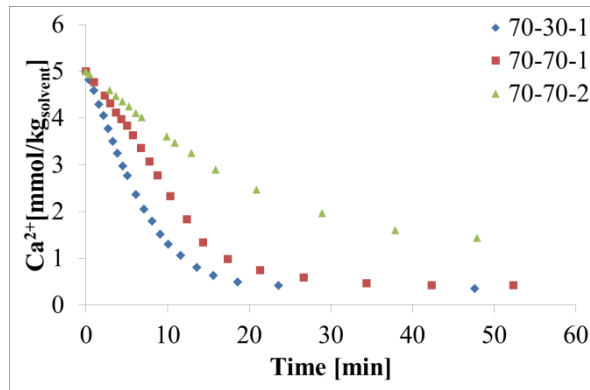


Figure 5.23: Decreasing calcium concentration over time for calcite in 30 and 70 wt% MEG at 70 °C.

The tendency shown at 40 °C, that increased MEG concentration reduces the time needed to reach equilibrium, recur at 70 °C. The reproducibility when the MEG content is 70 wt% is in spite of this poor. SEM pictures of the three experiments in MEG at 70°C are shown in Figure 5.24.

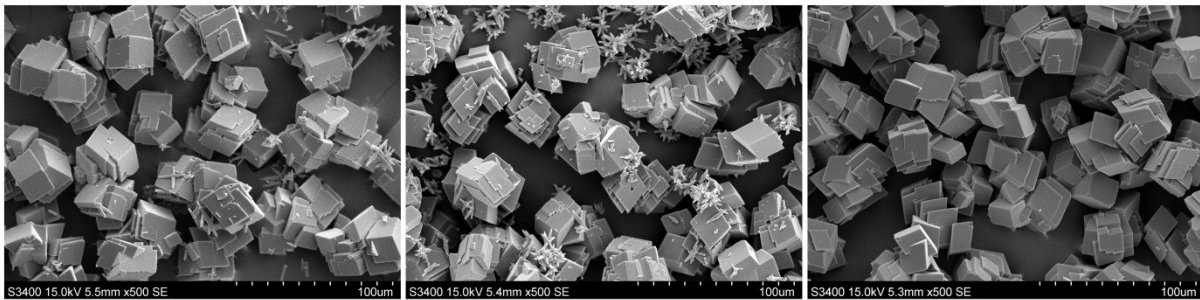


Figure 5.24: One and two calcite experiments grown in 30 and 70 wt%, respectively, at 70 °C after 50 minutes. From left: 70-30-1, 70-70-1 and 70-70-2. The scale bar is 100 µm.

Experiment 70-30-1 and 70-70-1 were conducted with an initial supersaturation, $S_{cal} = 5.0$. Similarly as for water experiments this induced nucleation of aragonite. Hence, for the second parallel with 70 wt% MEG S_{cal} was reduced to 4.0. No nucleation was then observed. The Teflon propeller and baffles were used in these MEG experiments, and no rust was seen. None of these MEG experiments appeared with rugged surfaces. It is difficult to draw any conclusions whether there is a connection between experiments with rust and the feature of the crystal surface from these experiments.

5.3.2 Calcite growth order and growth rate constants

Growth data for calcite are determined the same way as for vaterite. Details on calculations are given in Appendix B. However, because of its cubic shape, calcite has been calculated both as spheres and cubes for comparison. The growth data, from calcite calculated as cubes, for 0 and 70 wt% at 40 °C and 70 °C are shown in Figure 5.25. The experiments with 30 and 50 wt% MEG are excluded from the graphs for better visualization of the trends. It is referred to Appendix F for a complete collection of graphs.

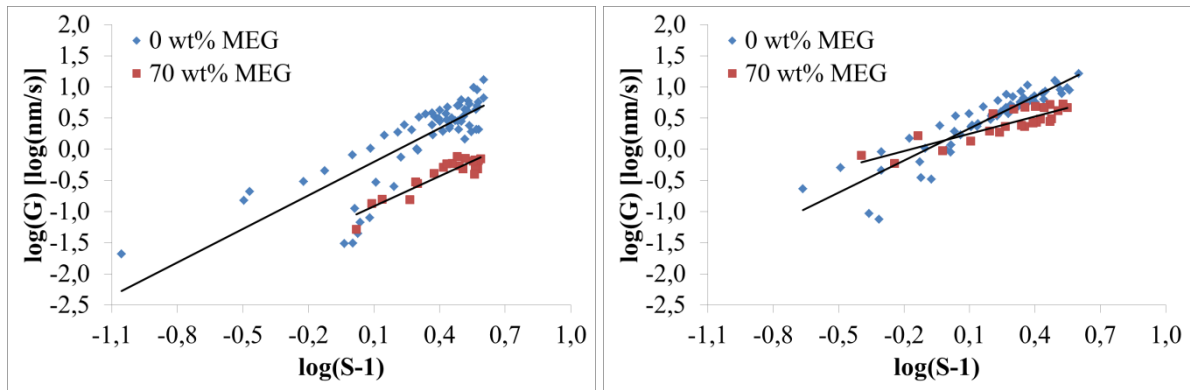


Figure 5.25: Log(G) as a function of log($S-1$) for calcite with 0 and 70 wt% MEG at 40 °C (left) and 70 °C (right).

Data points from all parallels at the given conditions are included in the graphs to obtain the linear regression models. The growth order and growth rate constants obtained from Figure 5.25 and corresponding graphs are reported in Table 5.9. Calculated values from both cubic and spherical shaped calcite particles are given in the table. For information on number of parallels it is referred to Table 4.1.

Table 5.9: Growth order, g , and growth rate constants, k_g , for calcite calculated as spheres and cubes. For number of parallel experiments it is referred to Table 4.1. *) These values are determined from an average of five parallel experiments with deviating growth rate constants. Hence, the standard deviation is larger than the actual average.

| MEG [wt%] | Sphere or Cube | g (40 °C) | g (70 °C) | k_g [nm/s] (40 °C) | k_g [nm/s] (70 °C) |
|-----------|----------------|-----------------|-----------------|----------------------|----------------------|
| 0 | Sphere | 2.54 ± 0.96 | 2.00 ± 0.51 | $0.50 \pm 0.53^*$ | 1.79 ± 0.95 |
| 30 | Sphere | 1.70 ± 0.38 | 1.38 | 0.55 ± 0.26 | 2.12 |
| 50 | Sphere | 1.30 ± 0.01 | - | 0.42 ± 0.04 | - |
| 70 | Sphere | 1.26 ± 0.10 | 0.92 ± 0.12 | 0.16 ± 0.04 | 1.94 ± 0.85 |
| 0 | Cube | 2.54 ± 0.96 | 1.99 ± 0.50 | $0.40 \pm 0.43^*$ | 2.41 ± 0.80 |
| 30 | Cube | 1.70 ± 0.38 | 1.38 | 0.44 ± 0.21 | 1.71 |
| 50 | Cube | 1.31 ± 0.02 | - | 0.34 ± 0.04 | - |
| 70 | Cube | 1.15 ± 0.26 | 0.92 ± 0.12 | 0.15 ± 0.07 | 1.57 ± 0.69 |

The difference in growth order between calcite calculated as spheres and as cubes is relatively low. For growth rate constants the difference is larger. The trends are however the same. Calcite will be considered as cubic shaped in all discussions onwards. The standard deviations of growth order and growth rate constants from the water experiments at both temperatures are large. This is a result of the difficulties of obtaining reproducible growth data at these conditions.

The growth order in water at 40 °C was found to be 2.54 ± 0.96 . Olderøy et al. (2011) reported that calcite, although with spherulitic seeds, at the same conditions followed a parabolic rate law with $g = 2$. Other researchers have also suggested that calcite follows a parabolic rate law (Nielsen and Toft, 1984) and (Kralj et al., 1997). Taken into consideration

the large standard deviation in this work a second order growth is not unreasonable. The growth order decreases as the MEG concentration is elevated. This trend was also seen for vaterite, and the possible explanation of reactant limitation was discussed by evaluating the concentration of free ions of calcium and carbonate, respectively. Thus, the concentration of free ions was also determined for calcite experiments. The concentrations are reported in Appendix I. As was seen for vaterite the deviation between concentrations of calcium and carbonate ions increases with increased wt% MEG. Consequently, this points toward a change from a parabolic to a linear rate law when the co-solvent concentration increases also for calcite.

As was done for vaterite, growth rate constants when assuming parabolic growth were determined. The graphs in Figure 5.26 illustrate how the growth rate constants are influenced by an increased MEG concentration at 40 °C and elevated temperature in water. The same trends were found for MEG concentrations at 70 °C and temperatures with 30 and 70 wt% MEG, respectively. These plots could be found in Appendix F.

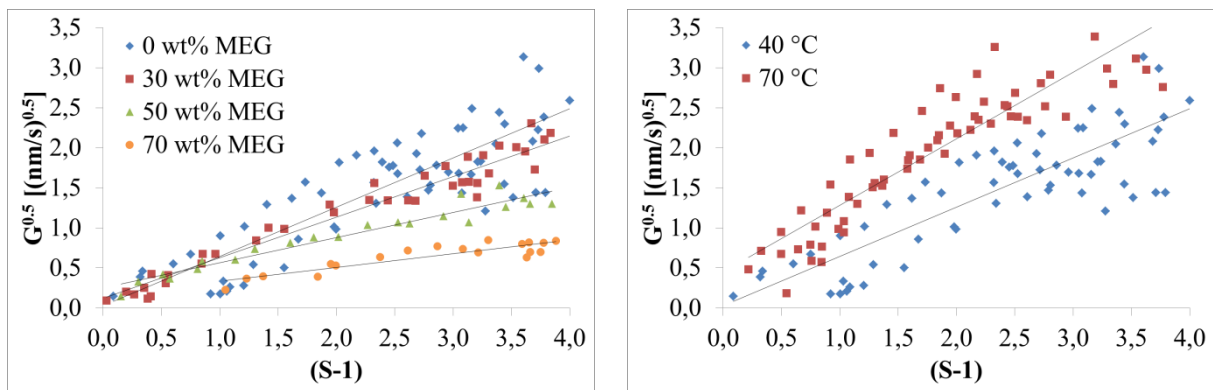


Figure 5.26: $G^{0.5}$ as a function of (S-1) for calcite with varying MEG concentration at 40 °C (left) and varying temperature in water (right).

Data points from all parallels at the given conditions are included in the graphs to obtain a linear regression model. A steeper slope gives a larger growth rate constant. All growth rate constants are reported in Table 5.10.

Table 5.10: Growth rate constants for calcite when assuming parabolic growth mechanism calculated as sphere and cube. *) These values are determined from an average of two parallel experiments with deviating growth rate constants. Hence, the standard deviation is larger than the actual average.

| MEG [wt%] | Sphere or cube | $k_{g=2}$ [nm/s] (40 °C) | $k_{g=2}$ [nm/s] (70 °C) |
|-----------|----------------|--------------------------|--------------------------|
| 0 | Sphere | 0.65 ± 0.20 | 1.23 ± 0.52 |
| 30 | Sphere | 0.32 ± 0.08 | 0.52 |
| 50 | Sphere | 0.14 ± 0.05 | - |
| 70 | Sphere | 0.02 ± 0.01 | $0.10 \pm 0.12^*$ |
| 0 | Cube | 0.54 ± 0.17 | 0.95 ± 0.40 |
| 30 | Cube | 0.26 ± 0.07 | 0.42 |
| 50 | Cube | 0.11 ± 0.05 | - |
| 70 | Cube | 0.02 ± 0.01 | $0.08 \pm 0.10^*$ |

The same trends that were seen for vaterite growth recur for calcite growth. Elevated temperature and absence of MEG constitute the fastest growing conditions for growth. From 0 – 70 wt% MEG, the growth rate constant reduces 27 times at 40 °C and almost 12 times at 70 °C.

Growth rate constants for calcite in water at 40 °C are reported in literature as shown in Table 5.11. The rate constant found in this work is however deviating from the literature values. There are different ways of preparing calcite seeds and different methods of performing growth experiments. It could be argued that these two matters could give varying growth rate constants.

Table 5.11: Growth rate constants for calcite in water at 40 °C reported in literature. *) This value was estimated from a polynomial function made on the basis of growth rate constants at 10.2 – 54.5 °C reported by Kralj et al. (1997).

| Work | $k_{g=2}$ [nm/s] |
|-----------------------|------------------|
| Kralj et al. (1997) | 0.07* |
| Flaten (2010) | 0.19 ± 0.06 |
| Olderøy et al. (2011) | 0.36 |
| This work | 0.54 ± 0.14 |

Kralj et al. (1997) made the supersaturated solution by mixing CaCl_2 and Na_2CO_3 solutions. The latter was the source of carbonate giving a high pH (~10), instead of CO_2 -bubbling which provides a low pH (~7). The growth was monitored by pH-measurements instead of titration (Kralj et al., 1997). Flaten (2010) executed the seeded calcite experiments the same way as in this work, but with a different type of seeds. By lowering the temperature from 30 to 10 °C and the stirring rate from 500 to 300 rpm, spherulitic calcite seeds are formed. Olderøy et al. (2011), who also prepared calcite seeds at 10 °C but with a stirring rate of 600 rpm, obtained spherulitic calcite seeds as well. Other researchers have also reported that a preparation of calcite seeds at 10 °C gives less aggregated particles (Beck and Andreassen,

2012). The experiments were conducted with NaOH solutions bubbled with CO₂ as the carbonate source and measurements of calcium depletion by titration (Olderøy et al., 2011). A pattern, of which type of seeds and which growth experiment method that gives higher or lower rate constants, is difficult to find.

For vaterite growth experiments, $k_{g=2}$ at 40 °C in water was found close to literature values independent on seeds and growth experiment method. When it for calcite growth is a variation of both $k_{g=2}$ and the method used, it is difficult to make any conclusions. It seems, however, that the growth rate constants in this work differ from literature values. Since the growth rate constant from literature in Table 5.11 also varies among themselves, this could imply that calcite growth is more difficult than vaterite growth to reproduce.

5.4 Comparison of vaterite and calcite growth

5.4.1 Growth order

The same tendency that was observed for vaterite, a reduced growth order with increased MEG concentration and elevated temperature is also seen for calcite. The growth orders are however higher for calcite than for vaterite. It should be mentioned that some of the standard deviations that were calculated for calcite are relatively large. With a growth of second order the possible rate determining steps could be diffusion at the surface, the integration jump or local diffusion at the kinks. To find which of these steps that limits the growth was not the aim of this work.

When the constituent ions, calcium and carbonate, move from the aqueous solution to the crystal surface, they must release their hydration water molecules before incorporation in the crystal lattice (Nielsen, 1984). This dehydration process requires energy, and it is stated that the activation energy for both adsorption and surface integration may be dependent on the dehydration. Nielsen (1982) found that the rate of surface integration was one thousand of the rate of dehydration of the cation (There is a much stronger bonding between the cation and the water molecule than to the anion(Nielsen, 1984)). Therefore, it is most likely that the surface integration is rate determining.

A change in growth order implies a change in the growth mechanism. It has been discussed that both vaterite and calcite experience a change from surface integration controlled to diffusion controlled growth when the growth order approaches one. All experiments were performed with non-stoichiometric ratios of calcium and carbonate. It was found both in vaterite and calcite seeded experiments, that the ratios of calcium and carbonate are becoming more non-stoichiometric as the co-solvent concentration increases. This implies that the low concentration of carbonate in the MEG-rich experiments possibly limits the supply of reactant to the crystal surface. First order kinetics could also mean that the growth is limited by transition of growth units to adsorption layer around the crystal surface. Whether the diffusion or adsorption is rate determining is difficult to decide, and outside the scope of this work.

Is it possible that the growth order could change during the growth in one experiment? The growth order is, as described in Chapter 2.3, dependent on supersaturation. While the reactants are consumed, the supersaturation decreases and the growth order could perhaps change. Consequently, it would be a different growth mechanism and a change in which processes that controls the growth rate. In this work an overall growth order for the entire de-supersaturation has been determined.

5.4.2 Growth rate constants

It is stated that at 70 °C in water calcite is the slowest growing polymorph, and vaterite the fastest (Ohtaki, 1998). The same trend is also seen in this work. Ohtaki (1998) does not

mention if the same tendency is seen at other temperatures. It is, however, shown in this work that calcite in water is the slowest growing polymorph also at 40 °C. A comparison of graphs for $G^{0.5}$ as a function of (S-1) for vaterite and calcite in water at the two different temperatures is illustrated in Figure 5.27.

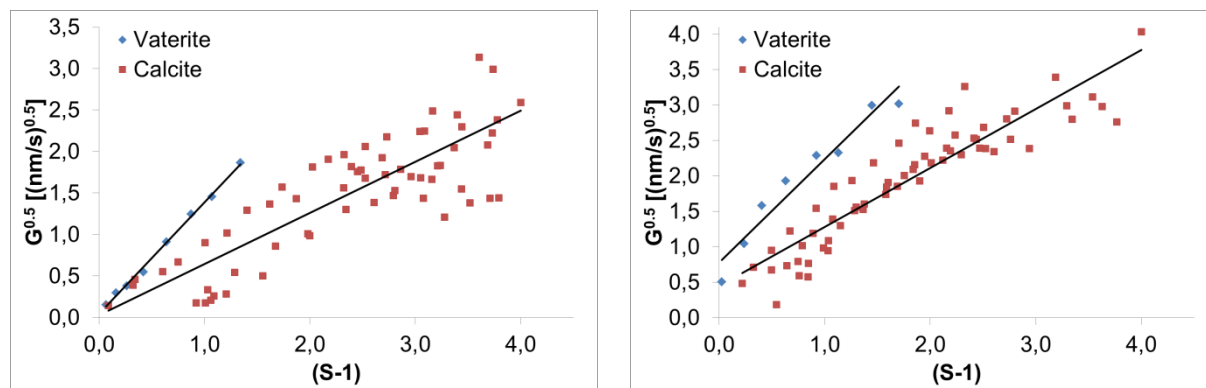


Figure 5.27: Comparison of $k_{g=2}$ for vaterite and calcite in water at 40 °C (left) and 70 °C (right).

As shown in Chapter 5.2 and 5.3, the growth rate constants at 40 °C found from these plots, when assuming second order growth is $k_{g=2} = 1.81$ nm/s for vaterite and 0.54 nm/s for calcite. At 70 °C the growth rate constants are $k_{g=2} = 2.12$ nm/s and 0.95 nm/s for vaterite and calcite, respectively. This means that, in water, calcite grows 70 % slower than vaterite at 40 °C, and 55 % slower at 70 °C. It is also seen that for both polymorphs the reduction of $k_{g=2}$ with increased MEG concentration is larger at 40 °C than at 70 °C.

5.4.3 Effect of MEG as solvent

The effect of MEG on the calcium carbonate growth may be described by examining physical parameters of the system as described in Chapter 2.7. The viscosity of aqueous MEG solutions increases with a higher concentration of MEG (Hayduk and Malik, 1971). The researchers also report that the viscosity of pure MEG reduces as the temperature is elevated. In the present work it has been demonstrated that MEG reduces the growth rate both for vaterite and calcite. A higher viscosity of the aqueous solution causes a lower diffusivity of growth units from the bulk solution to the crystal surface, thus decreasing the growth rate constant. For both vaterite and calcite growth the non-stoichiometric ratios between calcium and carbonate increased in such way that the activity of carbonate was more limited as the co-solvent concentration was raised. This could imply, that of the growth units, the diffusivity of carbonate is the most influenced by the co-solvent. It is observed that the reduction of growth rate constants with increased MEG concentration corresponds to the reduction of growth order and a possible change of growth mechanism. Consequently, there could possibly be a link between MEG's influence on respectively growth order and growth rate constants.

The effect of viscosity was investigated further. Growth rate constants from the vaterite experiments were calculated assuming linear rate law as seen in equation (4.10). The actual viscosities of MEG at given weight percentages and temperatures were found from Kidnay

and Parrish (2006). The rate constants were plotted as a function of these viscosities as shown in Figure 5.28. The trend is clear, increased concentrations of MEG gives enhanced viscosity and correspondingly a lowered growth rate constant.

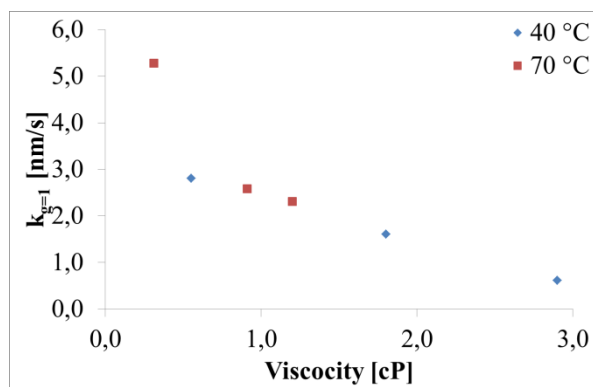


Figure 5.28: Growth rate constants for vaterite as a function of viscosity at 40 °C and 70°C (Kidnay and Parrish, 2006).

Even though it seems like a change in the viscosity could explain the reduced growth rates other parameters could also have an influence. In literature, it is stated that increased concentrations of MEG reduces the solubility, based on concentrations, of calcite (Kaasa et al., 2005). Later, it has been suggested that this is also expected for vaterite (Flaten, 2010). In accordance with Mullin (2001), a change in solubility could change the growth mechanism. With a lower solubility of the solute in the solvent, the crystal surface will become smoother due to a higher α -factor. A smoother surface means that fewer kinks are available for the integration of growth units, and hence the growth rates will be reduced (Davey, 1982). Generally, this implies that the mechanism is spiral growth with $g = 2$. Consistent with Davey (1982), reduced growth rates with reduced solubility (more MEG) were seen in this work. It has, however, been shown that increased amount of MEG causes a linear growth rate law with $g = 1$. Hence, the change in solubility alone cannot explain the change of growth mechanism.

Flaten et al. (2010b) studied MEG's effect on interfacial tension in unseeded experiments. It was found that the interfacial tension between the crystal and the solution decreased with increased MEG concentration. The tendency was the same regardless of whether the precipitating polymorph was calcite or vaterite. According to Ålander and Rasmuson ((2007 via Flaten (2010)) a lowered interfacial tension gives a shorter distance between the kinks at the crystal surface and will therefore cause a faster growth. In this work the opposite trend is observed. The lowered interfacial tension with increased MEG concentrations implies a slower growth. Consequently, the reduced growth rate constants with increased wt% MEG cannot only be explained by change in interfacial tension.

As stated by Davey (1982) specific adsorption of additives in mole fractions down to 10^{-9} could change the crystal growth rates. A solvent like MEG could be compared with an additive and it is realistic to assume that MEG, in a concentration range of 30 – 70 wt%, could be adsorbed as well. Adsorption of the solvent at specific sites on the crystal surface will reduce the growth rates. For instance could kink sites occupied by the solvent cause a higher

energy barrier for the growth to continue (Davey, 1982), and hence give a slower crystal growth. However, in this work it is seen that the growth order is closer to one when the MEG concentration increases. This means that the growth is not determined by surface integration and therefore most likely not determined by specific adsorption of MEG at kink sites either.

In the review of the co-solvent's effect on growth it is interesting to examine which polymorph that is the most influenced. Since the respective weight percentages of MEG have been varied for the two polymorphs, the rate constants could not be compared directly. An idea was to use a model of vaterite growth rates developed by Flaten (2010) to compare with calcite growth. The model is valid for vaterite growth, based on the parabolic rate law, for temperatures between 40 and 70 °C and MEG concentrations between 0 and 70 wt%:

$$G(T, \text{wt\% MEG}) = (-4.8 \cdot 10^{-9} + 2.6 \cdot 10^{-11} T - 2.3 \cdot 10^{-11} \text{wt\% MEG}) \cdot (S-1)^2 \quad (5.1)$$

The intention was to calculate the growth rate, G , for vaterite at 40 and 70 °C, 0 and 70 wt% MEG at a given supersaturation and compare it with the growth rate for calcite at the same temperature, wt% MEG and supersaturation. The attempt was not succeeded, and it could not be concluded whether MEG has the largest growth reducing effect on vaterite or calcite. In literature, however, it has been proposed that at 40 °C, MEG has the largest growth reducing influence on growth of calcite (Flaten, 2010).

5.4.4 Effect of temperature

Söhnle and Garside (1992) emphasize the importance of temperature influence on crystal growth rates. In the present work it has been shown that the growth rate constants both for vaterite and calcite increases as the temperature is elevated. The temperature dependency could be explained by the Arrhenius equation, which gives a reaction's rate constant, k , as a function of absolute temperature, T , and activation energy, E_a . On integrated form Arrhenius equation is expressed like

$$k = A'' \cdot \exp(-E_a / RT) \quad (5.2)$$

Where A'' is a pre-exponential factor and R is the universal gas constant. Arrhenius equation is valid for mostly all chemical reactions (Helbæk and Kjelstrup, 1999). The rate constant will increase with increased temperature as long as the activation energy is positive. Activation energy for crystal growth of vaterite has been found to be 57.1 kJ/mol (no standard deviation reported) (Kralj et al., 1990) and for calcite 55.29 ± 7.04 kJ/mol (Kralj et al., 1997). Consistent with Mullin (2001), activation energies for diffusion reactions are generally $\sim 10 - 20$ kJ/mol and for surface integration reactions $\sim 40 - 60$ kJ/mol. Furthermore, it is stated that crystal growth rates are likely to be diffusion controlled at high temperatures and surface integration controlled at low temperatures. This is due to that the rate of integration, compared to the rate of diffusion, increases more rapidly with temperature (Mullin, 2001).

In this work it has been shown that vaterite at 70 °C obtains a growth of first order. Whether this is caused by diffusion or adsorption determined growth is hard to define. If, however, the growth is diffusion controlled, the statement by Mullin (2001) could be an explanation. It is however not specified which temperatures that are defined high and low.

It is interesting to examine to which degree a change in temperature influences the growth of vaterite and calcite respectively. In water, the growth rate constant, $k_{g=2}$, for vaterite raises 15 % when the temperature is elevated from 40 to 70 °C, whereas for calcite the increase is 44 %. This implies that calcite growth is most sensitive to temperature variation compared to vaterite. One should however be cautious in drawing conclusions about the temperature effect since the standard deviation of calcite in water is relatively large.

5.5 Sensibility analysis and uncertainty

An important aspect with the seeded growth experiments is the certainty that inoculation of seeds should be highly reproducible for each experiment. Consequently, a complete examination of the seeds population should be done. In this work, the vaterite and calcite seeds have been investigated by the Coulter Counter. The aim has been to obtain a precise value for number and volume of the seeds. In the calculation of growth rates, from equation (2.15),

$$G = \frac{dL}{dt}$$

the characteristic dimension, L , of the particle are calculated from the particle volume. The increased particle volume, resulting from a decrease in calcium concentration, is obtained from equation (2.22):

$$\Delta V = \frac{-\Delta c \cdot M_w}{\rho \cdot N}$$

It is interesting to examine the parameters in this equation that comes from experimental measurements. Molecular weight, M_w , and density, ρ , of calcium carbonate are constants taken from literature and are therefore not evaluated. The equation is a function of number of seed particles, N . Thus, a correct number of seed particles and their initial volumes are important for the growth calculations. The uncertainty in determination of number and particles of seed is obtained from repeated Coulter Counter measurements. Additionally, the decreased calcium concentration, $-\Delta c$, are also a measured value which involve some uncertainty. During the conversion from calcium concentration to supersaturation ratios, and further to determination of growth order and growth rate constants in various linear regression models, there are several steps where uncertainty may be prevailing. Both these matters will be examined below.

5.5.1 Number and volume of particles

For calcite growth determination seeds from one batch were used throughout the experiments. The standard deviation reported in Table 5.2 for number and volume of particles were 9 % and 8 %, respectively. A sensibility analysis was executed in order to determine how these deviations influences the growth order and growth rate constants. It was chosen to vary the number and volume of particles with ± 10 %. It is assumed that a 10 % variation in number of particles will result in 10 % variation in volume of particles.

Two parallel calcite experiments, 40-0-1 and 40-0-4, performed at 40 °C with 0 wt% MEG, were tested. By altering the number and volume of particle ± 10 % new values of growth order, g , growth rate constants, k_g , and growth rate constants when assuming parabolic growth, $k_{g=2}$ were determined. It was found that the ± 10 % variation had the smallest influence on growth order. The growth order varied $\pm 0.7 - 3.0$ % from the actual value. The growth rate constant, k_g , varied $\pm 4 - 10$ %. The growth rate constant assuming parabolic growth varied the most. This rate constant altered $\pm 13 - 18$ % from the actual value and it was therefore decided to investigate $k_{g=2}$ further. $G^{0.5}$ was calculated, by inserting the different values for $k_{g=2}$ in the equation $G^{0.5} = k_{g=2}^{0.5}(S-1)$, and plotted against $S-1$. This resulted in six graphs, two for the actual $k_{g=2}$ and four for the $k_{g=2}$ from the ± 10 % variation, as shown in Figure 5.29.

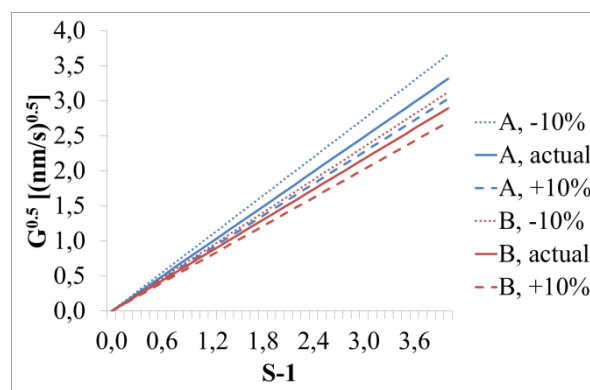


Figure 5.29: $G^{0.5}$ as a function of $(S-1)$ plotted with the actual $k_{g=2}$ for two parallels, 40-1-1 (A) and 40-0-4 (B), and with the $k_{g=2}$ when number and volume of particles have been varied ± 10 %.

It could be seen that the graphs, representing a variation of + 10 % and - 10% in number and volume of particles for experiment A and B, respectively, are overlapping each other. This implies that the standard deviation of number and volume of particles could result in growth rate constants that are approaching each other.

5.5.2 Growth data

The samples that were withdrawn from the supersaturated solution during the growth were weighted and titrated with EDTA to determine the calcium concentration. When the concentrations were plotted versus reaction time the curve showed an exponential decreasing

trend for the calcium depletion. Some data points, however, did not fit to the exponential curve. These points were considered as measurement errors and consequently removed.

After the conversion from calcium concentration to corresponding supersaturation ratios in MultiScale, $\log(G)$ and $G^{0.5}$ values were plotted against $\log(S-1)$ or $(S-1)$, respectively. The points constituted a linear trend but also here there was some scattering of the data points. Again, some points were removed. How the selection, of which points that were eliminated from the linear regression, was done could be discussed. It is interesting to investigate to which extent the choice of deviating points, that were removed, have had an influence on the determination of growth order and the growth rate constants.

One calcite experiment, 70-0-4, was selected for the investigation. The selected data points and the data points that were removed are shown in Figure 5.30. The determined growth order, g , growth rate constant, k_g , and growth rate constant assuming parabolic growth, $k_{g=2}$, for the two alternative selection of data points are reported in Table 5.12. The percentage deviations between the respective values are also shown.

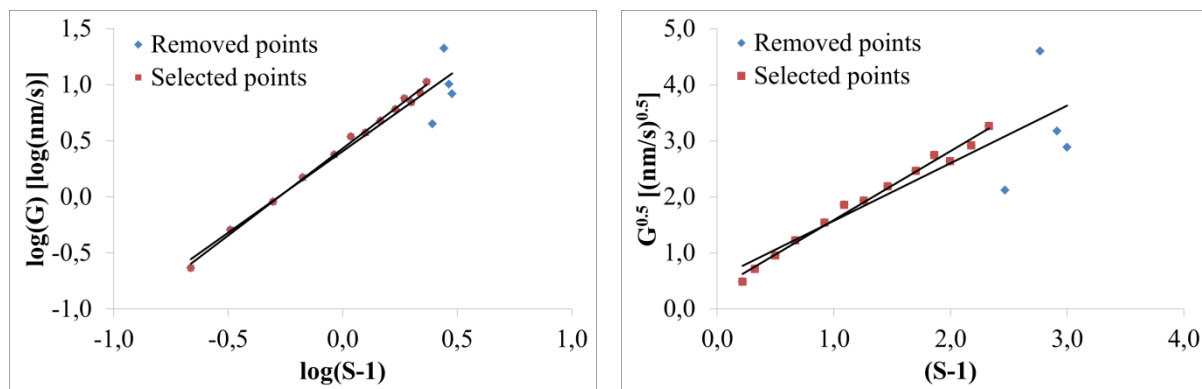


Figure 5.30: Influence of scattering of data points on crystal growth. Plots for determination of g and k_g (left) and $k_{g=2}$ (right).

Table 5.12: Percentage deviation of growth order and growth rate constants based on different data points.

| | g | k_g [nm/s] | $k_{g=2}$ [nm/s] |
|----------------------------|------|--------------|------------------|
| Selected points | 1.55 | 2.70 | 1.52 |
| With removed points | 1.45 | 2.56 | 1.06 |
| Deviation [%] | 6 | 5 | 30 |

It appears that the rate constant, $k_{g=2}$, is the most influenced value by which data points that are selected. The value differs 30 % depending on which points the linear regression model is based on. The same tendency was seen in the sensitivity analyse of influence of particle number and volume. It seems that the growth rate constant assuming parabolic rate law is the most sensitive parameter to variations caused by measurement errors.

6 Conclusions

Seeded batch experiments for vaterite and calcite at 40 and 70 °C with various MEG compositions have been performed in order to determine the effect of MEG on the growth rates. The results show that both polymorphs experience the highest growth rates with absence of MEG at high temperature.

The growth rate constant assuming parabolic growth mechanism for vaterite decreased from $k_{g=2} = 1.81$ to 0.24 nm/s when the MEG concentration increased from 0 – 60 wt% at 40 °C and from 2.12 to 0.63 nm/s at 70 °C. For calcite growth, with an increase of co-solvent concentration from 0 – 70 wt%, the reduction is from $k_{g=2} = 0.52$ to 0.02 nm/s at 40 °C and from 0.95 to 0.08 nm/s at 70 °C. For growth in water it is concluded that calcite is the slowest growing polymorph. It has also been shown that the rate constants of both polymorphs reduces the most at 40 °C compared to at 70 °C when the co-solvent concentration increases.

The results disclose a growth order close to two for vaterite in water at 40 °C. This implies a growth controlled by surface integration. Increasing the MEG concentration gives a growth approaching first order. At 70 °C $g = 1$ at all MEG concentrations and diffusion or adsorption controlled growth is suggested. The growth order for calcite in water at 40 °C is approximately 2.5. The same trend as for vaterite, with reduced order with increased co-solvent composition and temperature, is seen. To distinguish whether diffusion or adsorption are rate determining is without of the scope of this work. However, diffusion controlled growth is not expected at low growth rates caused by increased amount of MEG. Hence, it is assumed that the possible diffusion control is a result of reactant limitation of carbonate due to the experimental conditions with non-stoichiometric reactant ratios.

The influence of the co-solvent on the growth rates were discussed by examining different physical parameters of the system. It is likely that MEG reduces the growth rates due to its high viscosity. It is proposed that this lowers the diffusivity of growth units from the bulk to the crystal surface. The temperature effect on the growth could be described by Arrhenius equation.

It was found that there is a larger variation in number and volume of particles from different seed populations than from the same. Additionally, for seeds from the same population, number of particles varies more than volume of particles. Both observations could be explained by the stochastic nature of nucleation. Precise determination of number and volume of seed particles is important in calculation of growth rates. By implementing a sensitivity analysis it was revealed that the growth rate constant assuming parabolic rate law, $k_{g=2}$, is the most sensitive parameter to variations in number and volume of particles.

7 Further work

The scope of this project has been investigation of vaterite and calcite crystal growth at 40 °C and 70 °C in seeded batch experiments with a MEG concentration between 0 and 70 wt%. For further work it is suggested to examine growth with a wider temperature range, for example from 25 – 90 °C. The co-solvent composition could also be extended to 80 wt%. Additionally, it is an idea to carry out experiments with same amount of co-solvent for both polymorphs to better compare the MEG effect on vaterite and calcite, respectively.

The present experiments have been performed with non-stoichiometric calcium to carbonate ratios. It has been discussed to which extent reactant limitation have had an effect on the growth. To elucidate this it is proposed to do experiments with stoichiometric ratios.

All experiments in this work have been carried out with carbonate originating from CO₂-bubbling in an alkaline environment. This gives a low pH (~7). It would be interesting to carry out experiments with the same temperature and wt% MEG at high pH (~ 10) by using Na₂CO₃ as the source of carbonate. By doing this it could be determined how the rate of regeneration of carbonate from the CO₂ gas is affected by MEG.

The growth rates in this work have been determined by measurement of the depleting calcium concentration with titration in a batch reactor. The constant composition method, where the supersaturation is held steady, is an alternative technique for crystal growth studies as described in Chapter 3. Experiments with this method should be employed as it allows for growth studies at higher levels of supersaturation. By this means it could be determined if a different growth mechanism is obtained with a change in supersaturation as illustrated in Figure 2.6. Additionally, since several values of the growth rate at the constant supersaturation are provided, better statistics is provided.

In the present work it has been difficult to obtain a good reproducibility for calcite growth. Problems with corrosion in the reactor have been discussed as a possible explanation for this. Consequently, the reactor should be equipped so that rust problems are eliminated, for example with a propeller and baffles made of glass. To examine how corrosion affects the growth rates and crystal habit it could be an idea to study calcite growth with iron additives. Disregarding the corrosion problem in the lab scale reactor, iron ions are also present in the gas stream due to pipe line corrosion, and is therefore interesting to study independent on rust problems in this work (Flaten, 2010).

Another recommendation is to study growth in presence of other additives. It could be scale inhibitors or other ions that could be present in the gas processing process like magnesium or barium. Vaterite and calcite is not the only interesting polymorph. Thus crystal growth of aragonite could be investigated. Finally, there is always a good idea to carry out more parallel experiments in order to obtain better statistics.

References

- ANDREASSEN, J.-P., 2001. Growth and Aggregation Phenomena in Precipitation of Calcium Carbonate. Doctoral thesis, Department of Chemical Engineering, NTNU, Trondheim.
- ANDREASSEN, J.-P., and M. J. HOUNSLOW, 2004. Growth and Aggregation of Vaterite in Seeded-batch Experiments. *AIChE Journal* 50 (11): 2772-2782.
- AYLWARD, G., and T. FINDLAY., 2002. *SI Chemical Data*. 5 ed. Milton: John Wiley & Sons Australia LTD.
- BARLAND, A. O., 2012. Nucleation Kinetics and Polymorphism of Calcium Carbonate Particles in Natural Gas Production. Master's thesis, Department of Chemical Engineering, NTNU, Trondheim.
- BECK, R., and J.-P. ANDREASSEN, 2010. The Onset of Spherulitic Growth in Crystallization of Calcium Carbonate. *Journal of Crystal Growth* 312 (15): 2226-2238.
- BECK, R., and J. P. ANDREASSEN, 2012. Influence of Crystallization Conditions on Crystal Morphology and Size of CaCO₃ and Their Effect on Pressure Filtration. *AIChE Journal* 58 (1): 107-121.
- BREČEVIĆ, L., and A. E. NIELSEN, 1989. Solubility of Amorphous Calcium Carbonate. *Journal of Crystal Growth* 98 (3): 504-510.
- CLARKSON, J. R., T. J. PRICE, and C. J. ADAMS, 1992. Role of Metastable Phases in the Spontaneous Precipitation of Calcium-Carbonate. *Journal of the Chemical Society-Faraday Transactions* 88 (2): 243-249.
- DAVEY, R. J., 1982. Solvent Effects in Crystallisation Processes. In *Current topics in Material Science* (8), ed. E. Kaldis, 429-479. North-Holland Publishing Company.
- FLATEN, E. M., 2010. The Effect of MEG (Mono Ethylene Glycol) on the Precipitation Kinetics of Calcium Carbonate related to Natural Gas Production from Subsea Wells. Doctoral thesis, Department of Chemical Engineering, NTNU, Trondheim.
- FLATEN, E. M., M. SEIERSTEN, and J.-P. ANDREASSEN, 2009. Polymorphism and Morphology of Calcium Carbonate precipitated in mixed Solvents of Ethylene Glycol and Water. *Journal of Crystal Growth* 311 (13): 3533-3538.
- FLATEN, E. M., M. SEIERSTEN, and J.-P. ANDREASSEN, 2010a. Growth of the Calcium Carbonate Polymorph Vaterite in Mixtures of Water and Ethylene Glycol at conditions of Gas Processing. *Journal of Crystal Growth* 312 (7): 953-960.
- FLATEN, E. M., M. SEIERSTEN, and J.-P. ANDREASSEN, 2010b. Induction Time Studies of Calcium Carbonate in Ethylene Glycol and Water. *Chemical Engineering Research and Design* 88 (12): 1659-1668.

- FOSS, M., M., SEIERSTEN, AND K., NISANCIOGLU, 2006. *Interaction between Scale Inhibitors and FeCO₃ Precipitation on Carbon Steel*.
- FØRLAND, K. S., 2001. *Kvantitativ analyse*. Trondheim: Tapir.
- GEANKOPLIS, C. J., 2003. *Transport Processes and Separation Process Principles (includes Unit Operations)*. Upper Saddle River, N.J.: Prentice Hall.
- HAYDUK, W., and V. K. MALIK, 1971. Density, Viscosity, and Carbon Dioxide Solubility and Diffusivity in Aqueous Ethylene Glycol Solutions. *Journal of Chemical and Engineering Data* 16 (2): 143-146.
- HELBÆK, M., and S. KJELSTRUP, 1999. *Fysikalsk kjemi*. Bergen: Fagbokforlaget.
- INSTITUTE FOR ENERGY TECHNOLOGY, I., 2011. *Kjeller MEG Loop (KML)*. http://www.ife.no/departments/materials_and_corrosion_tech/projects/kml (accessed 2012/06/27).
- JIANG, S. F., and J. H. TER HORST, 2011. Crystal Nucleation Rates from Probability Distributions of Induction Times. *Crystal Growth & Design* 11 (1): 256-261.
- KAASA, B., K. SANDENGEN, and T. ØSTVOLD, 2005. Thermodynamic Prediction of Scale Potential, pH, and Gas Solubility in Glycol-Containing Systems. In *SPE International Symposium on Oilfield Scale* Aberdeen, United Kingdom.
- KASHCHIEV, D., and G. M. VAN ROSMALEN, 2003. Review: Nucleation in Solutions revisited. *Crystal Research and Technology* 30 (7-8): 555-574.
- KAZMIERCZAK, T. F., M. B. TOMSON, and G. H. NANCOLLAS, 1982. Crystal Growth of Calcium Carbonate. A Controlled Composition Kinetic Study. *The Journal of Physical Chemistry* 86 (1): 103-107.
- KIDNAY, A. J., and W. PARRISH, 2006. *Fundamentals of Natural Gas Processing*. Boca Raton: CRC Press.
- KRALJ, D., L. BREČEVIĆ, and J. KONTREC, 1997. Vaterite Growth and Dissolution in Aqueous Solution .3. Kinetics of Transformation. *Journal of Crystal Growth* 177 (3-4): 248-257.
- KRALJ, D., L. BREČEVIĆ, and A. E. NIELSEN, 1990. Vaterite Growth and Dissolution in Aqueous Solution I. Kinetics of Crystal Growth. *Journal of Crystal Growth* 104 (4): 793-800.
- MERSMANN, A., 2001. *Crystallization Technology Handbook*. New York: Marcel Dekker.
- MULLIN, J. W., 2001. *Crystallization*. Boston: Butterworth-Heinemann.
- MØRK, P. C., 2004. *Overflate og kolloidkjemi - Grunnleggende prinsipper og teorier*. Trondheim: NTNU.
- NIELSEN, A. E., 1984. Electrolyte Crystal Growth Mechanism. *Journal of Crystal Growth* 67: 289-310.

- NIELSEN, A. E., and J. M. TOFT, 1984. Electrolyte Crystal Growth Kinetics. *Journal of Crystal Growth* 67: 278-288.
- NJEGIĆ-DŽAKULA, B., L. BREČEVIĆ, G. FALINI, and D. KRALJ, 2009. Calcite Crystal Growth Kinetics in the Presence of Charged Synthetic Polypeptides. *Crystal Growth & Design* 9 (5): 2425-2434.
- NÝVLT, J., and J. ULRICH, 1995. *Admixtures in Crystallization*. Weinheim: VCH.
- OGINO, T., T. SUZUKI, and K. SAWADA, 1987. The Formation and Transformation Mechanism of Calcium Carbonate in Water. *Geochimica et Cosmochimica Acta* 51 (10): 2757-2767.
- OHTAKI, H., 1998. *Crystallization processes*. Chichester: Wiley.
- OLDERØY, M. O., M. L. XIE, B. L. STRAND, K. I. DRAGET, P. SIKORSKI, and J. P. ANDREASSEN, 2011. Polymorph Switching in the Calcium Carbonate System by Well-Defined Alginate Oligomers. *Crystal Growth & Design* 11 (2): 520-529.
- OLDERØY, M. Ø., XIE, M., STRAND, B.L., FLATEN, E.M., SIKORSKI, P. and ANDREASSEN, J.-P., 2009. Growth and Nucleation of Calcium Carbonate Vaterite Crystals in Presence of Alginate. *Crystal Growth & Design* 9: 5176-5183.
- OLJEDIREKTORATET, 2011. *Faktaheftet 2011*.
<http://www.npd.no/Publikasjoner/Faktahefter/Fakta-2011/Kap-7/> (accessed 2012/06/27).
- OLSEN, S., O. LUNDE, and A. DUGSTAD, 1999. Stabilizing pH in Troll Pipelines Solves Glycol-Regeneration Problems. *Oil & Gas Journal* 97 (26): 59-62.
- PLUMMER, L. N., and E. BUSENBERG, 1982. The Solubilities of Calcite, Aragonite and Vaterite in CO₂-H₂O Solutions between 0 and 90 °C, and an Evaluation of the Aqueous Model for the System CaCO₃-CO₂-H₂O. *Geochimica et Cosmochimica Acta* 46 (6): 1011-1040.
- SANDENGEN, K., 2006. Prediction of Mineral Scale Formation in Wet Gas Condensate Pipelines and in MEG (Mono Ethylene Glycol) Regeneration Plants. Doctoral thesis, Department of Materials Science and Engineering, NTNU, Trondheim.
- SUNAGAWA, I., 2005. *Crystals: Growth, Morphology, and Perfection*. Cambridge: Cambridge University Press.
- SÖHNEL, O., and J. GARSIDE, 1992. *Precipitation: Basic Principles and Industrial Applications*. Oxford: Butterworth-Heinemann.
- WALPOLE, R. E., R. H. MYERS, S. L. MYERS, and K. YE, 2002. *Probability & Statistics for Engineers & Scientists*. Boston, Mass.: Pearson.
- ÅLANDER, E. M., and A. C. RASMUSON, 2007. Agglomeration and Adhesion Free Energy of Paracetamol Crystals in Organic Solvents. *AIChE Journal* 53 (10): 2590-2605.

List of symbols

| Symbol | Unit | Name |
|-----------|---|--|
| a | - | Activity |
| a^* | - | Activity of a saturated solution |
| a^\pm | - | Mean ionic activity |
| A | m^3 or - | Crystal surface area or Debye-Hückel constant |
| A_T | $mmol/kg_{\text{solvent}}$ | Alkalinity |
| A' | - | Pre-exponential factor in nucleation rate |
| A'' | - | Pre-exponential factor in Arrhenius equation |
| c | mol/mL or mol/L or $mmol/kg_{\text{solvent}}$ | Concentration |
| c_i | | Solute concentration in the solution at the solid-liquid interface |
| c^* | | Equilibrium saturation concentration |
| C | - | Constant for the BET-equation |
| f | - | Overall shape factor |
| g | - | Growth order |
| G | nm/s or J/mol | Growth rate or Gibbs free energy |
| H | kJ/mol | Enthalpy |
| I | mol/L | Ionic strength |
| J | $1/m^3, s$ | Nucleation rate |
| k | J/K | Boltzmann constant |
| k_d | | Mass transfer coefficient for diffusion |
| k_g | m/s or nm/s | Growth rate constant |
| $k_{g=2}$ | m/s or nm/s | Growth rate constant assuming parabolic growth |
| $k_{g=1}$ | m/s or nm/s | Growth rate constant assuming linear growth |
| k_r | | Surface reaction rate constant |
| K_{sp} | | Solubility product |
| L | m | Characteristic dimension |
| m | g or mol/kg_{solvent} | Mass Molality |
| M_w | g/mol | Molecular weight |
| n | mol | Moles |
| N | #/mL | Number of particles in one mL suspension |
| N_A | 1/mol | Avogadro constant |
| P | Pa | Pressure |
| r | m or - | Radius or reaction order |
| R | J/K, mol | Gas constant |
| S | - | Supersaturation ratio |
| SR | - | Saturation ratio |
| t | s or min | Time |

| | | |
|----------|--------------------------|---|
| T | °C or K | Temperature |
| V | mL or cm ³ /# | Volume or volume per particle |
| z_i | - | Number of valences (charge number) of specie i |
| α | - | Volume shape factor or roughness factor |
| β | - | Surface shape factor |
| γ | - | Activity coefficient |
| μ | J/mol or cP | Chemical potential or viscosity |
| ν | - | Number of moles of ions in one mole of the solute |
| ξ | - | Anisotropy factor |
| ρ | g/cm ³ | Density |
| σ | - | Relative supersaturation |
| v | m ³ | Molecular volume |

List of abbreviations

| Abbreviation | Explanation |
|---------------------|---------------------------------|
| ACC | Amorphous calcium carbonate |
| BCF | Burton, Cabrera and Frank |
| B+S | Birth and Spread |
| EDTA | Ethylenediaminetetraacetic acid |
| IAP | Ionic Activity Product |
| MEG | Monoethylene glycol |
| NON | Nuclei on nuclei |
| PN | Polynuclear |
| PSD | Particle Size Distribution |
| SEM | Secondary Electron Microscope |
| XRD | X-ray Diffraction |

Appendix A – Chemicals

Chemicals used in the experiments are shown in Table A. 1.

Table A. 1: Chemicals

| Chemical | Formula | State | Molecular weight* [g/mol] | Purity [%] | Supplier |
|---|---|-------|------------------------------|------------|--------------------------------|
| Ammonia | NH ₃ | l | 17.0 | 25 | VWR International |
| Ammonium chloride | NH ₄ Cl | s | 53.5 | >99.0 | Fluka Chemika |
| Calcium chloride dihydrate | CaCl ₂ ·2H ₂ O | s | 147.02 | 99-103 | Fluka Analytical Sigma-Aldrich |
| Carbon dioxide | CO ₂ | g | 44.0 | | Yara Praxair |
| Ethylenediamine-tetraacetic acid (EDTA) | C ₁₀ H ₁₆ N ₂ O ₈ | aq | 292.24 | | Merck Chemicals |
| Ethanol | C ₂ H ₆ O | l | 46.10 | 96 | VWR International |
| Hydrochloric acid | HCl | l | 36.46 | 37 | VWR International |
| Monoethylene glycol (MEG) | C ₂ H ₆ O ₂ | l | 62.07 | | Fluka Analytical Sigma-Aldrich |
| Potassium chloride | KCl | s | 74.56 | 99.5 | Merck Chemicals |
| Silver chloride | AgCl | s | 143.3 | >99.0 | Fluka Chemika |
| Sodium carbonate | Na ₂ CO ₃ | s | 105.99 | ≥99 | Fluka Analytical Sigma-Aldrich |
| Sodium hydroxide | NaOH | s | 40.00 | >99 | VWR International |
| Sodium nitrate | NaNO ₃ | s | 85.00 | | Merck Chemicals |

*(Aylward and Findlay, 2002)

Appendix B – Calculations

B.1 Number and volume of seed particles

The number and volume of the vaterite and calcite seed particles are determined with the Coulter Counter. An imbibition of 100 μL and 2 000 μL for vaterite and calcite seeds, respectively, in saturated NaNO_3 solution is determined by the Coulter Counter. A calculation example for vaterite seeds is shown below. The average number of particles per 100 μL from 12 measurements is for one experiment 21 700. Number of particles, N per mL is calculated by

$$\frac{N_{part./100\mu L}}{0.1} = \frac{21\,700}{0.1} = \underline{2.17 \cdot 10^5 \# / mL}$$

The average volume of particles, $V_{part.}$, per 100 μL from the same experiment is $6.19 \cdot 10^6 (\mu\text{L}^3)^3$. The volume of particles per mL is calculated by

$$\frac{V_{part./100\mu L}}{10^{17}} = \frac{6.19 \cdot 10^6 \mu\text{L}^9}{10^{17}} = \underline{6.19 \cdot 10^{-11} m^3 / mL}$$

The average volume per particle is calculated by

$$V_{part} = \frac{V_{part} / mL}{N_{part} / mL} = \frac{6.19 \cdot 10^{-11} m^3 / mL}{2.17 \cdot 10^5 \# / mL} = \underline{\underline{2.85 \cdot 10^{-16} m^3 / \#}}$$

Nucleation, agglomeration and breakage of the particles are assumed non-existing.

B.2 Growth rates

A calculation example for vaterite growth is shown below. The samples withdrawn during the growth experiments are weighted in order to determine amount of calcium

$$m_{Ca^{2+}} = m_{cup\ with\ sample} - m_{empty\ cup} = 58.00g - 47.82g = \underline{10.18g}$$

It is assumed that the mass of calcium in solution is equal to the volume of calcium in solution

$$m_{Ca^{2+}} \approx V_{Ca^{2+}} = 10.18mL$$

EDTA is used as titrant in the titration. The number of moles EDTA is determined from the volume EDTA used at the titration endpoint and the known EDTA concentration from

$$n_{EDTA} = c_{EDTA} \cdot V_{EDTA} = 9.92 \cdot 10^{-6} \text{ mol/mL} \cdot 4.28 \text{ mL} = 4.25 \cdot 10^{-5} \text{ mol}$$

and corresponds to the number of moles of calcium

$$n_{Ca^{2+}} = n_{EDTA} = \underline{4.25 \cdot 10^{-5} \text{ mol}}$$

The concentration of calcium in a sample is calculated from

$$c_{Ca^{2+}} = \frac{n_{Ca^{2+}}}{V_{Ca^{2+}}} = \frac{4.25 \cdot 10^{-5} \text{ mol}}{10.18 \text{ mL}} = \underline{4.17 \cdot 10^{-6} \text{ mol/mL}}$$

The calculated concentrations are plotted against time, t , to show the depleting calcium concentration during the growth. The difference in $c_{Ca^{2+}}$ between sample 1 and 2.

$\Delta c_{Ca^{2+},1} = c_{Ca^{2+},1} - c_{Ca^{2+},0}$ is found, and the volume increase of each seed particle is then calculated

$$\Delta V_1 = \frac{-\Delta c_{Ca^{2+},1} \cdot Mw_{CaCO_3}}{\rho_{CaCO_3,v} \cdot N} = \frac{-(-6.13 \cdot 10^{-7} \text{ mol/mL}) \cdot 100.09 \text{ g/mol}}{2.440 \text{ g/cm}^3 \cdot 2.17 \cdot 10^5 \text{ \#/mL}} = 1.16 \cdot 10^{-10} \text{ cm}^3 / \#$$

where Mw_{CaCO_3} is the molecular weight of calcium carbonate. $\rho_{CaCO_3,v}$ is the density of vaterite (Flaten et al., 2010a) and N is the number of seed particles in one mL suspension, #/mL, determined by the Coulter Counter. The initial volume of a particle, V_0 , is also measured with the Coulter Counter, and the volume of the particle in the first sample is determined from

$$V_1 = V_0 + \Delta V_1 = 2.85 \cdot 10^{-10} \text{ cm}^3 + 1.16 \cdot 10^{-11} \text{ cm}^3 = \underline{3.26 \cdot 10^{-10} \text{ cm}^3 / \#}$$

The radius of the seed particle is determined from the volume, $V_1 = \frac{4}{3} \pi \cdot r_1^3$, by

$$r_1 = \left(\frac{3 \cdot V_1}{4 \cdot \pi} \right)^{\frac{1}{3}} = \left(\frac{3 \cdot 3.26 \cdot 10^{-10} \text{ cm}^3}{4 \cdot \pi} \right)^{\frac{1}{3}} = 4.27 \cdot 10^{-4} \text{ cm} = \underline{4.27 \cdot 10^{-6} \text{ m}}$$

The increase of radius between the initial particle, r_0 , and the particle in the first sample, r_1 is

$$\Delta r_1 = r_1 - r_0 = 4.27 \cdot 10^{-6} \text{ m} - 4.08 \cdot 10^{-6} \text{ m} = \underline{1.90 \cdot 10^{-7} \text{ m}}$$

The growth rate, G , is then determined from

$$G_1 = \frac{\Delta r_1}{\Delta t_1} = \frac{1.90 \cdot 10^{-7} \text{ m}}{26 \text{ s}} = 7.31 \cdot 10^{-9} \text{ m/s} = \underline{\underline{7.31 \text{ nm/s}}}$$

Calcite growth is calculated the same way as vaterite except for the spherical volume considerations. Calcite is cubic formed, thus volume is obtained from

$$V_1 = s_1^3 = (2L_1)^3$$

where s is one side of the cube. The characteristic dimension, L , which is half of the cube side is calculated from

$$L_1 = \left(\frac{V_1}{8} \right)^{\frac{1}{3}}$$

Hence, the growth rate is determined from

$$G_1 = \frac{\Delta L_1}{\Delta t_1}$$

B.3 Supersaturation ratios

In order to determine the growth order, g , and the growth rate constant, k_g , the supersaturation ratios must be calculated. This is performed in MultiScale, which calculates saturation ratios for calcite, SR_{cal} , based on activity. To obtain supersaturation ratios for vaterite, S_{vat} , the equilibrium constant – temperature relation in equation (2.38) must be considered. The alkalinity of the system must also be known, calculated from equation (2.31)

$$A_{T,1} = A_{T,0} - 2 \cdot \Delta c_{\text{Ca}^{2+},1} = 166.19 \text{ mmol/kg}_{\text{solvent}} - 2 \cdot 0.613 \text{ mmol/kg}_{\text{solvent}} = \underline{\underline{164.96 \text{ mmol/kg}_{\text{solvent}}}}$$

MultiScale returns a SR_{cal} value of 26.49, which corresponds to SR_{vat} from the following equation

$$SR_{\text{vat},1} = \frac{SR_{\text{cal},1} \cdot K_{\text{sp,cal}}(T)}{K_{\text{sp,vat}}(T)} = \frac{26.49 \cdot 2.52 \cdot 10^{-9}}{8.89 \cdot 10^{-9}} = 7.51$$

The supersaturation ratio for vaterite is then determined by

$$S_{\text{vat},1} = \sqrt{SR_{\text{vat},1}} = \sqrt{7.51} = \underline{\underline{2.74}}$$

Alternatively, for calcite growth calculations, S_{cal} could be determined directly from the SR_{cal} value given from MultiScale.

B.4 Mother-liquids and solutions for growth experiments

B.4.1 Mother-liquids

All experiments were carried out with $\text{CaCl}_2 \cdot 2\text{H}_2\text{O}$ and NaOH solutions prepared from mother-liquids. This was done to minimize uncertainty when weighting out chemicals. A calculation example for the calcium mother-liquid is shown below. It is emphasized that the term “solution” in $\text{kg}_{\text{solution}}$ means water/MEG and solid substance, and “solvent” in $\text{kg}_{\text{solvent}}$ means only water/MEG.

2 kg 100 mmol/ $\text{kg}_{\text{solution}}$ $\text{CaCl}_2 \cdot 2\text{H}_2\text{O}$ solution was prepared as the calcium mother-liquid. This requires

$$100 \frac{\text{mmol}}{\text{kg}_{\text{solution}}} \cdot 2 \text{ kg}_{\text{solution}} = 200 \text{ mmol} = 0.2 \text{ mol } \text{CaCl}_2 \cdot 2\text{H}_2\text{O}$$

and an amount of

$$0.2 \text{ mol} \cdot 147.012 \frac{\text{g}}{\text{mol}} = 29.40 \text{ g } \text{CaCl}_2 \cdot 2\text{H}_2\text{O}$$

is weighted out. Amount of deionized water added is therefore

$$2 \text{ kg}_{\text{solution}} - 29.40 \text{ g } \text{CaCl}_2 \cdot 2\text{H}_2\text{O} = 1970.60 \text{ g } \text{H}_2\text{O}$$

The number of moles $\text{CaCl}_2 \cdot 2\text{H}_2\text{O}$ is 0.2 which results in 0.4 moles of crystallization water. Molecular weight of water is 18.016 g/mol which means that

$$0.40 \text{ mol} \cdot 18.016 \frac{\text{g}}{\text{mol}} = 7.21 \text{ g } \text{H}_2\text{O}$$

should be accounted for when calculating the relation between amount water and amount solution as

$$\frac{(1970.40 + 7.21) \text{ g}_{\text{water}}}{(1970.40 + 29.40) \text{ g}_{\text{solution}}} = 0.99 \frac{\text{g}_{\text{water}}}{\text{g}_{\text{solution}}}$$

The NaOH mother-liquid is made the same way, except that calculations for crystallization water is not needed.

B.4.2 Solutions

A calculation example for a calcium solution used in a vaterite growth experiment is given below. The initial calcium concentration is $5.0 \text{ mmol/kg}_{\text{solvent}}$ for all experiments. The concentration of the calcium solution before mixing with NaOH in the reactor is therefore $10.0 \text{ mmol/kg}_{\text{solvent}}$. Amount of each solution before mixing is $0.375 \text{ kg}_{\text{solvent}} = 375 \text{ g}_{\text{solvent}}$ giving a total reactor content of $0.750 \text{ kg} = 750 \text{ g}$. Number of moles $\text{CaCl}_2 \cdot 2\text{H}_2\text{O}$ needed is

$$10.0 \text{ mmol/kg}_{\text{solvent}} \cdot 0.375 \text{ kg}_{\text{solvent}} = 3.75 \text{ mmol}$$

which means that

$$\frac{3.75 \text{ mmol}}{100 \text{ mmol/kg}_{\text{solution}}} = 0.0375 \text{ kg}_{\text{solution}} = 37.5 \text{ g}_{\text{solution}}$$

is weighted out from the calcium mother liquid. Amount of water included in $37.5 \text{ g}_{\text{solution}}$ is

$$37.5 \text{ g}_{\text{solution}} \cdot 0.99 \text{ g}_{\text{water}}/\text{g}_{\text{solution}} = 37.13 \text{ g}_{\text{water}}$$

resulting in remaining water needed is

$$375 \text{ g}_{\text{solvent}} - 37.13 \text{ g}_{\text{water in calcium solution}} = 337.87 \text{ g}_{\text{water}}$$

When MEG is introduced in the system, for example for an experiment with 50 wt% MEG, amount of water added is

$$(375 \text{ g}_{\text{solvent}} \cdot 0.50) - 37.13 \text{ g}_{\text{water in calcium solution}} = 150.37 \text{ g}_{\text{water}}$$

Amount of MEG added will therefore be

$$375 \text{ g}_{\text{solvent}} \cdot 0.5 = 187.5 \text{ g}_{\text{MEG}}$$

The preparation of solutions for a calcite growth experiment is slightly different due to that the amount of calcite seed solution of $60 \text{ mL} = 0.06 \text{ L} = 60 \text{ g}$ and its concentration of ions are taken into account. (For vaterite growth experiments the amount of 15 mL seed solution is ignored in the calculations). Samples from the calcite seed solution reactor are withdrawn frequently to determine its calcium concentration. This was measured to 2.2 mmol/L giving

$$0.06 \text{ L} \cdot 2.2 \text{ mmol/L} = 0.13 \text{ mmol Ca}^{2+}$$

in the seed solution, which makes the need of moles calcium reduced from 3.75 mmol to 3.62 mmol. The new initial concentration of calcium, being the basis for the calculations above, is therefore

$$\frac{3.62 \text{ mmol}}{0,750 \text{ kg}_{\text{solvent}}} = 4.83 \text{ mmol} / \text{kg}_{\text{solvent}}$$

instead of 5.0 mmol/kg_{solvent}.

Additionally, the amount of water in the seed solution is taken into account when calculating amount of water added. In the example above 150.37 g_{water} is reduced to 150.37 g_{water} – (60/2) g_{water in seeds} = 120.37 g_{water}. The remaining 30 g water from seed solution is included in the NaOH solution calculations.

Moreover, in determination of supersaturation rations in MultiScale the 60 mL calcite seed solution is also taken into account. The seed solution has a concentration of 0.2 mol/L NaCl and 0.1 mol/L CaCO₃. This gives an increased chloride concentration from 10.0 mmol/kg_{solvent} to 26.0 mmol/kg_{solvent}. The sodium concentration will also be increased due to this. For instance with an initial sodium concentration of 146.29 mmol/kg_{solvent} (and the same as the alkalinity level), the new sodium concentration will be 162.29 mmol/kg_{solvent}. The carbonate influence on the alkalinity level is ignored.

Appendix C – Experimental setup

All vaterite growth experiments were done with an initial $S_{\text{vat}} = 3.0$ which corresponds to $SR_{\text{cal}} = 30.39$ at 40 °C and $SR_{\text{cal}} = 26.13$ at 70 °C according to equation (2.13) and (2.38). The experimental conditions with alkalinity, SR, amount of mother-liquids, water and MEG is reported in Table C. 1.

Table C. 1: Experimental conditions for vaterite growth experiments.

| Temperature [°C] | 40 | | | 70 | | |
|---|----------|-----------|-----------|----------|-----------|-----------|
| MEG content [wt%] | 0 | 40 | 60 | 0 | 40 | 60 |
| Alkalinity [mmol/kg_{solvent}] | 166.190 | 101.650 | 71.020 | 46.605 | 28.259 | 20.267 |
| SR_{cal} | 30.3997 | 30.3990 | 30.4011 | 26.1306 | 26.1307 | 26.1310 |
| CaCl₂ solution | | | | | | |
| CaCl ₂ from mother-liquid [g] | 37.50 | 37.50 | 37.50 | 37.50 | 37.50 | 37.50 |
| H ₂ O [g] | 337.92 | 187.92 | 112.92 | 337.92 | 187.92 | 112.92 |
| MEG [g] | 0.00 | 150.00 | 225.00 | 0.00 | 150.00 | 225.00 |
| NaOH solution | | | | | | |
| NaOH from mother-liquid [g] | 124.64 | 76.24 | 53.27 | 34.95 | 21.19 | 15.20 |
| H ₂ O [g] | 255.34 | 151.81 | 98.87 | 341.44 | 204.65 | 135.41 |
| MEG [g] | 0.00 | 150.00 | 225.00 | 0.00 | 150.00 | 225.00 |

Calcite growth experiments were carried out with an initial $S_{\text{cal}} = 5.0$ which correspond to $SR_{\text{cal}} = 25.00$. Due to nucleation of aragonite at some experiments at 70 °C, the initial S_{cal} was reduced to 4.0 ($SR_{\text{cal}} = 16.00$). The experimental conditions with alkalinity, SR, amount of mother-liquids, water and MEG is reported in Table C. 2.

Table C. 2: Experimental conditions for calcite growth experiments.

| Temperature [°C] | 40 | | | | 70 | | |
|---|-----------|-----------|-----------|-----------|-----------|-----------|-----------|
| MEG content [wt%] | 0 | 30 | 50 | 70 | 0 | 30 | 70 |
| Alkalinity [mmol/kg_{solvent}] | 146.290 | 105.800 | 78.520 | 54.410 | 48.920 | 34.765 | 18.594 |
| SR_{cal} | 24.9991 | 25.0018 | 24.9951 | 24.9983 | 24.9975 | 25.0003 | 24.9999 |
| CaCl₂ solution | | | | | | | |
| CaCl ₂ from mother-liquid [g] | 36.12 | 36.18 | 36.18 | 36.18 | 36.18 | 36.18 | 36.18 |
| H ₂ O [g] | 309.28 | 196.72 | 121.72 | 46.72 | 309.22 | 196.72 | 46.72 |
| MEG [g] | 0.00 | 112.50 | 187.50 | 262.50 | 0.00 | 112.50 | 262.50 |
| NaOH solution | | | | | | | |
| NaOH from mother-liquid [g] | 109.72 | 79.35 | 58.89 | 40.81 | 36.69 | 26.07 | 13.95 |
| H ₂ O [g] | 239.67 | 156.32 | 100.97 | 43.32 | 309.78 | 207.47 | 69.11 |
| MEG [g] | 0.00 | 112.50 | 187.50 | 262.50 | 0.00 | 112.50 | 262.50 |

Initial IAP for seeds and all experiments were calculated and plotted as illustrated in Figure C. 1. To be able to calculate IAP, the activities of calcium and carbonate have to be determined as shown in equation (2.11). Activities of these ions are calculated from the product of concentration and the activity coefficient as seen in equation (2.4). This gives

$$IAP = a_{Ca^{2+}} \cdot a_{CO_3^{2-}} = \gamma^2 \cdot c_{Ca^{2+}} \cdot c_{CO_3^{2-}}$$

Combining this with equation (2.12) and (2.13) gives, for calcite,

$$SR_{cal} = \frac{IAP}{K_{sp,cal}} = \frac{\gamma^2 \cdot c_{Ca^{2+}} \cdot c_{CO_3^{2-}}}{K_{sp,cal}}$$

The activity coefficient, γ , is determined as shown below:

$$\gamma = \sqrt{\frac{SR_{cal} \cdot K_{sp,cal}}{c_{Ca^{2+}} \cdot c_{CO_3^{2-}}}}$$

where SR_{cal} , $K_{sp,cal}$ and concentrations of free ions of Ca^{2+} and CO_3^{2-} are obtained from MultiScale.

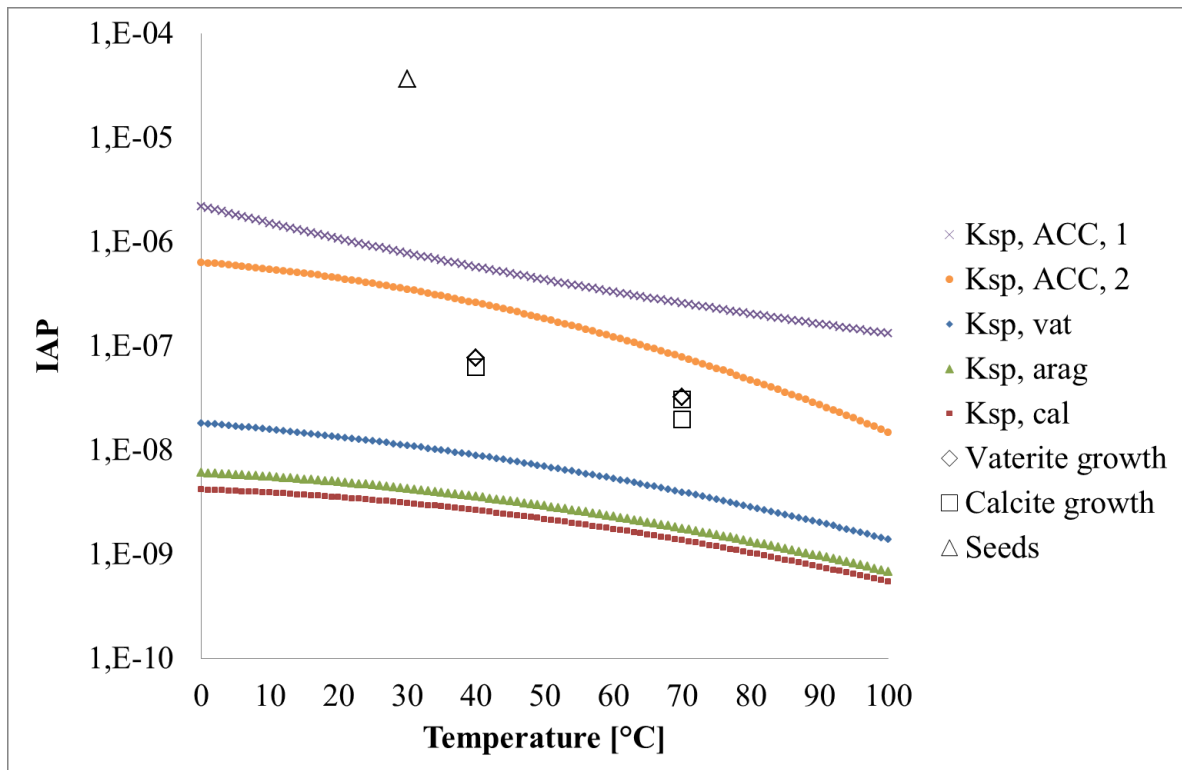


Figure C. 1: IAP as a function of temperature for the ACC, vaterite, aragonite and calcite. Initial IAP as a function of temperature for seeds, vaterite growth and calcite growth are also shown in the diagram. The y-axis is logarithmic. $K_{sp, vat}$, $K_{sp, arag}$ and $K_{sp, cal}$ from Plummer and Busenberg (1982), $K_{sp, ACC, 1}$ from Clarkson et al. (1992) and $K_{sp, ACC, 2}$ from Brečević and Nielsen (1989).

Appendix D – Uncertainty

Uncertainty is always an issue when doing experiments in the laboratory. Errors are involved in all measurements that are carried out during an experiment. Generally, errors could be classified either as random errors or systematic errors (Førland, 2001).

Typical systematic errors are impurities in chemicals, poor calibration of instruments as pH-meters and weights, and errors in the experimental technique. Systematic errors will give inaccurate results compared to for instance results from literature or results from a different experimental technique. Independent of how many parallels that are done, the result will not get closer to the ‘correct’ value. Systematic errors could be difficult to detect, but when it is found it is not impossible to eliminate.

Random errors are harder to avoid since they vary for each time the experiment is done. This type of error will give imprecise results. An increased amount of parallel experiments will reduce the imprecision. A measure of precision in a series of experiment is standard deviation.

When parallel experiments have been done in this work, the average value has been determined as (Walpole et al., 2002)

$$\bar{x} = \sum_{i=1}^n \frac{x_i}{n}$$

where n is the number of parallels. Precision is expressed as sample variance, denoted s^2 , given by

$$s^2 = \sum_{i=1}^n \frac{(x_i - \bar{x})^2}{n-1}$$

where the sample standard deviation, s , is

$$s = \sqrt{s^2}$$

When only one parallel has been executed standard deviation could not be reported. Thus, for these experiments, linear regression models are reported with a correlation coefficient, R^2 . Another often used term for R^2 is coefficient of determination (Walpole et al., 2002). R^2 is a number between 0 and 1 that gives information on how closely the estimated values for the trendline corresponds with the actual data. When R^2 is equal to 1.0 the fit is perfect, whereas if $R^2 = 0$ the fit is very poor. If for instance $R^2 = 0,970$ this means that 97.0 % of the variation has been expressed in the linear regression model.

From Microsoft Excel, R^2 , has been calculated as the Pearson product moment correlation coefficient, R

$$R = \frac{\sum (x - \bar{x})(y - \bar{y})}{\sqrt{\sum (x - \bar{x})^2 \sum (y - \bar{y})^2}}$$

where R^2 is the square root of this.

Appendix E – Number and volume of seed particles

Table E. 1: Number and volume of vaterite seed particles.

| Experiment | Number of particles [10 ³ # part./mL] | Volume of particles [10 ⁻¹² m ³ /mL] | Volume pr. particle [10 ⁻¹⁶ m ³ /part.] |
|-----------------------------------|---|---|---|
| V.1 | 224.97 ± 49.63 | 64.21 ± 5.32 | 2.93 ± 0.40 |
| V.2 | 220.20 ± 4.64 | 56.02 ± 1.68 | 2.54 ± 0.10 |
| V.3 | 354.90 ± 33.85 | 75.65 ± 2.40 | 2.15 ± 0.16 |
| V.4 | 297.25 ± 27.50 | 75.20 ± 3.19 | 2.54 ± 0.13 |
| V.5 | 401.69 ± 22.76 | 71.69 ± 1.49 | 1.79 ± 0.07 |
| V.6 | 380.61 ± 19.32 | 74.87 ± 2.96 | 1.97 ± 0.05 |
| Average | 313.27 | 69.61 | 2.32 |
| Standard deviation | 78.49 | 7.92 | 0.43 |
| Standard deviation/Average | 0.25 | 0.11 | 0.18 |

Table E. 2: Number and volume of calcite seed particles.

| Experiment | Number of particles [10 ³ # part./mL] | Volume of particles [10 ⁻¹² m ³ /mL] | Volume pr. particle [10 ⁻¹⁶ m ³ /part.] |
|-----------------------------------|---|---|---|
| C.1 | 4.93 ± 0.22 | 179.21 ± 15.61 | 362.86 ± 1.94 |
| C.2 | 4.33 ± 0.12 | 151.62 ± 3.94 | 350.55 ± 0.42 |
| C.3 | 4.55 ± 1.11 | 163.82 ± 37.75 | 361.12 ± 0.80 |
| C.4 | 4.02 ± 0.22 | 149.70 ± 6.31 | 372.80 ± 1.30 |
| Average | 4.46 | 161.09 | 361.83 |
| Standard deviation | 0.38 | 13.60 | 9.11 |
| Standard deviation/Average | 0.09 | 0.08 | 0.03 |

Appendix F – Additional graphs

F.1 Vaterite growth experiments

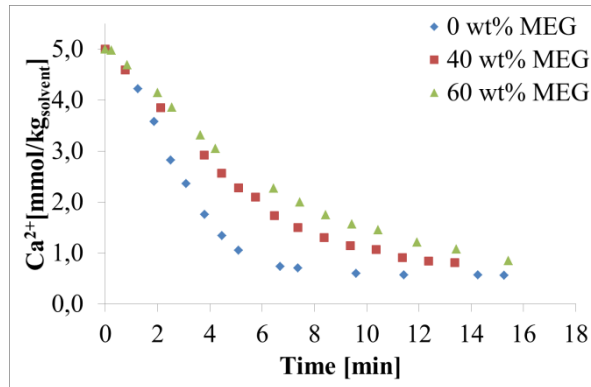


Figure F. 1: Decreasing calcium concentration over time for vaterite with varying MEG concentration at 70 °C.

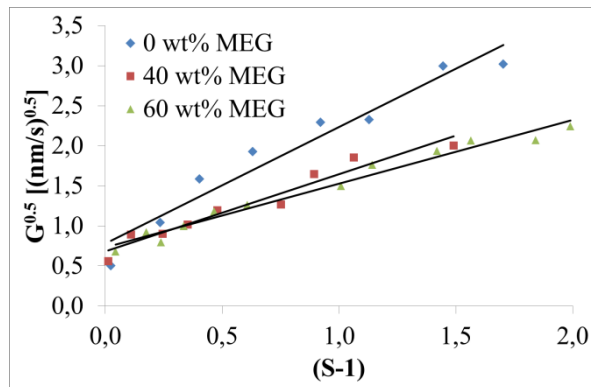


Figure F. 2: $G^{0.5}$ as a function of (S-1) for vaterite with varying MEG concentration at 70 °C.

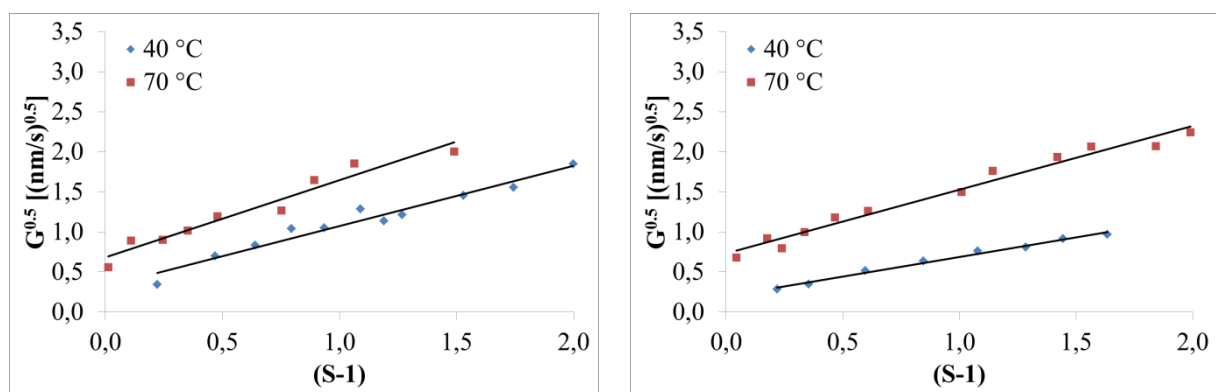


Figure F. 3: $G^{0.5}$ as a function of (S-1) for vaterite with varying temperature in 40 wt% MEG (left) and 60 wt% MEG (right).

F.1 Calcite growth experiments

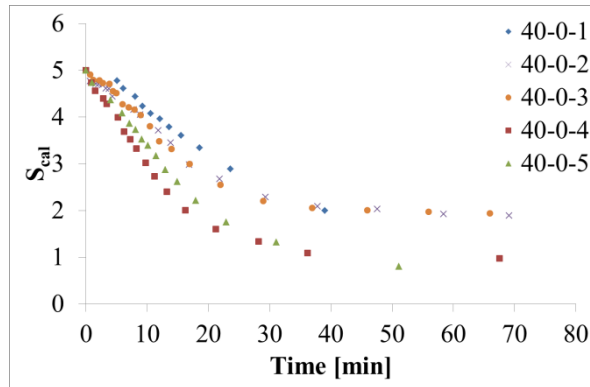


Figure F. 4: De-supersaturation profiles for calcite in water at 40 °C for five parallel experiments. The notation 40-0-i means temperature - wt% MEG - parallel number.

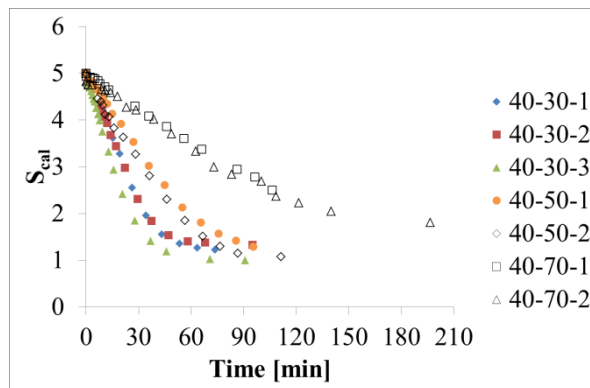


Figure F. 5: De-supersaturation profiles for calcite in 30, 50 and 70 wt% MEG at 40 °C. The notation 40-X-i means temperature - wt% MEG - parallel number.

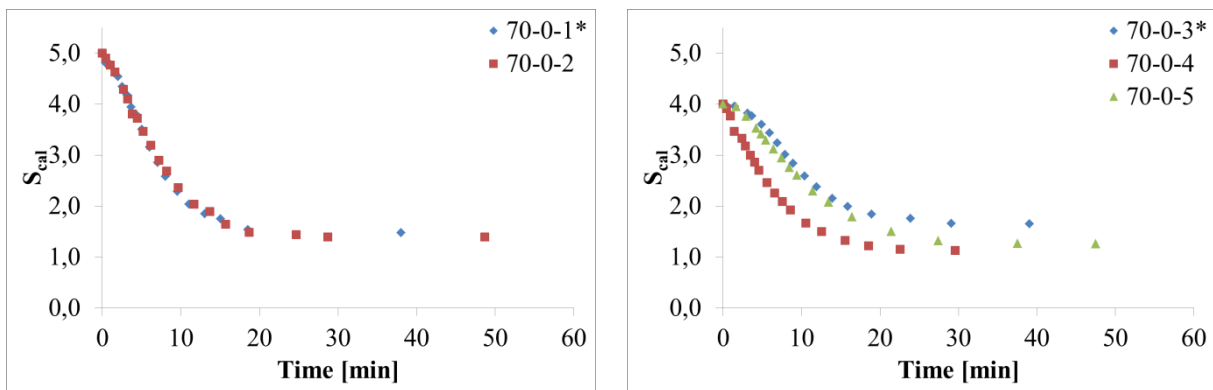


Figure F. 6: De-supersaturation profiles for calcite in water at 70 °C with initial $S_{cal}=5.0$ (left) and $S_{cal}=4.0$ (right). The notation 70-0-i means temperature - wt% MEG - parallel number.

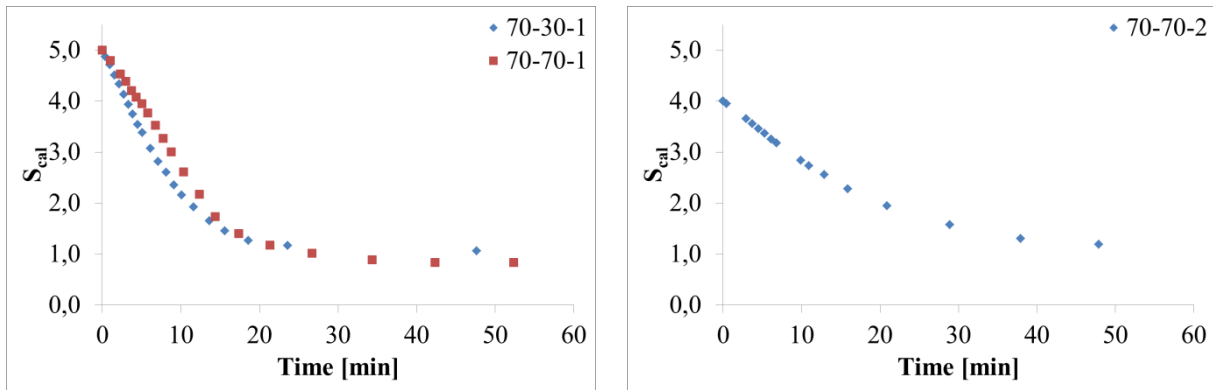


Figure F. 7: De-supersaturation profiles for calcite in 30 and 70 wt% MEG at 70 °C with initial $S_{cal}=5.0$ (left) and $S_{cal}=4.0$ (right). The notation 70-X-i means temperature - wt% MEG - parallel number.

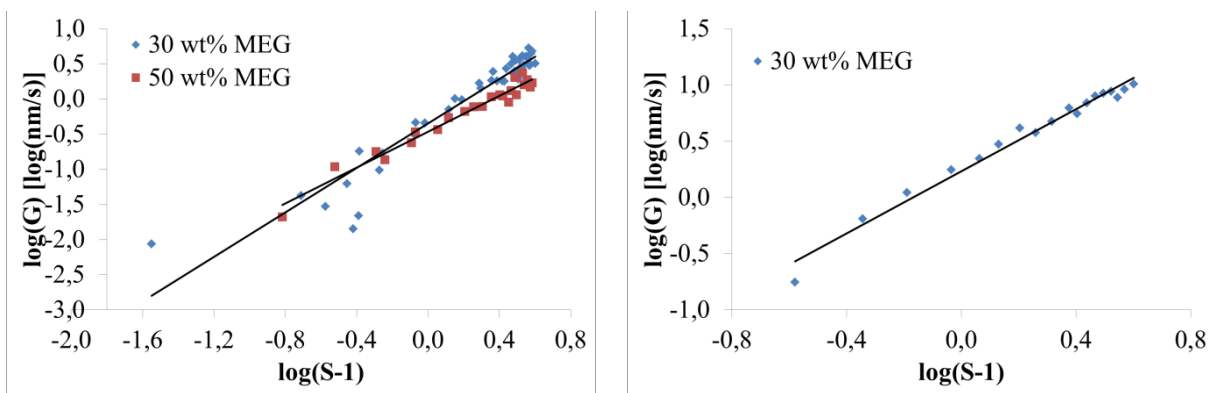


Figure F. 8: $\log(G)$ as a function of $\log(S-I)$ for calcite with 30 and 50 wt% MEG at 40 °C (left) and 30 wt% MEG at 70 °C (right).

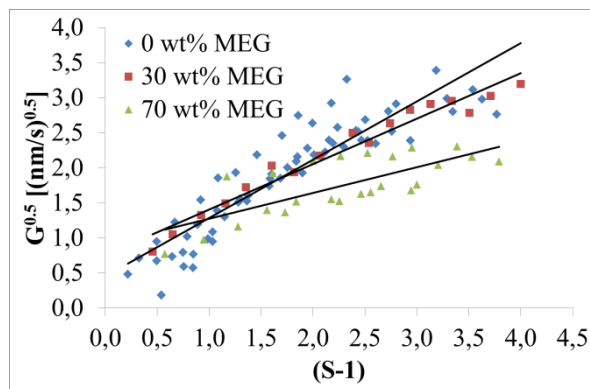


Figure F. 9: $G^{0.5}$ as a function of $(S-1)$ for calcite with varying MEG concentration at 70 °C.

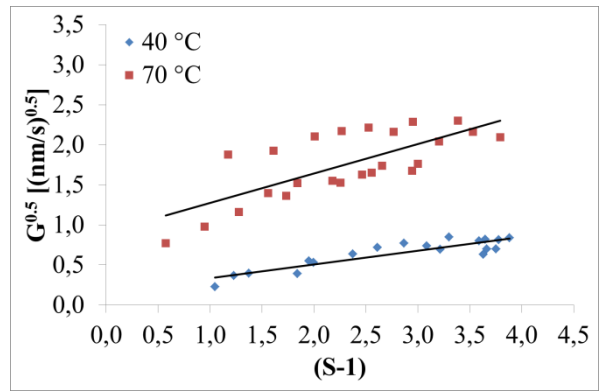
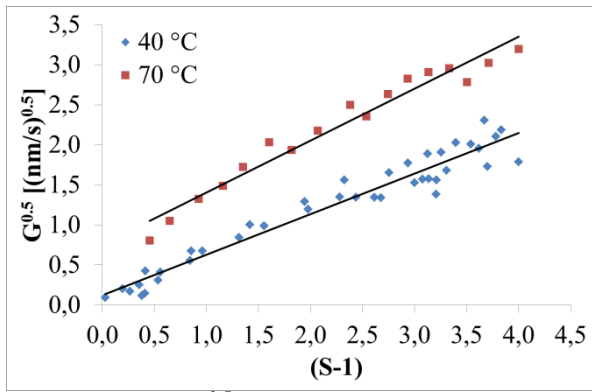


Figure F. 10: $G^{0.5}$ as a function of (S-1) for calcite with varying temperature in 30 wt% MEG (left) and 70 wt% MEG (right).

Appendix G – XRD scans

XRD analyses were prepared with single crystal sample holders. The intensity values at the y-axis are not shown due to that the curves are displaced vertically to better distinguish between them. The interval of diffraction angle is 20 – 60 °. XRD analysis was used qualitatively for determination of constituent polymorphs in a crystal sample. Some of the peaks are sheared off to better distinguish between the lower peaks.

Characteristic peaks for vaterite seeds and vaterite grown at 40 °C at varying MEG concentrations are illustrated in Figure G. 1. The labels ‘v’ and ‘c’ denotes vaterite and calcite, respectively.

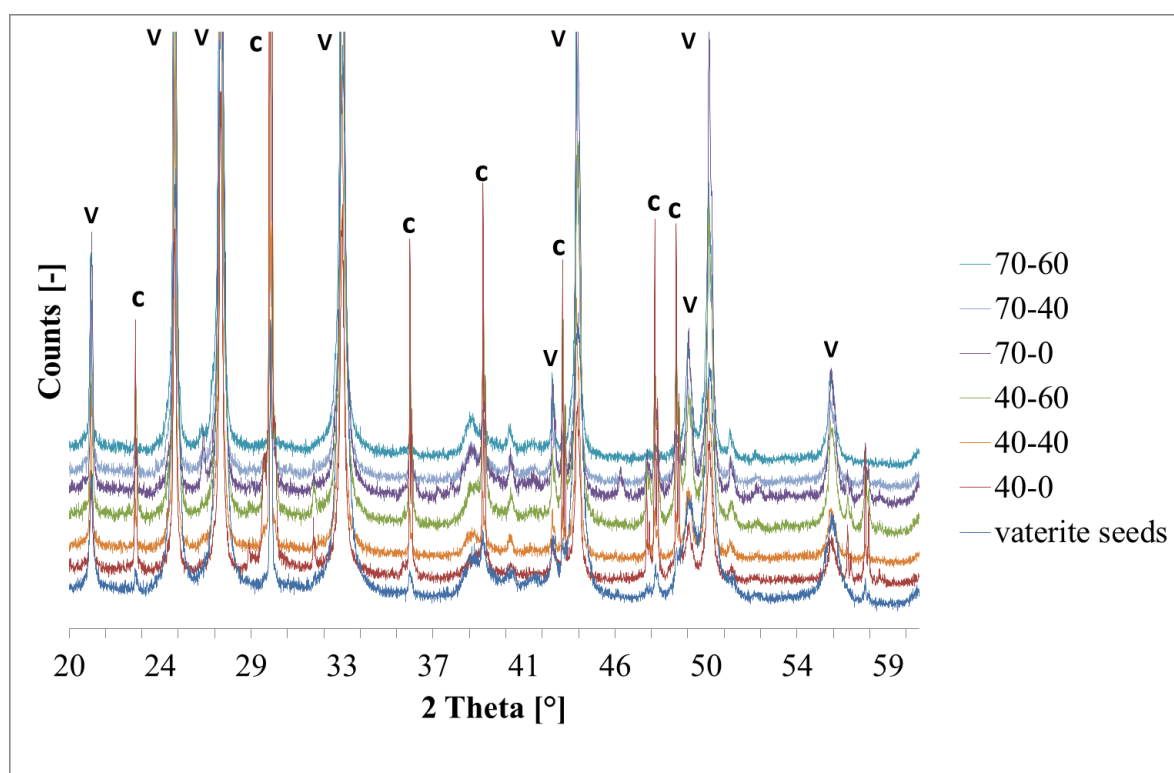


Figure G. 1: Powder XRD for vaterite seeds and vaterite grown at 40 °C and 70 °C with 0, 40 and 60 wt% MEG.

Characteristic peaks for calcite seeds and calcite grown at 40 °C at varying MEG concentrations are illustrated in Figure G. 2. All peaks are characteristic for calcite. No other elements were identified.

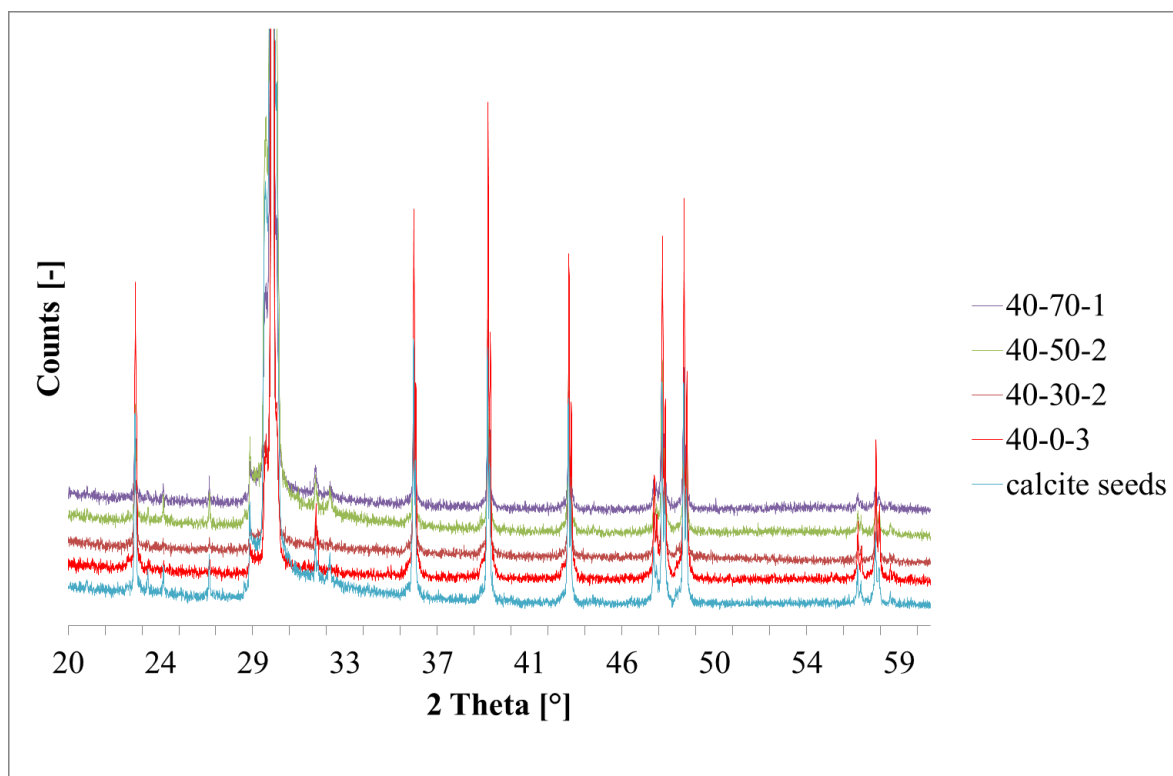


Figure G. 2: Powder XRD for calcite seeds and calcite grown at 40 °C with 0, 30, 50 and 70 wt% MEG. One parallel from each MEG concentration is shown.

Characteristic peaks for calcite seeds and calcite grown at 70 °C at varying MEG concentrations are illustrated in Figure G. 3. All peaks are characteristic for calcite. No other elements were identified.

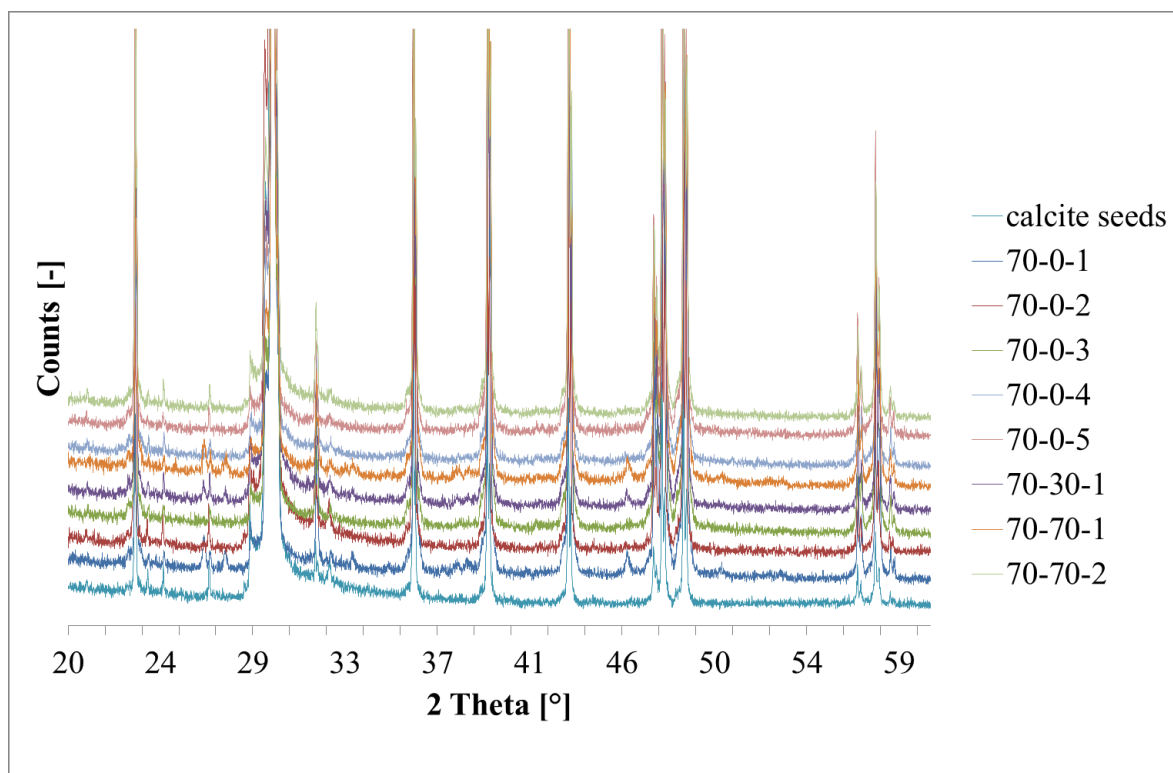


Figure G. 3: Powder XRD for calcite seeds and calcite grown at 70 °C with 0, 30, 50 and 70 wt% MEG. All parallels are shown.

Appendix H – Pictures of the reactor equipment



Figure H. 1: Reactor lid with propeller and baffles made of steel (left) and Teflon (right).

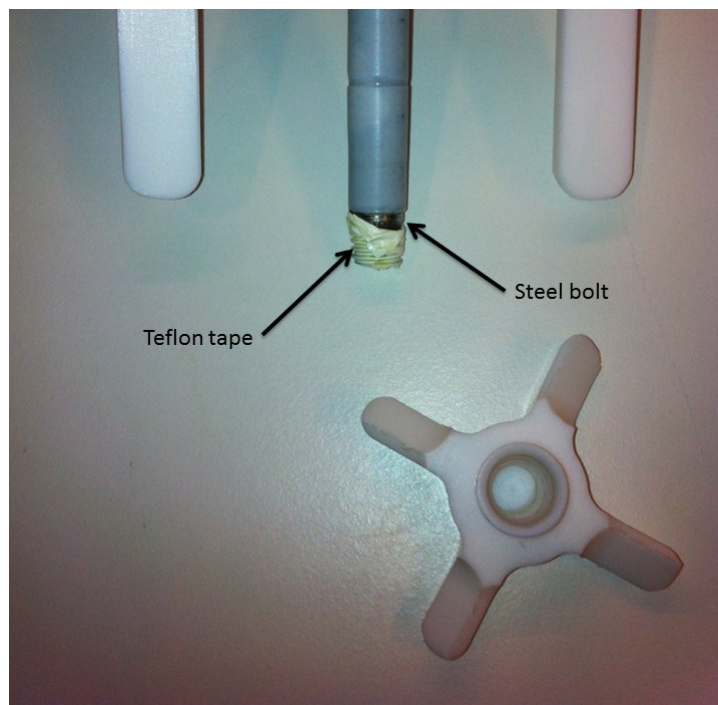



Figure H. 2: Teflon propeller with steel bolt covered with Teflon tape.

Appendix I – Concentration of free ions for calcite growth

Table I. 1: Concentration of free ions in mmol/kg_{solvent} of calcium and carbonate initially and in the end of the growth.

| Temperature [°C] | MEG [wt%] | Initial S _{cal} | Initial Ca ²⁺ * | Initial CO ₃ ²⁻ | End Ca ²⁺ | End CO ₃ ²⁻ |
|------------------|-----------|--------------------------|----------------------------|---------------------------------------|----------------------|-----------------------------------|
| 40 | 0 | 5 | 4.85 | 0.23 | 0.25 | 0.19 |
| 40 | 30 | 5 | 4.85 | 0.09 | 0.23 | 0.08 |
| 40 | 50 | 5 | 4.85 | 0.04 | 0.56 | 0.03 |
| 40 | 70 | 5 | 4.85 | 0.02 | 1.98 | 0.01 |
| 70 | 0 | 5 | 4.82 | 0.06 | 0.59 | 0.04 |
| 70 | 0 | 4 | 4.88 | 0.03 | 0.67 | 0.02 |
| 70 | 30 | 5 | 4.82 | 0.03 | 0.48 | 0.01 |
| 70 | 70 | 5 | 4.82 | 0.006 | 0.74 | 0.002 |
| 70 | 70 | 4 | 4.88 | 0.003 | 1.95 | 0.001 |

Appendix J – Risk assessment form

| NTNU HMS /KS | | Risk assessment | | | | Utarbeidet av | Nummer | Dato | | |
|---|---|---|------------------|--------------|-------------------|------------------------|------------------|-----------|------------|------------------------------------|
|  | | | | | | HMS-avd. | HMSRV2603 | | | |
| | | | | | | Godkjent av | Side | Erstatter | | |
| | | | | | | | | | | |
| Unit: | | <i>Chemical Engineering</i> | | Date: | | 7.10.2011 | | | | |
| Line manager: | | <i>Øyvind Gregersen</i> | | | | | | | | |
| Participants in the identification process (including their function): | | Jens-Petter Andreassen (supervisor) og Charlotte K. Krossholm (student) | | | | | | | | |
| Signatures: | | | | | | | | | | |
| ID no. | Activity from the identification process form | Potential undesirable incident/strain | Likelihood: | | | Consequence: | | | Risk value | Comments/status Suggested measures |
| | | | Likelihood (1-5) | Human (A-E) | Environment (A-E) | Economy/material (A-E) | Reputation (A-E) | | | |
| 1 | HCl | Søi, sprut på hud, klær | 3 | A | | | | | A3 | |
| 2 | MEG | Søi, sprut på hud, klær | 3 | A | | | | | A3 | Bruk avtrekksskap |
| 3 | NaOH | Søi, sprut på hud, klær | 3 | A | | | | | A3 | |
| 4 | Glassutstyr | Knusing av glass | 2 | B | | | | | B2 | |
| 5 | Gassylinder med CO2 | Trykk overstiger temperatur | 3 | A | | | | | A3 | |
| 6 | Vannbad/Gummislanger | | 3 | A | | | | | A3 | |
| Likelihood, e.g.: | | | | | | | | | | |
| 1. Minimal | | | | | | | | | | |
| 2. Low | | | | | | | | | | |
| 3. Medium | | | | | | | | | | |
| 4. High | | | | | | | | | | |
| 5. Very high | | | | | | | | | | |
| Consequence, e.g.: | | | | | | | | | | |
| A. Safe | | | | | | | | | | |
| B. Relatively safe | | | | | | | | | | |
| C. Dangerous | | | | | | | | | | |
| D. Critical | | | | | | | | | | |
| E. Very critical | | | | | | | | | | |
| Risk value (each one to be estimated separately): | | | | | | | | | | |
| Human = Likelihood x Human Consequence | | | | | | | | | | |
| Environmental = Likelihood x Environmental consequence | | | | | | | | | | |
| Financial/material = Likelihood x Consequence for Economy/material | | | | | | | | | | |